225
11-87 JGM (5)
I. 30416 DE87 006232-1

SANDIA REPORT
SAND86—2927 • UC—71
Unlimited Release
Printed April 1987

A Phenomenological Constitutive Model for Low Density Polyurethane Foams

Michael K. Neilsen, Harold S. Morgan, Raymond D. Krieg

Prepared by
Sandia National Laboratories
Albuquerque, New Mexico 87185 and Livermore, California 94550
for the United States Department of Energy
under Contract DE-AC04-76DP00789

SF2900Q(8 81)

DISCLAIMER

This report was prepared as an account of work sponsored by an agency of the United States Government. Neither the United States Government nor any agency Thereof, nor any of their employees, makes any warranty, express or implied, or assumes any legal liability or responsibility for the accuracy, completeness, or usefulness of any information, apparatus, product, or process disclosed, or represents that its use would not infringe privately owned rights. Reference herein to any specific commercial product, process, or service by trade name, trademark, manufacturer, or otherwise does not necessarily constitute or imply its endorsement, recommendation, or favoring by the United States Government or any agency thereof. The views and opinions of authors expressed herein do not necessarily state or reflect those of the United States Government or any agency thereof.

DISCLAIMER

Portions of this document may be illegible in electronic image products. Images are produced from the best available original document.

Issued by Sandia National Laboratories, operated for the United States Department of Energy by Sandia Corporation.

NOTICE: This report was prepared as an account of work sponsored by an agency of the United States Government. Neither the United States Government nor any agency thereof, nor any of their employees, nor any of their contractors, subcontractors, or their employees, makes any warranty, express or implied, or assumes any legal liability or responsibility for the accuracy, completeness, or usefulness of any information, apparatus, product, or process disclosed, or represents that its use would not infringe privately owned rights. Reference herein to any specific commercial product, process, or service by trade name, trademark, manufacturer, or otherwise, does not necessarily constitute or imply its endorsement, recommendation, or favoring by the United States Government, any agency thereof or any of their contractors or subcontractors. The views and opinions expressed herein do not necessarily state or reflect those of the United States Government, any agency thereof or any of their contractors or subcontractors.

Printed in the United States of America
Available from
National Technical Information Service
U.S. Department of Commerce
5285 Port Royal Road
Springfield, VA 22161

NTIS price codes
Printed copy: A05
Microfiche copy: A01

SAND--86-2927

DE87 009108

Distribution
Category UC-71

SAND86-2927
Unlimited Release
Printed April 1987

A Phenomenological Constitutive Model for Low Density Polyurethane Foams*

by

Michael K. Neilsen, Harold S. Morgan, and Raymond D. Krieg
Applied Mechanics Division I
Sandia National Laboratories
Albuquerque, NM 87185

ABSTRACT

Results from a series of hydrostatic and triaxial compression tests which were performed on polyurethane foams are presented in this report. These tests indicate that the volumetric and deviatoric parts of the foam behavior are strongly coupled. This coupling behavior could not be captured with any of several commonly used plasticity models. Thus, a new constitutive model was developed. This new model was based on a decomposition of the foam response into two parts: (1) response of the polymer skeleton, and (2) response of the air inside the cells. The air contribution was completely volumetric. The new constitutive model was implemented in two finite element codes, SANCHO and PRONTO. Results from a series of analyses completed with these codes indicated that the new constitutive model captured all of the foam behaviors that had been observed in the experiments. Finally, a typical dynamic problem was analyzed using the new constitutive model and other constitutive models to demonstrate differences between the models. Results from this series of analyses indicated that the new constitutive model generated displacement and acceleration predictions that were between predictions obtained using the other models. This result was expected.

*This work performed at Sandia National Laboratories supported by the U.S. Department of Energy under contract number DE-AC04-76DP00789.

DISTRIBUTION OF THIS DOCUMENT IS UNLIMITED

MASTER

ACKNOWLEDGEMENTS

The authors acknowledge the early contributions of Richard Yoshimura, 6323, Rod May, 7544 and Karl Schuler, 1522, who defined the tests. Karl Schuler also participated in the early model development stages. The NMERI/CERF tests were completed by Debbie Hamberg at the University of New Mexico. During the implementation of the constitutive model in the finite element codes, valuable assistance was provided by Mike Stone, 1521, and Lee Taylor, 1523. The efforts of the above researchers are gratefully acknowledged.

CONTENTS

FIGURES

FIGURES CONTINUED

FIGURES CONTINUED

APPENDIX FIGURES

APPENDIX FIGURES CONTINUED

APPENDIX FIGURES CONTINUED

TABLES

1. INTRODUCTION

Rigid, closed-cell, polyurethane foams are used in a variety of applications as house insulation, fillers and rigidizers in airplane wings, for material packaging, and in impact limiters for shipping containers [1]. Low density polyurethane foam is used in impact limiters in a variety of nuclear waste shipping containers [2,3]. During a hypothetical nuclear waste shipping accident, the foam is expected to absorb a significant amount of impact energy by undergoing large inelastic volume reductions. Consequently, the crushing of polyurethane foams must be well characterized if the overall response of a shipping container is to be properly predicted for various accident scenarios.

Unfortunately, test data on the crushing of low density foams are quite limited. Manufacturers of polyurethane foams usually provide mechanical properties for their products based on results from unconfined, uniaxial, compressive tests. The uniaxial stress-strain responses are easy to measure, but they provide minimal information on the volumetric response of foam and no information on the interactions between the volumetric and deviatoric (shear) responses. In response to this need for experimental data, Sandia National Laboratories decided in 1979 to perform extensive laboratory tests to characterize the behavior of low density polyurethane foams. At the request of the Transportation System Development Department, now 6320, members of the Engineering Analysis Department, now 1520, defined a series of hydrostatic and triaxial compression tests to be performed on foams supplied by General Plastics Manufacturing Company. The tests were performed by the New Mexico Engineering Research Institute (NMERI) at their Civil Engineering Research Facility (CERF) in 1979 and 1980. The test procedures and results were never formally documented but were reported in a letter from NMERI/CERF to Sandia National Laboratories [4].

A variety of constitutive models have been developed to predict the behavior of foams within a variety of load ranges. For example, a linear elastic constitutive model for foams has recently been developed by Kraynik and Warren [5] at Sandia National Laboratories. This model accurately describes the behavior of foams in the linear elastic regime. In this

report, a phenomenological constitutive model that accurately predicts the linear and post-yield behavior of low-density, polyurethane foams is presented.

The purpose of this report is to provide formal documentation of the results from the NMERI/CERF tests and to present a constitutive model which captures the foam behavior exhibited in the tests. First, the NMERI/CERF tests are described and the measured foam responses are presented. Next, three different constitutive models that have been used in the past to model foam behavior are shown to have shortcomings when applied to the foam behavior observed in the experimental NMERI/CERF tests. This is followed by the presentation of a new constitutive model which accounts for foam behavior observed in the experiments. Numerical implementation of the new model is also described. Then, a hypothetical impact problem is analyzed with the new model, and the results are compared to results obtained with (1) a conventional deviatoric plasticity model and (2) a combined volumetric plasticity with pressure dependent deviatoric plasticity model. This report ends with a few conclusions about the use of the new model and a discussion of model limitations and future work.

2. TEST DESCRIPTION AND RESULTS

Six different General Plastics foams with identification numbers (ID's) of 6602, 6703, 9503, 9703, 6704, and 9505 were used in the NMERI/CERF tests. The densities of these foams, as indicated by the last digit of their ID's, ranged from 2 lb/ft^3 to 5 lb/ft^3. All samples from each foam type were taken from a single block. The samples were oriented such that the axes of the cylinders were in the "rise" direction of the foam. The edges of the blocks were avoided in order to insure homogeneity. Hydrostatic tests were performed on all six foams. Also, several triaxial compression tests were performed on all foams except 6704. A matrix of the tests is shown in Table 2.1. The numbers in the table represent the number of tests performed for a given test condition.

In the hydrostatic tests, cylindrical test samples with nominal heights and diameters of 5.60 in. and 2.73 in., respectively, were jacketed with a very thin latex jacket and placed in a 2000 psi triaxial pressure chamber typically used for soil tests. The cell was then filled with water and sealed. The samples were allowed to float freely in the pressure cell. A 4 in. diameter piston displacing at a rate of approximately 0.002 in/sec was then used to increase the pressure within the cell. Cell pressure was measured with a 200 psi pressure gage, and volume changes of the samples were determined from piston displacement measurements. The volume measurements were corrected for expansion of the pressure cell and compressibility of the water. Volume changes from these sources were shown to be negligible compared with volume changes of the samples.

The triaxial tests were performed in another pressure vessel typically used for testing soils. In these tests, jacketed samples were loaded hydrostatically to a prescribed confining pressure. Then, additional axial displacement was applied at a rate of 0.9 in/sec in the rise direction of the foam. The axial load and displacement were measured and converted to axial stress and strain. Measurements of the change in volume of the water surrounding the samples were used to determine changes in sample volume. Standard uniaxial compression tests were performed on unjacketed samples of three of the foams.

In all hydrostatic tests and in all triaxial tests, except the uniaxial tests, the samples were jacketed so air could not escape. All tests were performed at room temperature and at very low strain rates. Consequently, no data on temperature or strain rate effects were obtained.

Table 2.1. Tests Performed on Low Density Polyurethane Foams

NUMBER OF TESTS								
FOAM ID	HYDROSTATIC	TRIAXIAL CONFINING PRESSURE (PSI)						
		0*	6	10	15	20	30	31
6602	3	1	0	1	2	1	0	0
6703	3	0	0	0	1	1	0	0
9703	3	1	1	1	1	0	0	0
9503	3	0	0	1	0	1	0	1
6704	3	0	0	0	0	0	0	0
9505	3	1	1	0	0	1	1	0

* Uniaxial test

The combination of hydrostatic and triaxial tests in Table 2.1 was chosen to provide sufficient data to describe both the volumetric and deviatoric (shear) behaviors of the foams and the coupling between the two responses. The volumetric response is defined as the relationship between pressure, p, and volume strain, γ, where

$$p = \frac{-\sigma_{kk}}{3} \qquad 2.1$$

and

$$\gamma = \epsilon_{kk} \tag{2.2}$$

σ_{ij} and ϵ_{ij} are the foam stress and strain components in an orthonormal basis. Conventional summation notation is used throughout this entire report. The deviatoric stress components, S_{ij}, and the deviatoric strain components, e_{ij}, are defined as

$$S_{ij} = \sigma_{ij} + p\delta_{ij} \tag{2.3}$$

and

$$e_{ij} = \epsilon_{ij} - \frac{\gamma}{3}\delta_{ij} \tag{2.4}$$

Results from the various tests performed on the General Plastics foams are presented in Figures 2.1 - 2.6. Both the volumetric and axial stress-axial strain responses are shown for each test. The only exception is for 6704 Foam in Figure 2.5. Only hydrostatic tests were performed on this foam. The foam axial stress-axial strain responses are presented for use in the development of the new constitutive model presented in a later section. The triaxial tests consisted of two phases: an initial hydrostatic loading phase followed by a triaxial loading phase. The triaxial test results in Figures 2.1 - 2.6 do not start at zero stress and strain because the response from the initial hydrostatic loading phase was measured only at the end of the hydrostatic phase of these tests. The volumetric and axial strains presented in these figures are compressive and are defined by $(V_0 - V)/V_0$ and $(L_0 - L)/L_0$, respectively, where V is the volume of the sample, L is the sample height, and the subscript 0 indicates the initial value of the quantity. The stresses are also compressive. The hydrostatic results were plotted on the axial stress-axial strain plots by assuming that the axial stress was equal in magnitude to the pressure and the strain was isotropic such that the axial strain was given by the following equation

$$\frac{(L_0 - L)}{L_0} = 1 - \left[1 - \frac{(V_0 - V)}{V_0}\right]^{1/3} \tag{2.5}$$

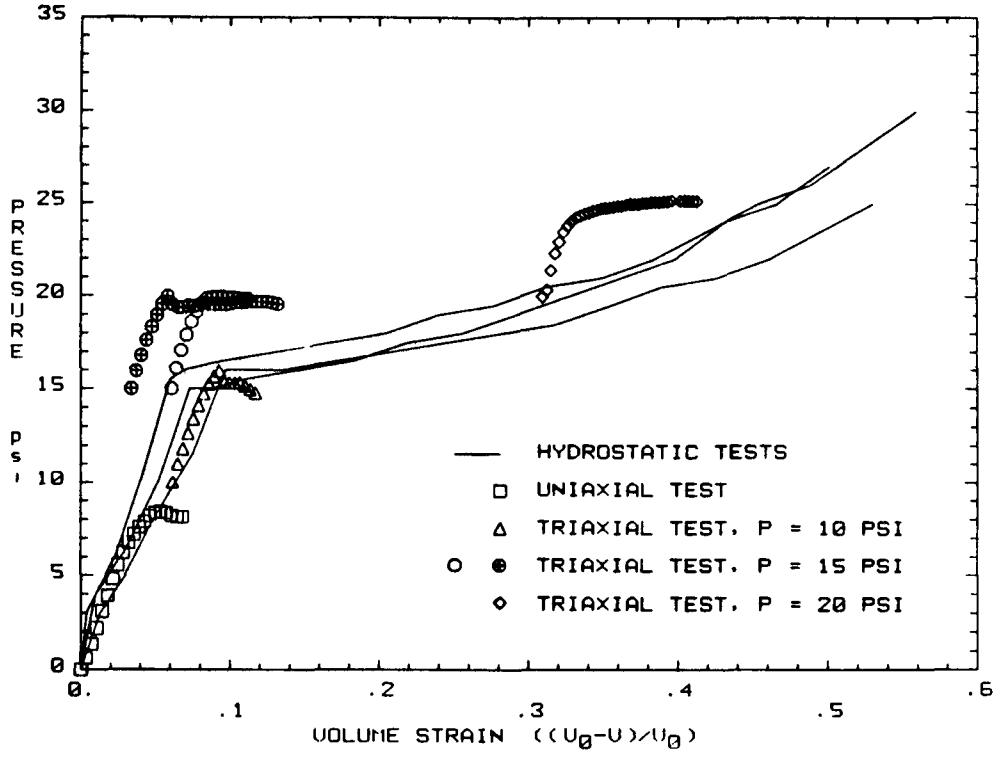

FIGURE 2.1a. Volumetric Responses from All Tests on Foam 6602

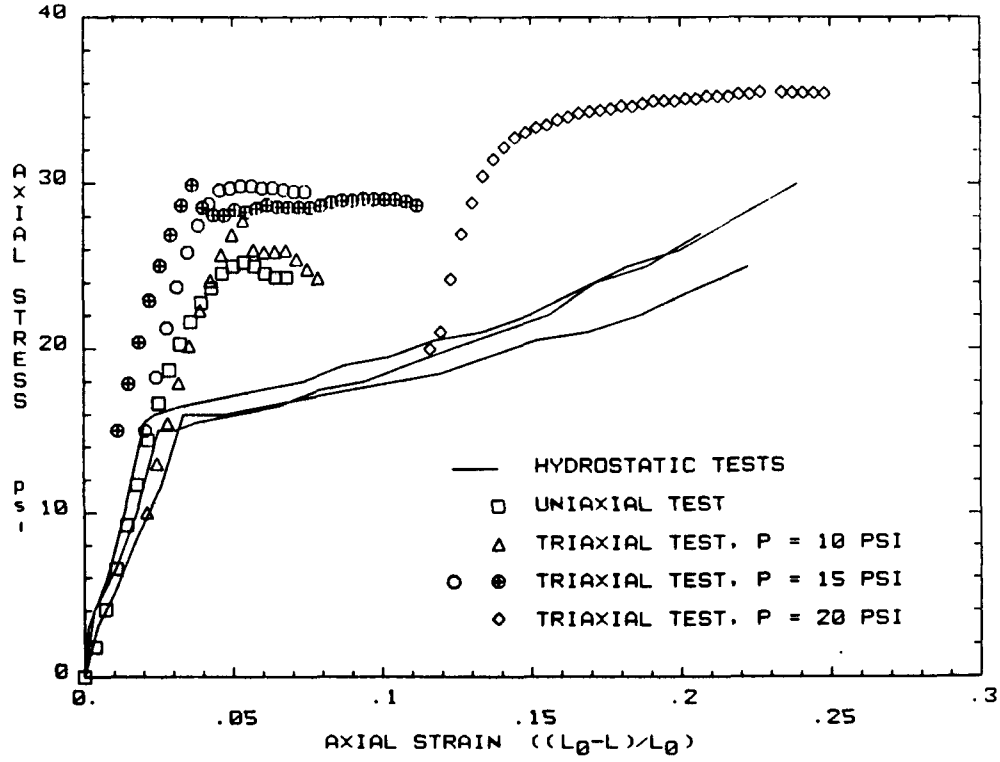

Figure 2.1b. Axial Responses from All Tests on Foam 6602

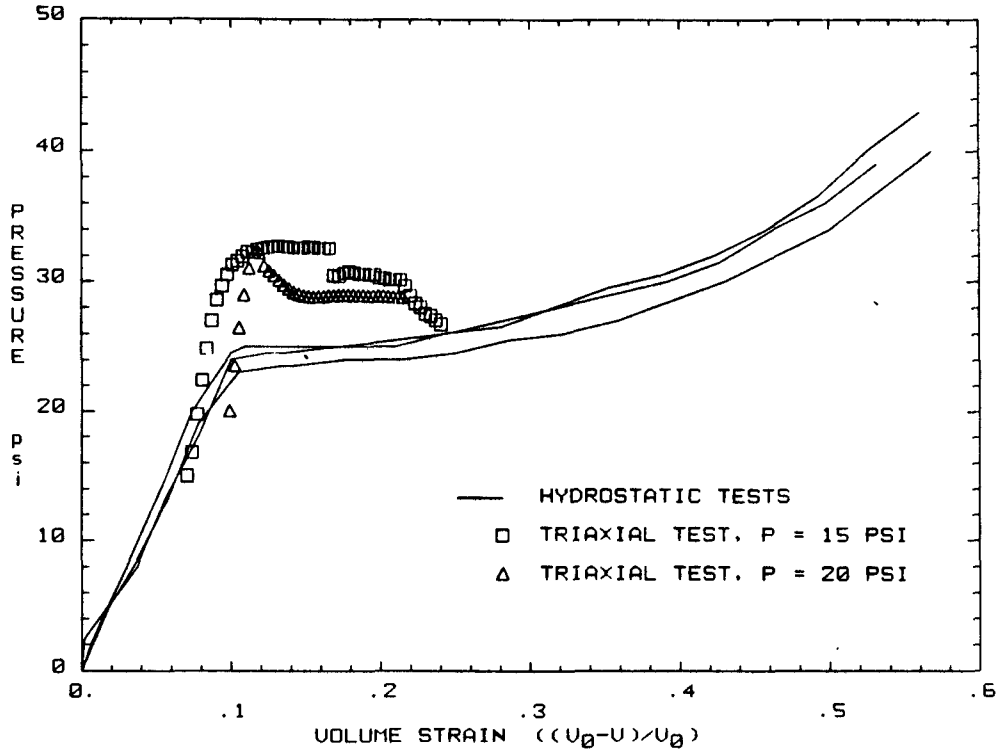

FIGURE 2.2a. Volumetric Responses from All Tests on Foam 6703

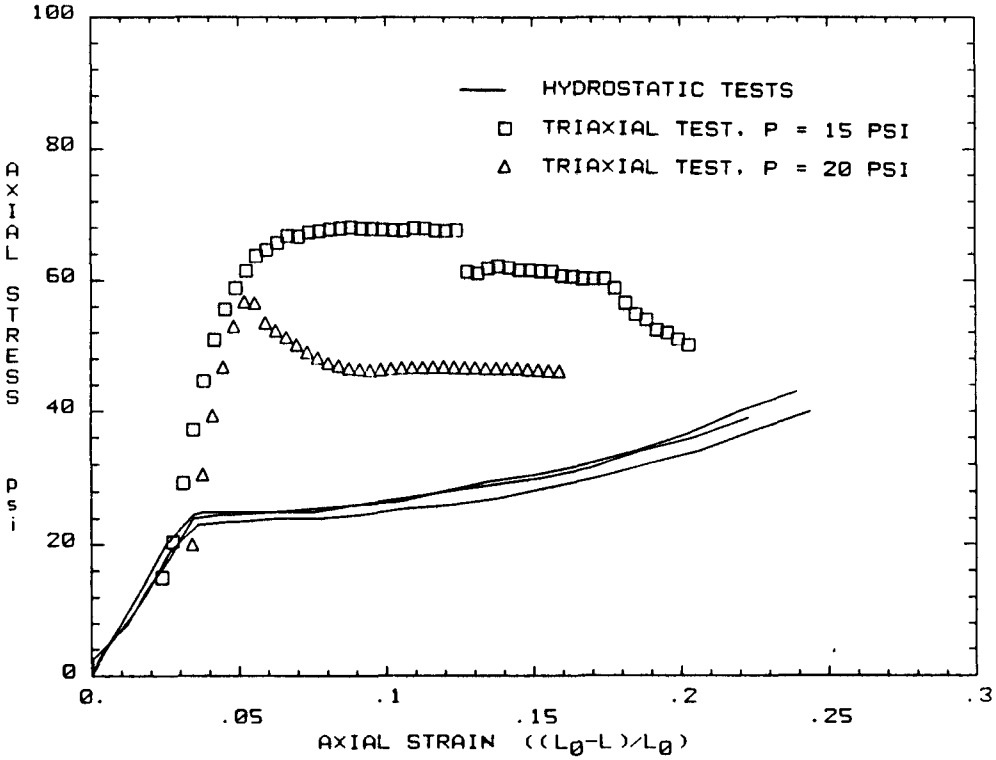

FIGURE 2.2b. Axial Responses from All Tests on Foam 6703

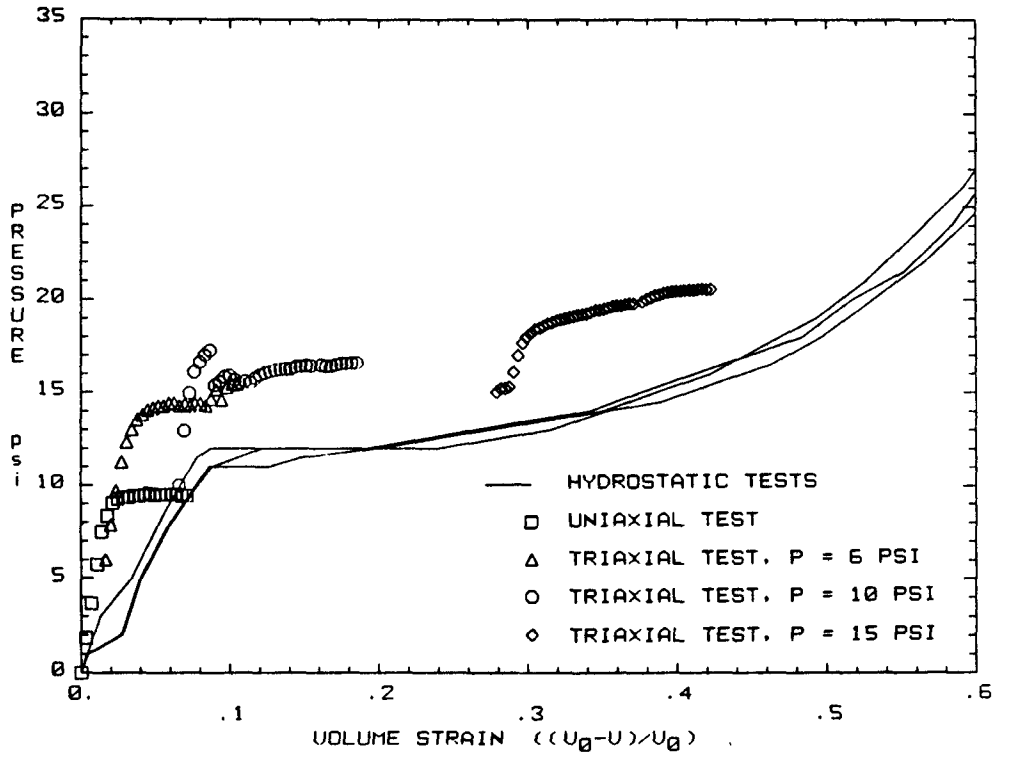

FIGURE 2.3a. Volumetric Responses from All Tests on Foam 9703

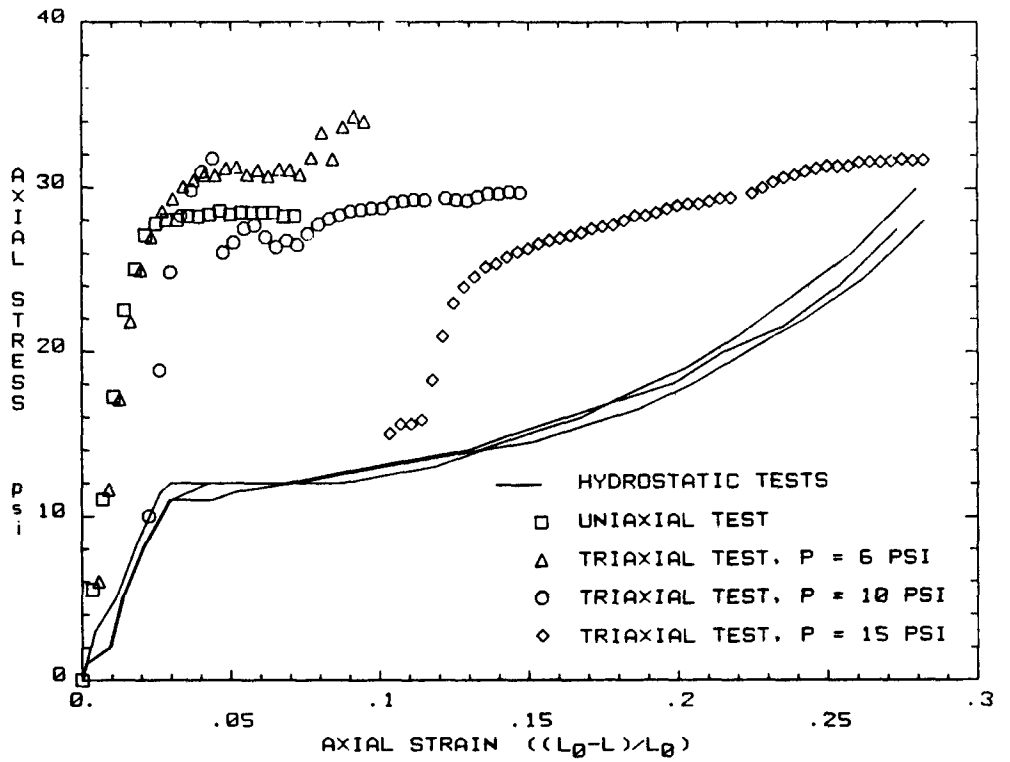

FIGURE 2.3b. Axial Responses from All Tests on Foam 9703

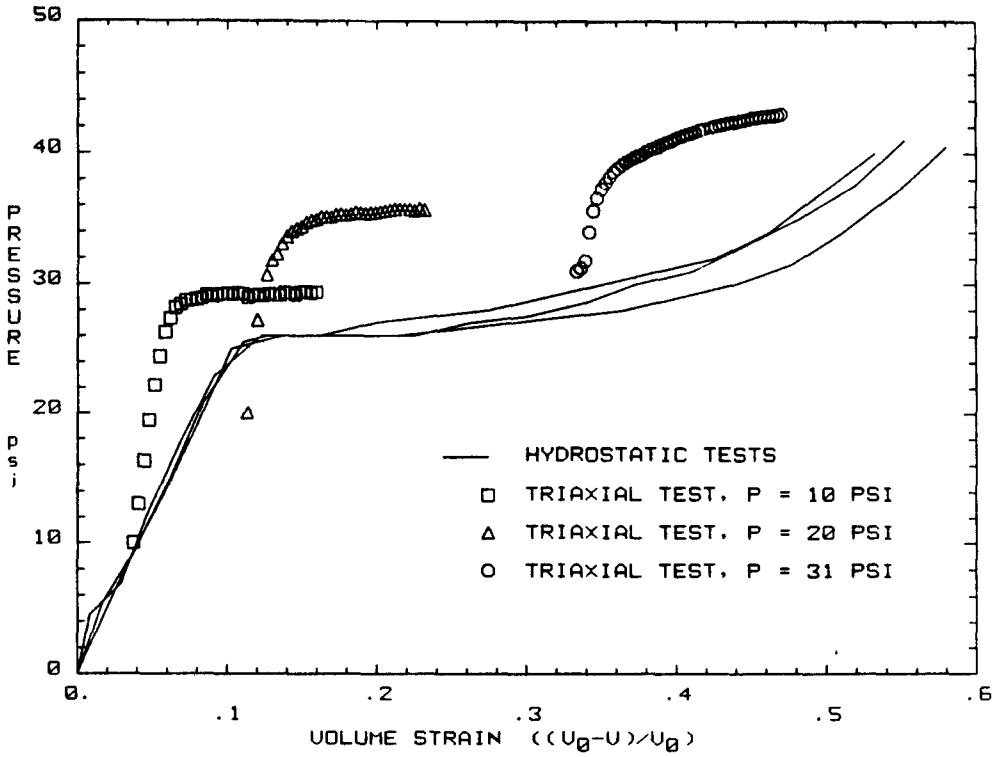

FIGURE 2.4a. Volumetric Responses from All Tests on Foam 9503

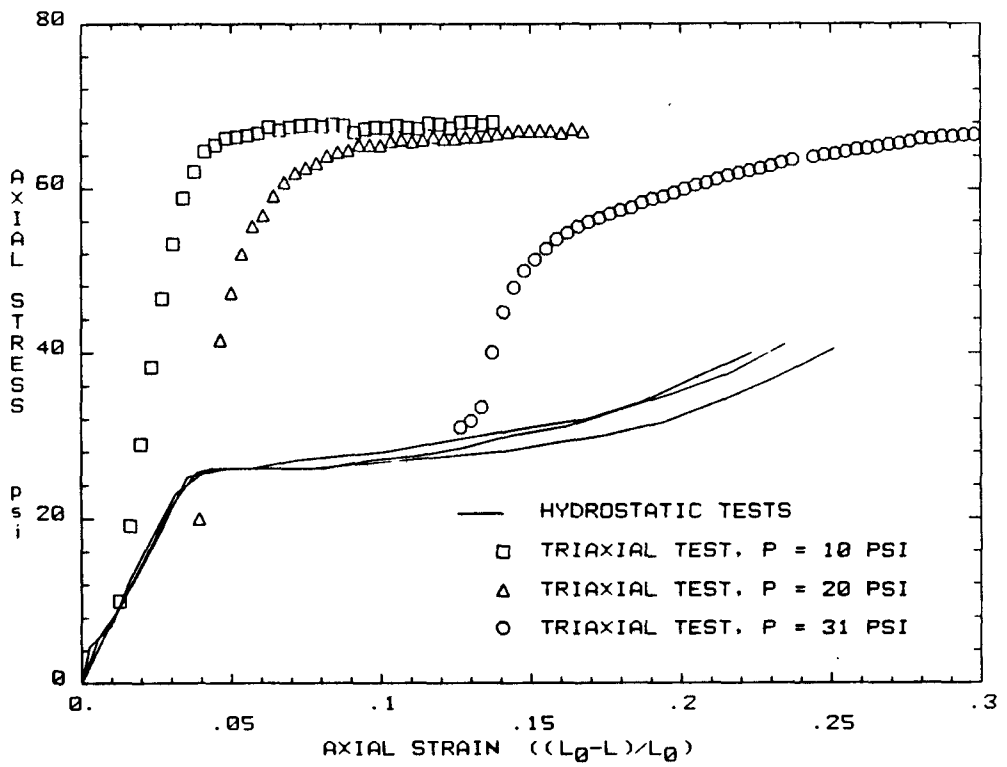

FIGURE 2.4b. Axial Responses from All Tests on Foam 9503

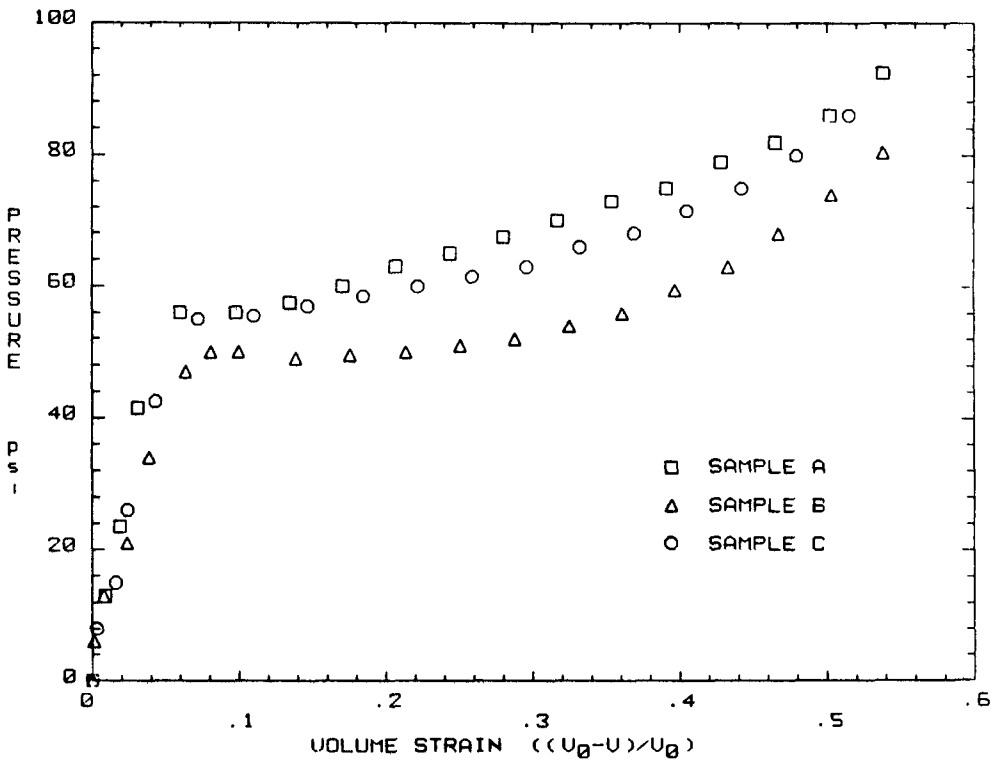

FIGURE 2.5. Hydrostatic Test Results for Foam 6704

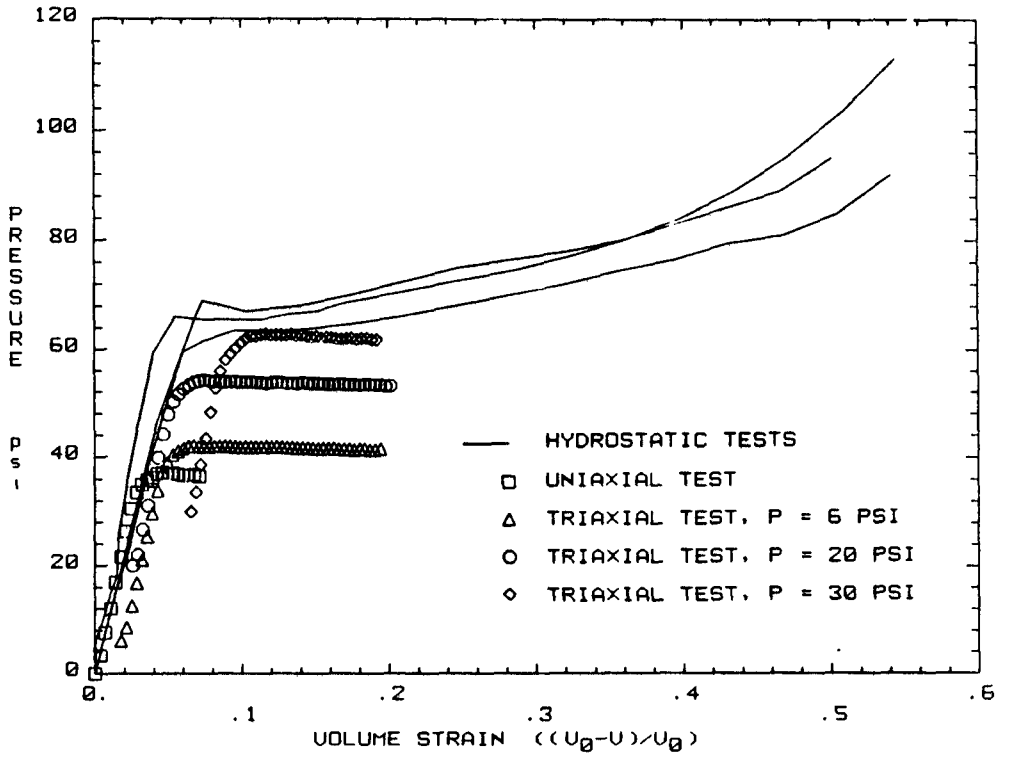

FIGURE 2.6a. Volumetric Responses from All Tests on Foam 9505

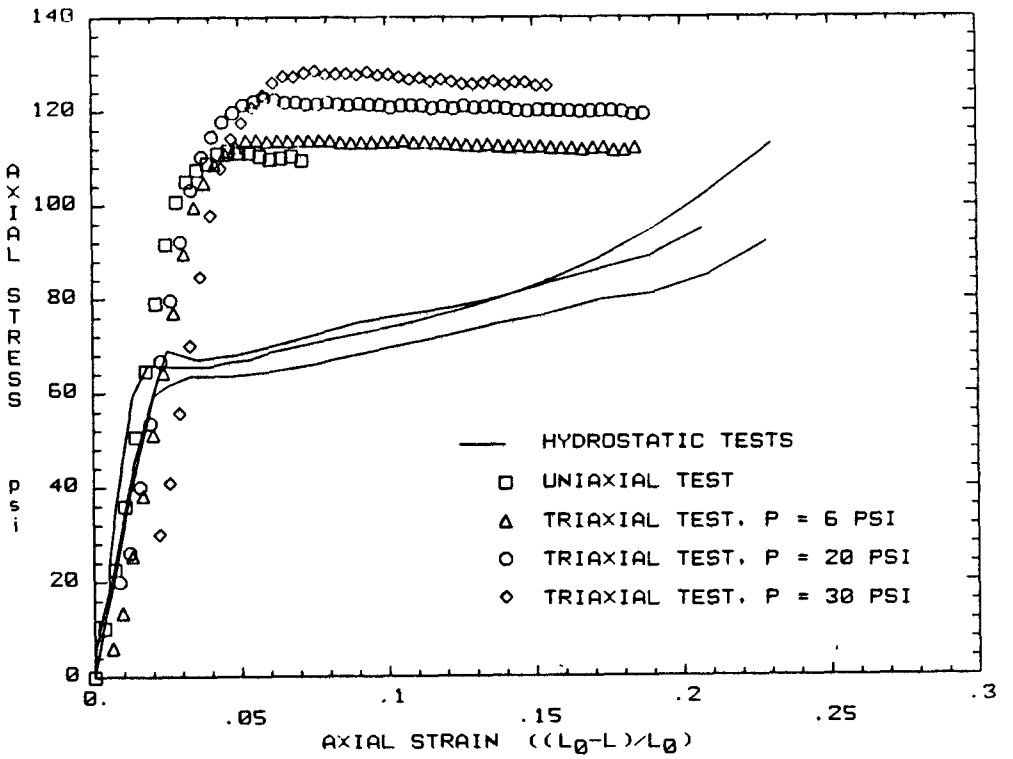

FIGURE 2.6b. Axial Responses from All Tests on Foam 9505

The results in Figures 2.1 - 2.6 indicate only a small amount of scatter between the three hydrostatic tests performed on each foam. The volume strains measured at the ends of the hydrostatic loading phases of the triaxial tests are also consistent with the volumetric strains measured in the hydrostatic tests. However, the pressure at which volumetric yielding occurs is highly dependent on the test conditions. For 6602 foam, the pressure at yield under hydrostatic loading is approximately 15 psi whereas the pressure at yield under uniaxial loading is about 8 psi and for the triaxial test with a confining pressure of 10 psi is approximately 15 psi. In the triaxial tests with confining pressures of 15 psi and 20 psi, the foam actually yields twice, once at 15 psi during the hydrostatic phase of the tests and then again at 19.5 psi for the test with 15 psi confining pressure and at 25 psi for the test with 20 psi confining pressure. For these two triaxial tests, the data indicate that when the additional axial loads are finally applied, the foam has higher resistance to the axial loads than to continued hydrostatic loading. This type of behavior is not commonly observed for most materials and is an indication of the unusual coupling between the volumetric and shear responses of the foam. This coupling can also be seen in the axial stress-axial strain curves in Figures 2.1b - 2.6b.

3. APPLICATION OF EXISTING CONSTITUTIVE MODELS TO LOW-DENSITY POLYURETHANE FOAMS

The logical first step in the development of a constitutive model for low density polyurethane foams is to try to fit existing constitutive models to the test data. In this section, three types of models which have been used in the past to model low density foam behavior [6] are evaluated with respect to the NMERI/CERF data. The three types of models considered in this section include: (1) a uniaxial crush model, (2) a conventional deviatoric plasticity model which is commonly used to describe the behavior of metals, and (3) a "soils" model which combines volumetric plasticity with pressure dependent deviatoric plasticity.

3.1. Uniaxial Crush Model

The usual method of testing foam is in a conventional uniaxial compression test. This is a convenient method because the most common application for foam crushing involves a uniaxial crush. The uniaxial stress-strain curve can be directly used to compute displacements from loads or vice versa. This simple uniaxial model has a severe limitation, however, whenever the foam is used in a multiaxial crush mode. The uniaxial behavior cannot be applied by simply ignoring stresses in the other directions. This is seen in Figure 2.1b. where the axial stress-axial strain curve is shown to be not unique but instead very sensitive to the applied pressure. It is obvious that a multiaxial model is necessary if multiaxial loading is involved.

3.2. Conventional Deviatoric Plasticity Model

A second method of modeling foam is to use a conventional plasticity model, which is the simplest multiaxial model. Uniaxial yield strengths can be measured and generalized to multiaxial conditions using conventional deviatoric plasticity assumptions. One of the assumptions which must be evaluated, however, is that a model of this type allows only elastic volume

strains. The hydrostatic data in Figures 2.1a to 2.6a indicate that the foams undergo large plastic volume strains when subjected to sufficient load. Thus, conventional deviatoric plasticity models are unable to capture the plastic volumetric behavior of polyurethane foams. Another assumption made in conventional plasticity models is that the volumetric and deviatoric responses are not coupled. That is, deviatoric loading is assumed to have no effect on volumetric behavior, and deviatoric yield is not affected by the pressure. If a deviatoric volumetric decomposition were valid, all of the volumetric responses in Figures 2.1a to 2.6a would be the same regardless of the load history. The curves in Figures 2.1a to 2.6a indicate that the volumetric response is clearly dependent on load history and the occurrence of deviatoric loading. Thus, conventional deviatoric plasticity models fail to capture two important features of polyurethane foam behavior, volumetric plasticity and volumetric-deviatoric coupling.

3.3. Combined Volumetric Plasticity with Pressure Dependent Deviatoric Plasticity Model

Another class of multiaxial models which combine volumetric plasticity with pressure dependent deviatoric plasticity were examined next. These models were attractive because they have features which deviatoric plasticity models do not; namely, capabilities for volumetric plasticity and coupling between the volumetric and deviatoric responses. A particular model of this type, developed by Krieg [7] for soil and concrete, was examined in detail for its applicability to foam. In this model, the yield function is assumed to be separable into the product of deviatoric and volumetric parts. The volumetric yield function is independent of the deviatoric stresses, but the deviatoric portion of the yield function is dependent on the pressure. The shape of the deviatoric yield surface is a paraboloid of revolution about the pressure axis as shown in Figure 3.1. The volumetric, Φ_v, and deviatoric, Φ_s, yield functions are given by the following equations

$$\Phi_v = p - f(\gamma) \qquad 3.1$$

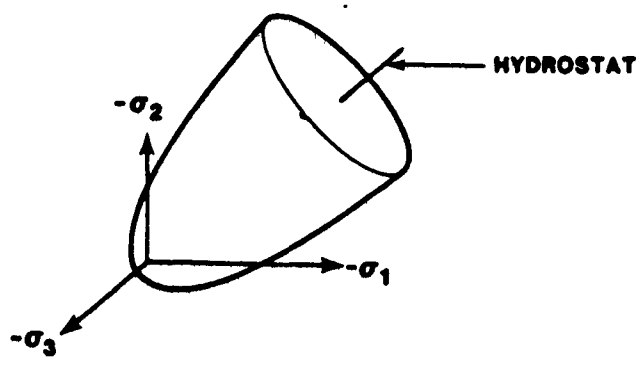

FIGURE 3.1. Yield Surface in Principal Stress Space [7]

$$\Phi_s = J_2 - (a_0 + a_1 p + a_2 p^2) \qquad 3.2$$

where p is the pressure (defined in Equation 2.1), f is a function of the volumetric strain and defines the materials volumetric stress-strain behavior, J_2 is the second invariant of the deviatoric stresses, and a_0, a_1 and a_2 are material constants. Since f in Equation 3.1 is defined from volumetric stress-strain data, this model captures the volumetric plasticity of polyurethane foam. However, in this model, the volumetric response is considered to be independent of the deviatoric response. This assumption is obviously not valid for the data presented in Figures 2.1a to 2.6a.

Neither uniaxial models, conventional deviatoric plasticity models, nor models which combine volumetric plasticity with pressure dependent deviatoric plasticity are appropriate for low density polyurethane foams. Therefore, a new constitutive model was developed and is presented in the next section.

4. NEW CONSTITUTIVE MODEL FOR LOW DENSITY POLYURETHANE FOAMS

The first step in the development of a new constitutive model for low density polyurethane foams was to examine the individual components of the foam structure. Each of the foams used in the NMERI/CERF tests was a closed cell foam with air inside the cells. Therefore, each foam consisted of two structural components: (1) the polymer structure or skeleton and (2) the air inside the foam. In applications where the air could not escape from the skeleton during loading, the air could carry a substantial part of the load. In all of the NMERI/CERF tests, except the uniaxial tests, the samples were jacketed and air could not escape. Thus, a model which considered the contribution of the air to the overall structural response of the foams was appropriate for the foam behavior exhibited in the NMERI/CERF tests.

Total foam response can be decomposed into the response of the skeleton and the response of the air in the following manner. Since, the air does not resist any shear deformation, the air contribution is completely volumetric. For convenience, the skeleton is assumed to occupy the same space as the foam. This implies that the skeleton strain components are equal to the foam strain components. Also, the foam stress components, σ_{ij}, are given by the following equation

$$\sigma_{ij} = \sigma_{ij}^{sk} + \sigma^{air}\,\delta_{ij} \qquad 4.1$$

where σ_{ij}^{sk} are the skeleton stress components and $\sigma^{air}\delta_{ij}$ represents the air contribution to the normal stress components. To better understand this equation, consider a hydrostatic compression test in which the foam sample is jacketed and the air is not allowed to escape. If the skeleton was structured so that it could not carry any load, then the external pressure applied to the foam would equal the internal air pressure. In other words, the foam stress components would equal the air contribution. This foam would not be able to resist any deviatoric loading. In most foams, however, the skeleton is structured so that it can carry load and the contribution of the skeleton must be added to the air contribution to determine how much

load the foam can carry. In the next section, an expression for the air contribution as a function of foam strain components is derived.

The ideal gas law was used to derive an expression for the air contribution, σ^{air}. If the foam is compressed from initial volume V_0 to a final volume of V_1, the volume strain, γ, can be expressed as

$$\gamma = (V_1 - V_0)/V_0 \qquad 4.2$$

The volume of the foam is equal to the sum of volume of the polymer from which it is made, V^p, and the volume of the air trapped inside, V^{air}. The volume of the polymer is fixed when the foam is manufactured and merely changes its position as the foam deforms. Thus, the volume strain becomes

$$\gamma = (V_1^{air} - V_0^{air})/(V_0^{air} + V^p) \qquad 4.3$$

or

$$\gamma = \left(\frac{V_1^{air}}{V_0^{air}} - 1\right)/\left(1 + \frac{V^p}{V_0^{air}}\right) \qquad 4.4$$

The denominator of Equation 4.4 can be expressed as

$$\left(1 + \frac{V^p}{V_0^{air}}\right) = \frac{1}{1 - \phi} \qquad 4.5$$

where ϕ is the volume fraction of solid material. If the ideal gas law is expressed as

$$p^{air}V^{air} = n\ R\ T \qquad 4.6$$

where p^{air} is the air pressure, V^{air} is the air volume, n is the mole fraction of air, R is the universal gas constant, and T is the absolute temperature, Equation 4.4 can be rewritten as

$$\gamma = \left(\frac{T_1 \, p_0^{air}}{T_0 \, p_1^{air}} - 1 \right)(1 - \phi) \qquad 4.7$$

and rearranged to give

$$p_1^{air} = p_0^{air} \frac{(1 - \phi) \, T_1}{(\gamma + 1 - \phi) \, T_0} \qquad 4.8$$

The pressure p_0^{air} is the internal air pressure when no load is applied to the foam. Thus, p_1^{air} can be expressed as

$$p_1^{air} = p_0^{air} - \sigma^{air} \qquad 4.9$$

The negative sign is needed in front of σ^{air} because p_0^{air} and p_1^{air} are positive in compression whereas σ^{air} is positive in tension. Substitution of Equation 4.9 into Equation 4.8 leads to an expression for the air contribution, σ^{air}.

$$\sigma^{air} = \frac{p_0^{air}\left[\gamma + (1 - \phi)\left(1 - \frac{T_1}{T_0}\right)\right]}{(\gamma + 1 - \phi)} \qquad 4.10$$

For a prescribed foam volume strain, γ, Equation 4.10 describes the stress carried by the air. Note that for isothermal conditions when the foam volume strain is equal to zero the air contribution is also equal to zero. Also, the air contribution approaches infinity as the foam volume strain approaches $\phi - 1$ or in other words as the foam volume approaches the polymer volume. A plot of the air contribution as a function of volume strain is shown in Figure 4.1. For applications in which the air can escape from the foam, the stress carried by the air can be neglected by setting p_0^{air} equal to zero.

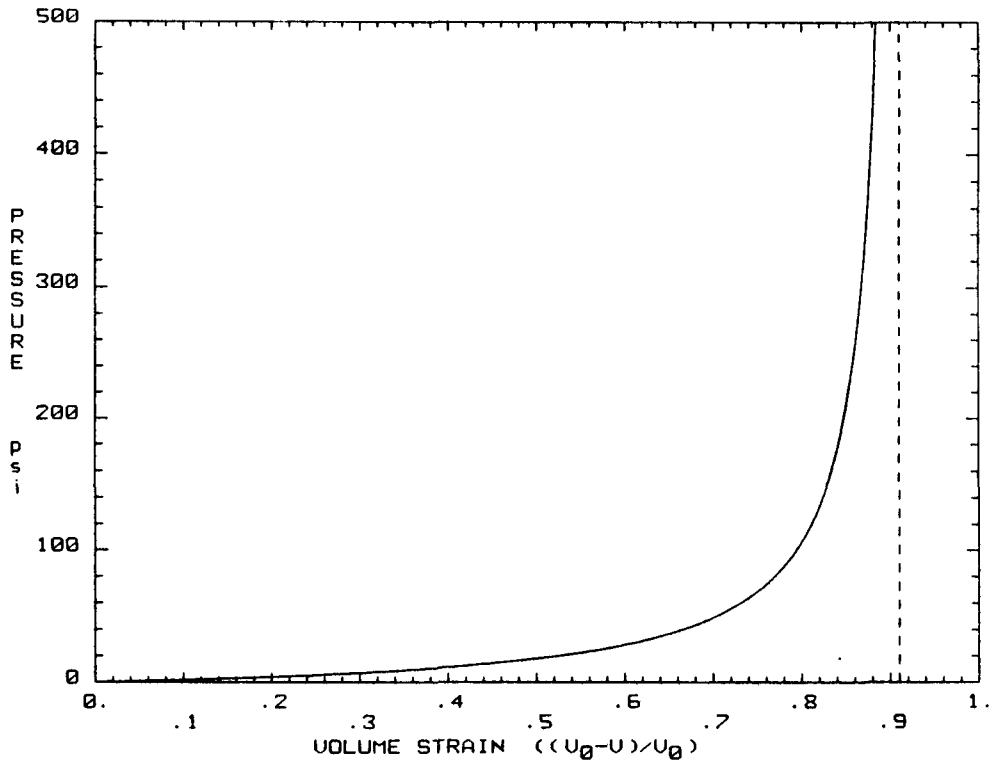

FIGURE 4.1 Air Contribution for 9505 Foam (ϕ = 0.09)

The response of the skeleton can now be determined from the NMERI/CERF tests. Since the foam and the skeleton occupy the same volume, the foam and skeleton strains are the same. Also, the skeleton stress components can be derived from Equation 4.1 written in the following form

$$\sigma_{ij}^{sk} = \sigma_{ij} - \sigma^{air}\delta_{ij} \qquad 4.11$$

The skeleton stress components are determined by subtracting the expression given by Equation 4.10 for the stress carried by the air from the foam normal stress components. The skeleton responses have been found in this way using the data plotted in Figures 2.1 - 2.6 and are shown in Figures 4.2 - 4.7. Equation 4.10 should rather accurately describe the air behavior and Figures 4.2 - 4.7 describe the skeleton behavior.

The volumetric responses for hydrostatic loading indicate that the skeleton may soften or harden slightly after yield. In addition, the volumetric skeleton responses are affected by the deviatoric loading conditions. Furthermore, the lateral strains are zero for the uniaxial tests. This implies that Poisson's ratio for the skeleton is equal to zero. That is, the skeleton response in a principal stress direction is not affected by the other principal skeleton stresses. The skeleton responses for 6602 Foam in Figure 4.2 indicate that for hydrostatic loading the yield stress can be expressed as a function of the volume strain, γ. If the loading is deviatoric, the axial yield stress appears to be equal to the axial yield stress for hydrostatic loading plus a constant. Thus, the yield stress in each principal stress direction can be expressed as

$$g = A \langle II' \rangle + B\,(1 + C\,\gamma) \qquad 4.12$$

where II' is the second invariant of the deviatoric strains, $\langle\ \rangle$ is the heavyside step function, γ is the volume strain or first invariant of the foam strains, and A, B, and C are constants. Constant B is the yield stress of the skeleton for purely hydrostatic loading, and the product of B and C is the slope of the skeleton volumetric response after yielding for purely hydrostatic loading. Constant A is equal to the difference between the axial yield stress for hydrostatic loading and the axial yield stress for

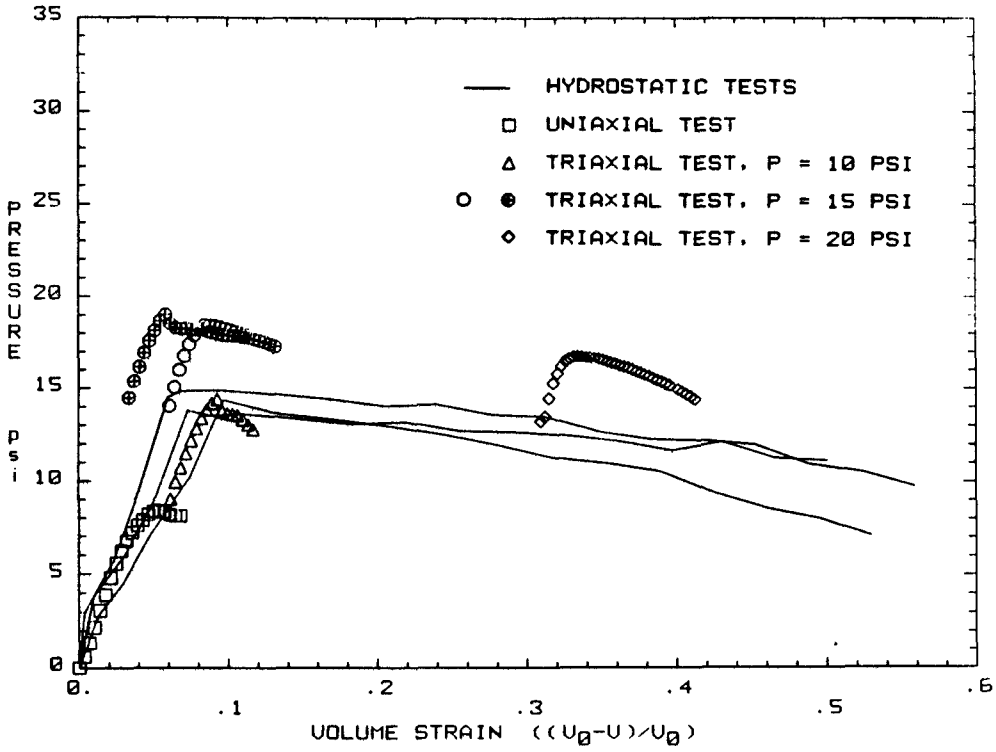

FIGURE 4.2a. Skeleton Volumetric Responses from All Tests on Foam 6602

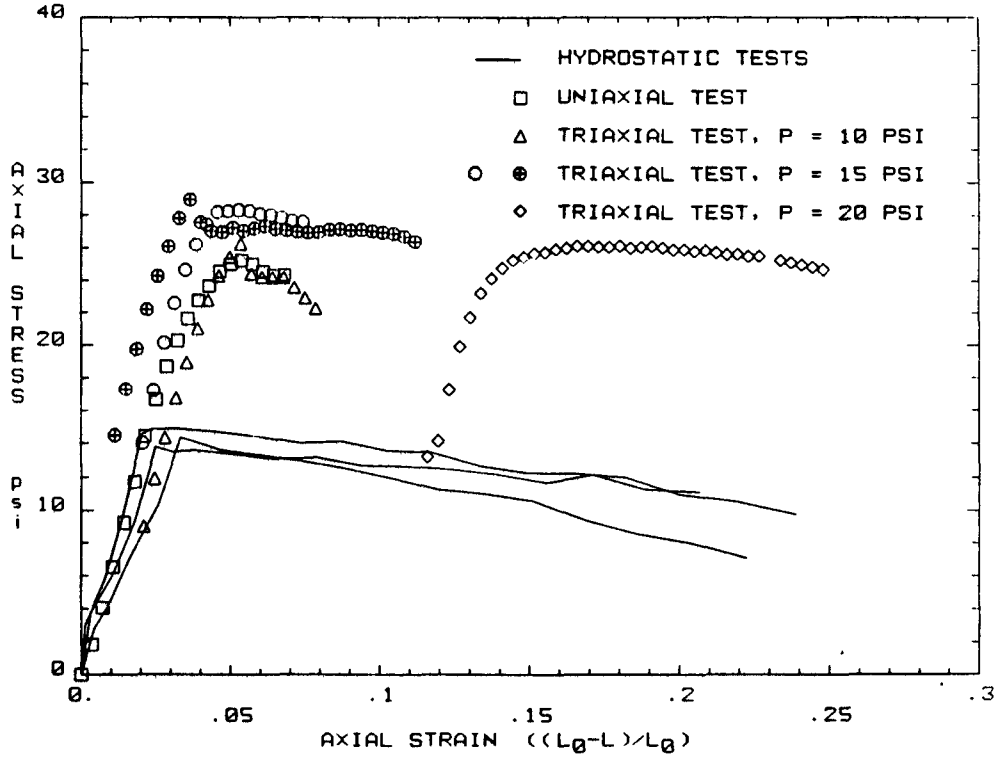

FIGURE 4.2b. Skeleton Axial Responses from All Tests on Foam 6602

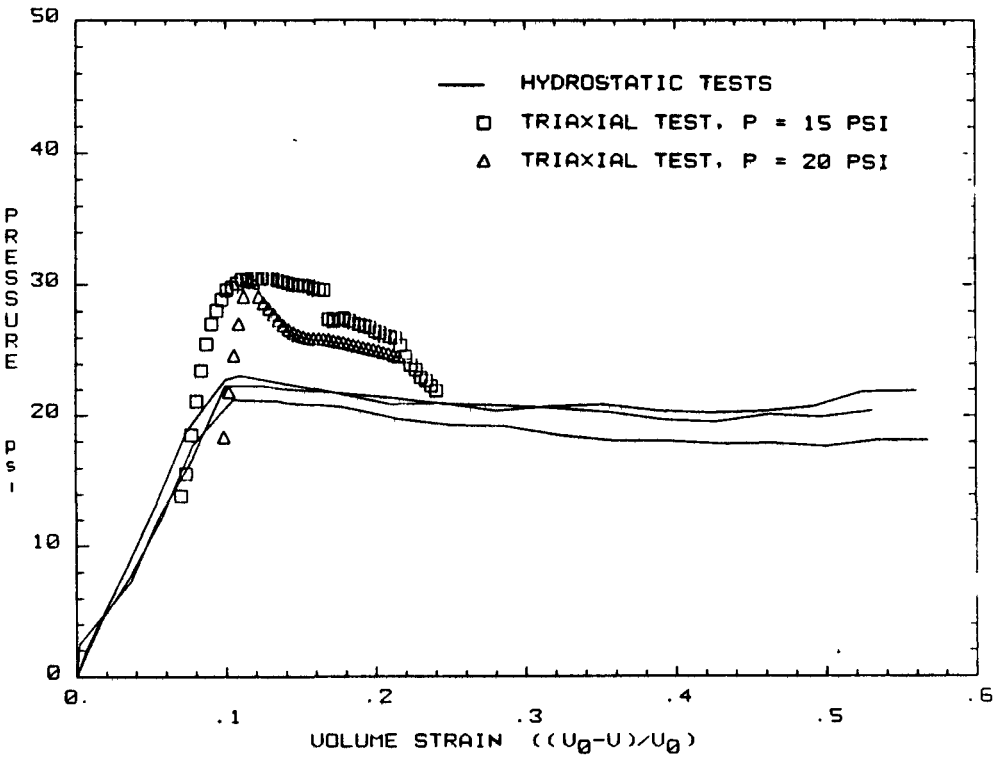

FIGURE 4.3a. Skeleton Volumetric Responses from All Tests on Foam 6703

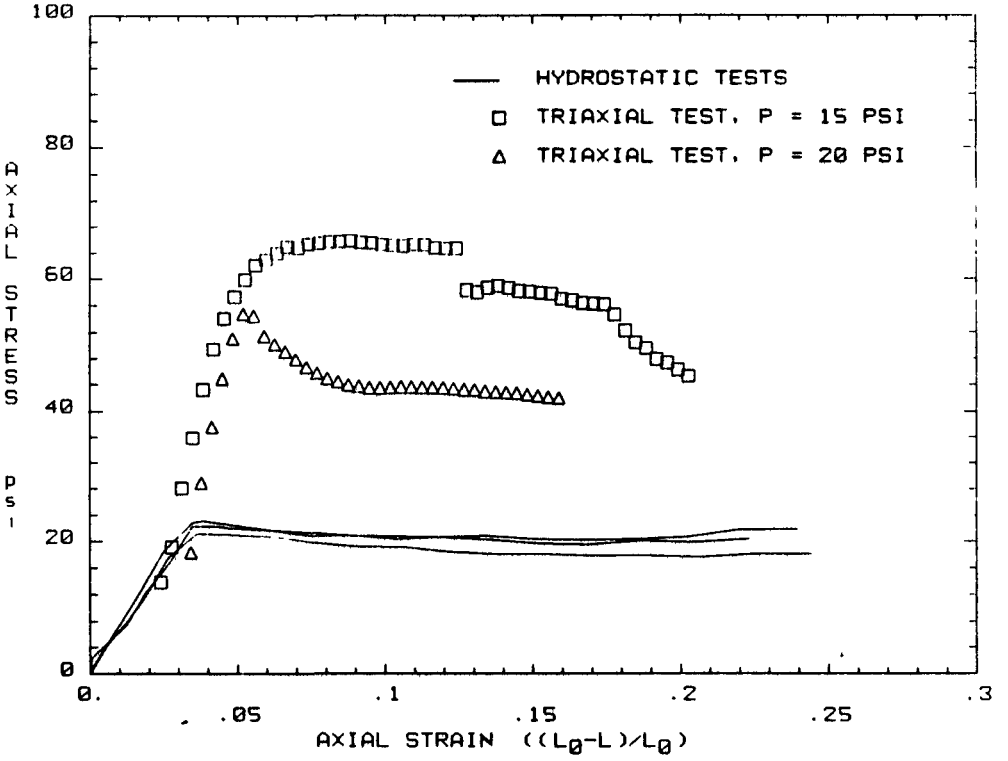

FIGURE 4.3b. Skeleton Axial Responses from All Tests on Foam 6703

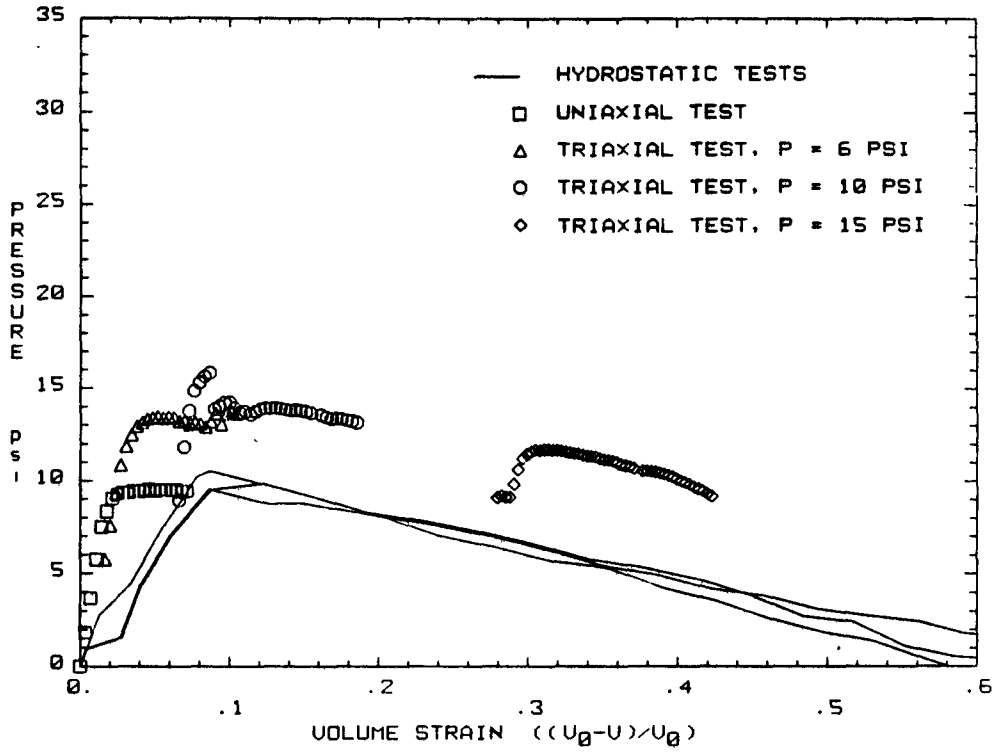

FIGURE 4.4a. Skeleton Volumetric Responses from All Tests on Foam 9703

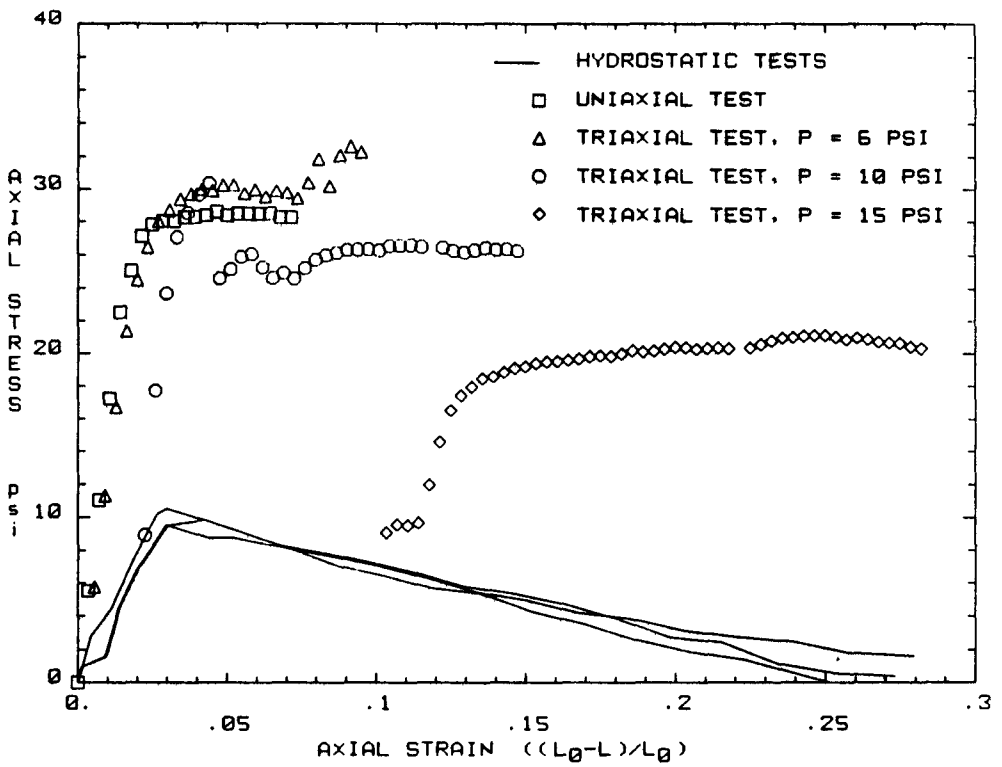

FIGURE 4.4b. Skeleton Axial Responses from All Tests on Foam 9703

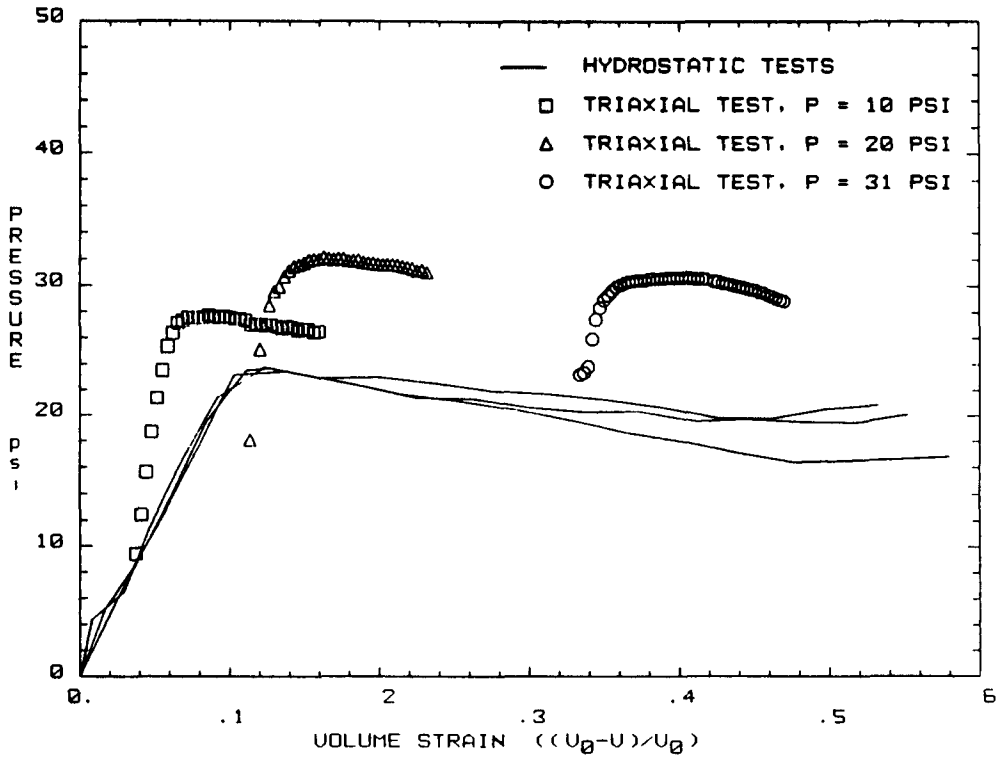

FIGURE 4.5a. Skeleton Volumetric Responses from All Tests on Foam 9503

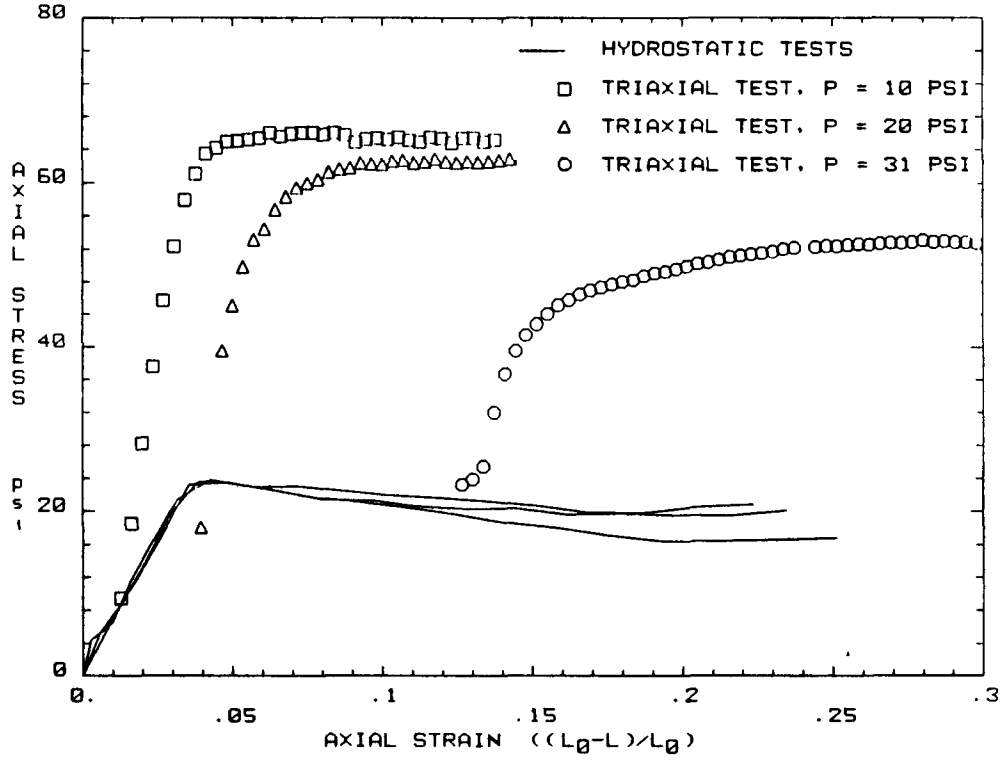

FIGURE 4.5b. Skeleton Axial Responses from All Tests on Foam 9503

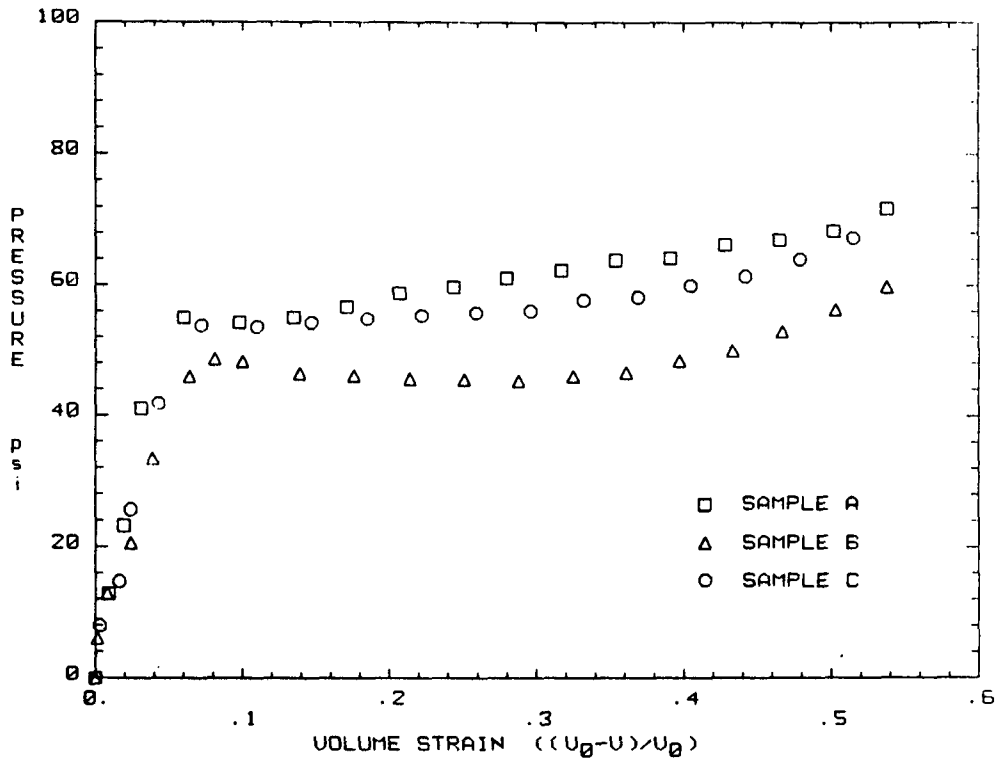

FIGURE 4.6. Skeleton Volumetric Responses for Foam 6704

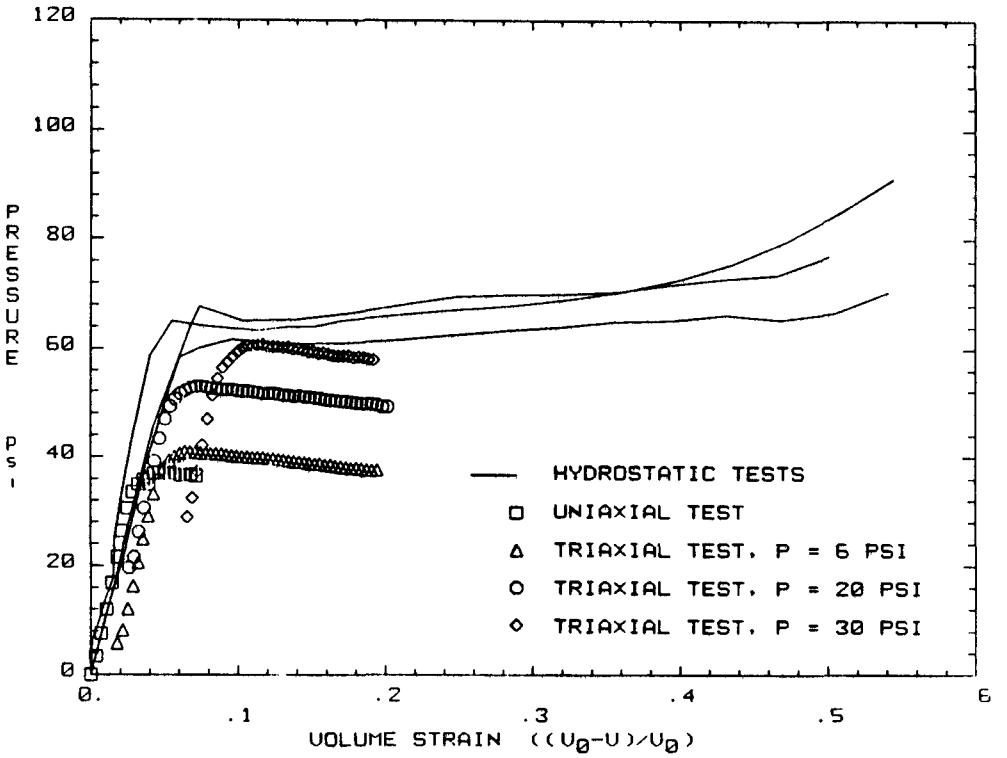

FIGURE 4.7a. Skeleton Volumetric Responses from All Tests on Foam 9505

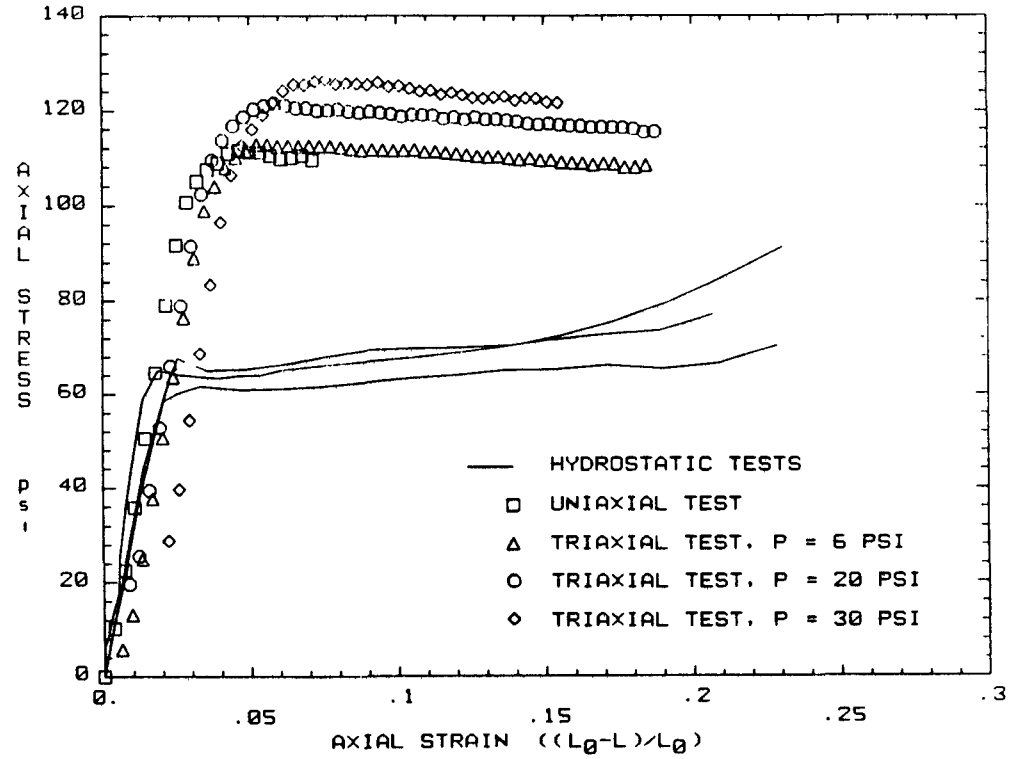

FIGURE 4.7b. Skeleton Axial Responses from All Tests on Foam 9505

deviatoric loading. The first term in Equation 4.12 is active only if the loading is deviatoric. The principal skeleton stresses must be less than or equal to the yield function g. If the principal skeleton stresses are less than g, the behavior is elastic. If the principal skeleton stresses are equal to g, the behavior may be plastic. Constants B and C are determined from a hydrostatic test, and constant A is determined from a triaxial or uniaxial test. Thus, at least one hydrostatic test and one triaxial or uniaxial test are needed to characterize the foam behavior. Material properties for the various foams (Table 4.1) were determined from the hydrostatic and uniaxial skeleton data. The foam elastic modulus, E, was taken as the slope of a best fit curve through the data in the elastic regime. Yield function parameter C was determined from the slope of a best fit curve through the data in the plastic regime of the hydrostatic tests.

Table 4.1. Material Properties for NMERI/CERF Foams

FOAM	E	A	B	C	ϕ
6602	462	9.5	15.5	0.738	0.035
6703	644	37.0	21.3	0.218	0.050
9703	344	19.5	11.8	1.590	0.050
9503	650	36.0	24.5	0.511	0.060
6704	2050	49.8	48.8	-0.613	0.080
9505	3010	49.2	60.8	-0.517	0.090

E - YOUNG'S MODULUS, psi

A - YIELD FUNCTION PARAMETER, psi

B - YIELD FUNCTION PARAMETER, psi

C - YIELD FUNCTION PARAMETER

ϕ - VOLUME FRACTION OF SOLID MATERIAL

The next step in the model building process was to express the characterizing parameters in terms of volume fraction. A consideration of the physical meaning of the constants showed that parameters A, B and E should approach zero as volume fraction goes to zero. For this reason these parameters were fitted with a power function. Parameter C was fitted with a linear function of volume fraction. This least squares fitting process produced the values given in Equations 4.13 – 4.16. The fitted curves and supporting data are shown in Figure 4.8.

$$A = 3440\ \phi^{1.676} \qquad 4.13$$

$$B = 2780\ \phi^{1.645} \qquad 4.14$$

$$C = 2.21 - 31.1\ \phi \qquad 4.15$$

$$E = 454000\ \phi^{2.20} \qquad 4.16$$

Equation 4.16 indicates a $\phi^{2.2}$ dependence for Young's Modulus. Kraynik and Warren [5] have reported a $\phi^{2.0}$ dependence for Young's Modulus for low density foams. Equations 4.13 to 4.16 could be used to estimate input parameters for the new constitutive model if the only data available for the foam was its volume fraction. However, further experimental testing should be completed to improve our confidence in Equations 4.13 to 4.16.

The constitutive model is summarized in the flowchart shown in Figure 4.9. For a given initial stress and strain state, the foam stress components can be determined from the expressions for the stress carried by the air and by the skeleton. Initial foam stress components and air pressure are used to compute the initial skeleton stress components. Foam strains are updated using the strain rate and time step size. Trial skeleton stress components are computed by assuming that the skeleton behavior remains elastic over the time step. The trial skeleton stress components are then rotated to principal stress directions, and each principal trial stress is compared with the yield stress. If a principal

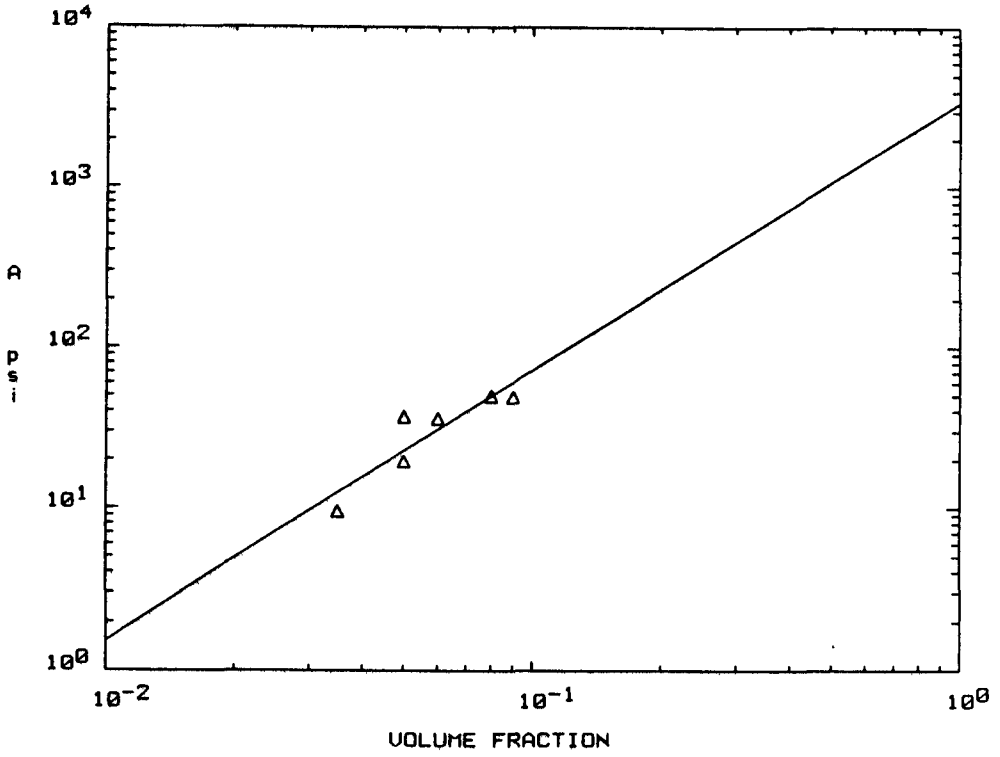

FIGURE 4.8a. Foam Parameter A as a Function of Density Ratio

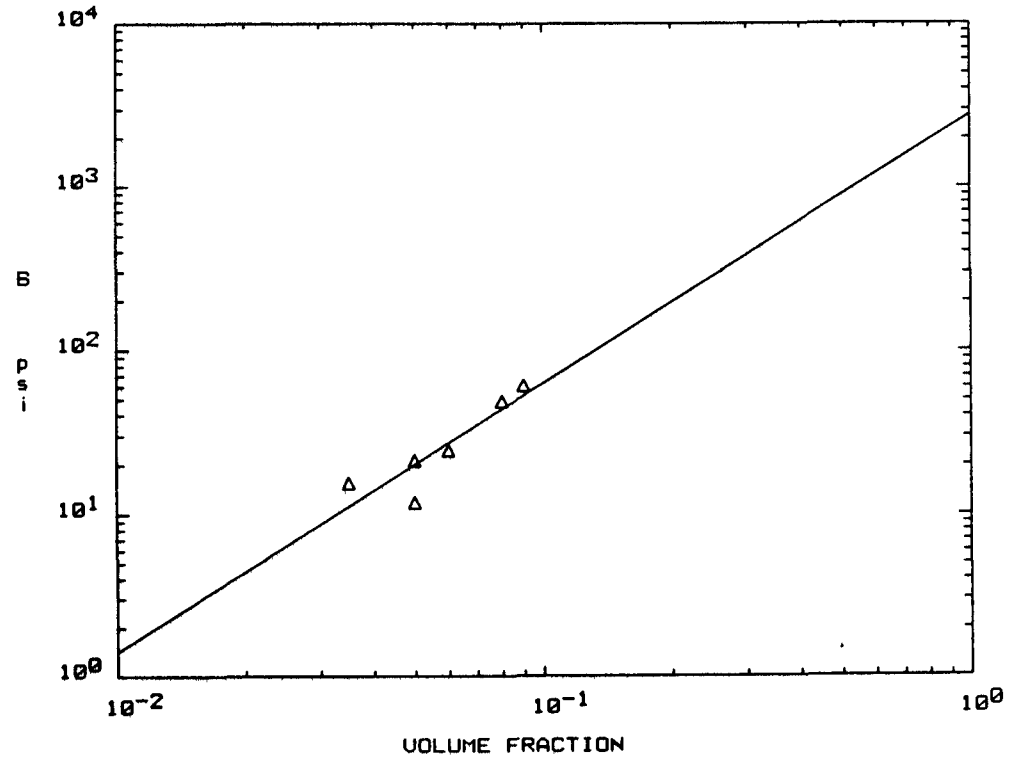

FIGURE 4.8b. Foam Parameter B as a Function of Density Ratio

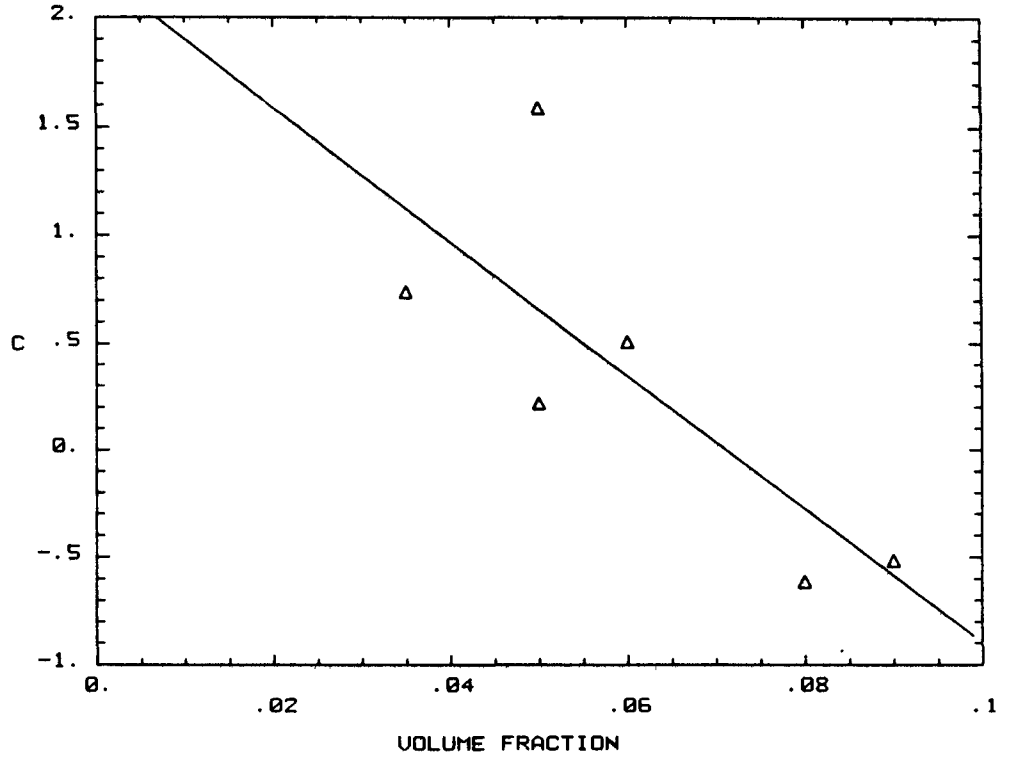

FIGURE 4.8c. Foam Parameter C as a Function of Density Ratio

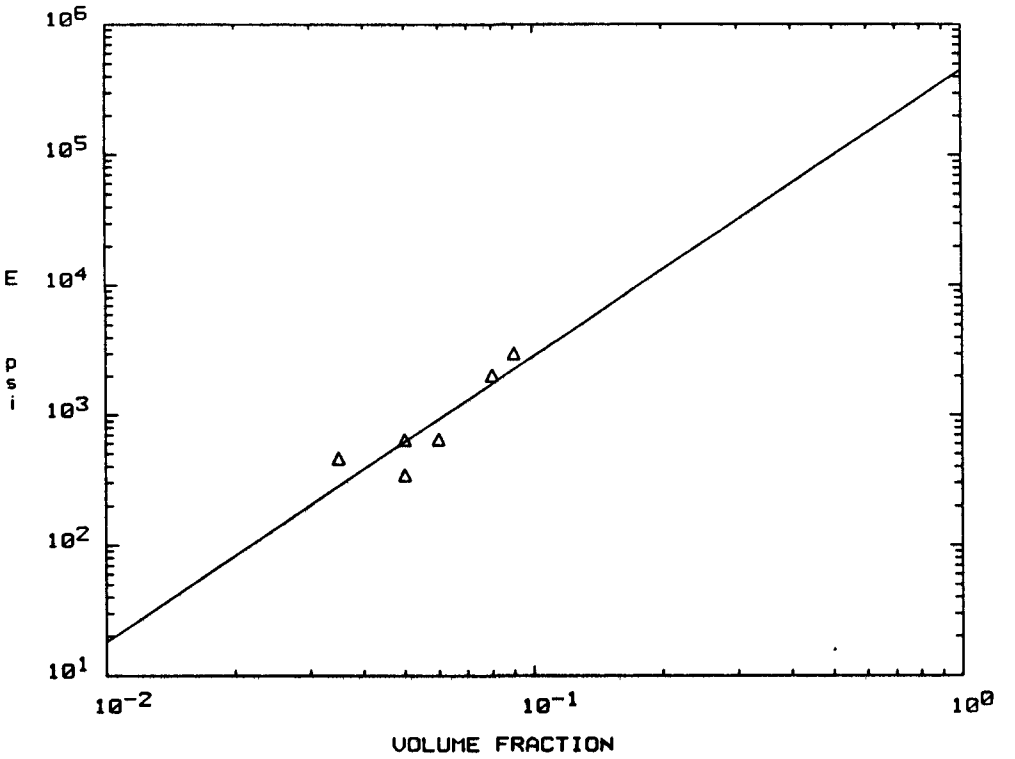

FIGURE 4.8d. Foam Elastic Modulus E as a Function of Density Ratio

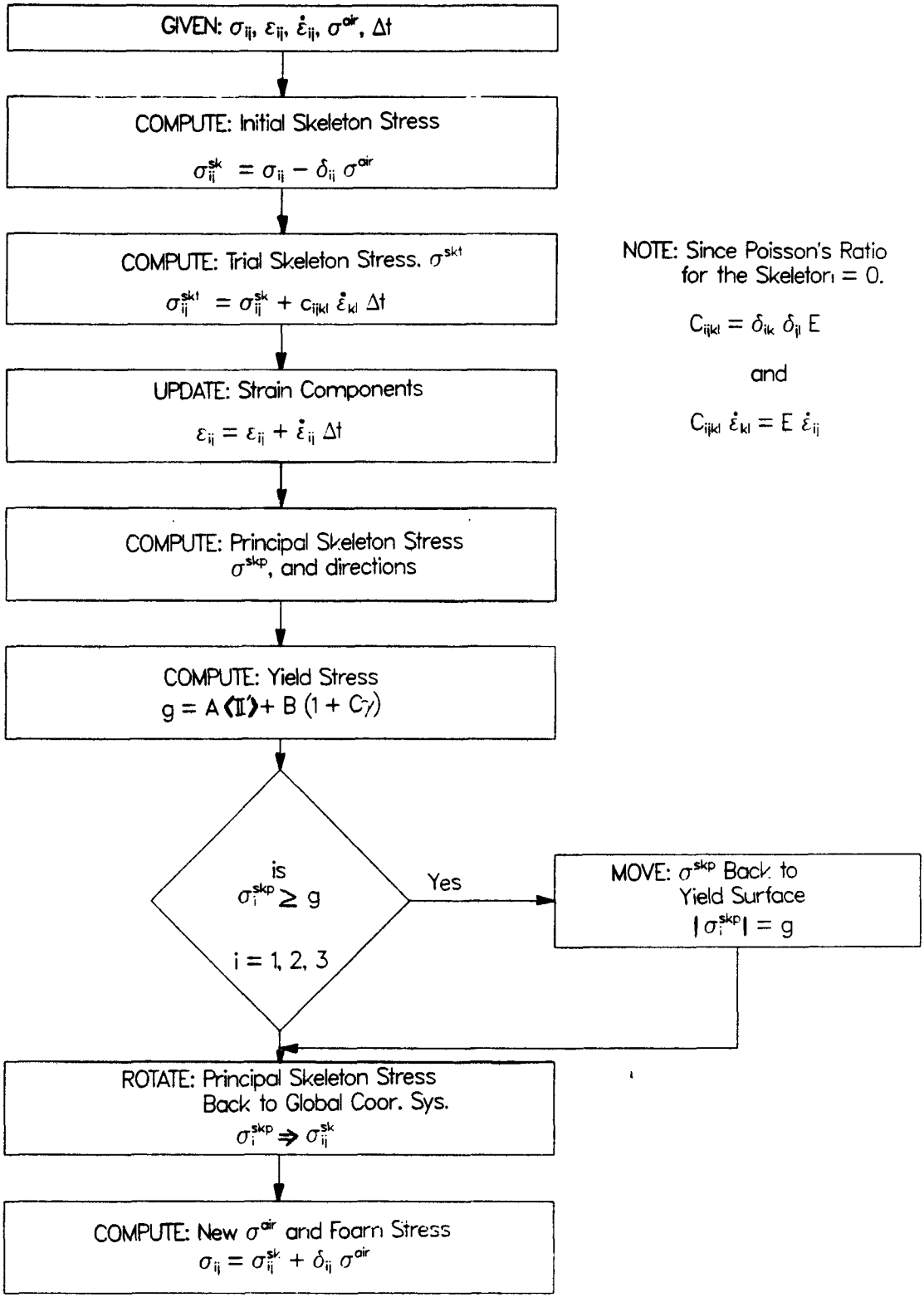

FIGURE 4.9. Flowchart of New Constitutive Model

trial skeleton stress is smaller in magnitude than the yield stress, it becomes the actual principal skeleton stress at the end of the time step. Principal skeleton stresses with magnitudes that are equal to or greater than the yield stress are set equal in magnitude to the yield stress. Once the principal skeleton stresses are determined, they are rotated back to the global coordinate system. The stress carried by the air is then computed using the updated volume strain. Finally, foam stress components for this time step are computed by adding the stress carried by the air to the normal skeleton stress components.

The next step in the development of the new constitutive model was its implementation in finite element computer codes. The model was incorporated in SANCHO [8], a quasistatic dynamic relaxation code, and in PRONTO [9], a transient dynamics code. The implementation in both codes was relatively straightforward and followed the flow chart in Figure 4.9. However, there were two minor modifications made to the constitutive model during the implementation phase. The first modification involved the step function used in the yield criterion for the skeleton (Equation 4.12). The step function acts as an "on-off" switch with values of either 0 or 1. The discontinuous jumps between the values of 0 and 1 caused some convergence difficulties, but these difficulties were easily solved by replacing the step function with a steep sine function which allowed a continuous variation between 0 and 1 (Figure 4.10). The second modification affected the air pressure contribution and yield stress equations. These equations were written as functions of engineering volume strain but the computer codes in which this model was implemented used logarithmic strain in their constitutive model routines. The engineering volume strain, γ, can be expressed as a function of the current logarithmic strain components as follows

$$\gamma = e^{\xi_{kk}} - 1 \qquad 4.17$$

where ξ_{ij} are the logarithmic strain components, and e is the base of the natural logarithm system. Equation 4.17 was used in the implementation of the model in the computer codes to express the air pressure contribution and the yield stress as functions of the logarithmic strain components.

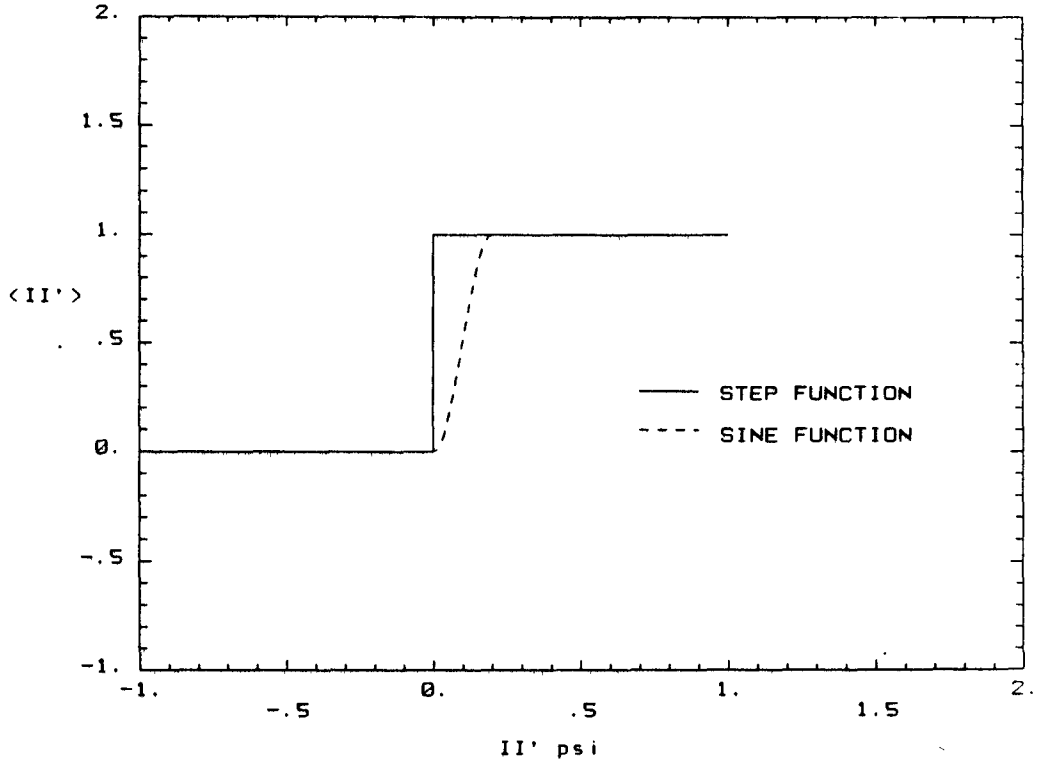

FIGURE 4.10. Modification to Step Function in Yield Equation

The last step in the development of this new constitutive model was to verify that the model accurately represented the polyurethane foam behavior. To verify the model, a series of analyses was completed using the new constitutive model in SANCHO and PRONTO. This series of analyses was completed using an axisymmetric, one element model of a NMERI/CERF test sample. Boundary conditions on the model were varied to represent the various NMERI/CERF tests. Experimental foam behavior and constitutive model behavior from a hydrostatic test for 6602 Foam are shown in Figures 4.11a and 4.11b. The new constitutive model accurately modeled this hydrostatic test. This result was expected because parameters for the constitutive model were selected based on results from the experimental hydrostatic and uniaxial tests. Experimental foam behavior and constitutive model behavior from a uniaxial test for 6602 Foam are shown in Figures 4.12a and 4.12b. Again, the constitutive model accurately represented the experimental foam behavior. Experimental foam behavior and constitutive model behavior from triaxial tests for 6602 Foam are shown in Figures 4.13 - 4.15. The new constitutive model accurately represented the foam behavior for all of the triaxial tests. Also, there was no significant difference between results obtained using SANCHO and results obtained using PRONTO. Comparisons between experimental results and model behavior for other foams are shown in Appendix A.

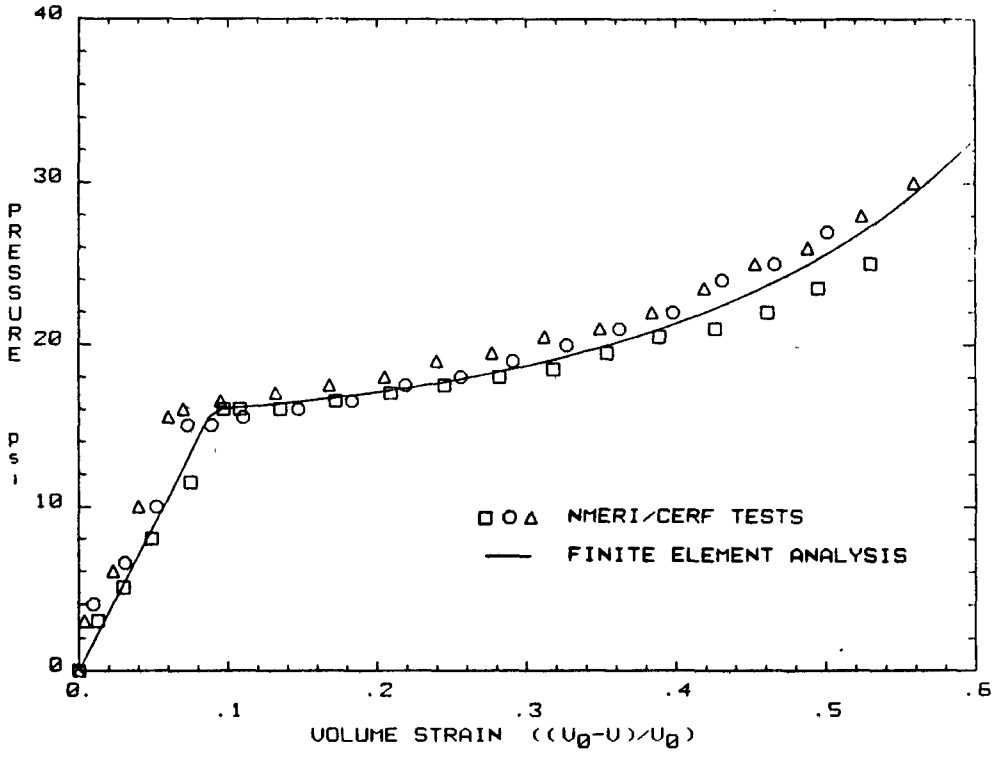

FIGURE 4.11a. Comparison of Analytical and Experimental Results - Volumetric Responses from Hydrostatic Tests on Foam 6602

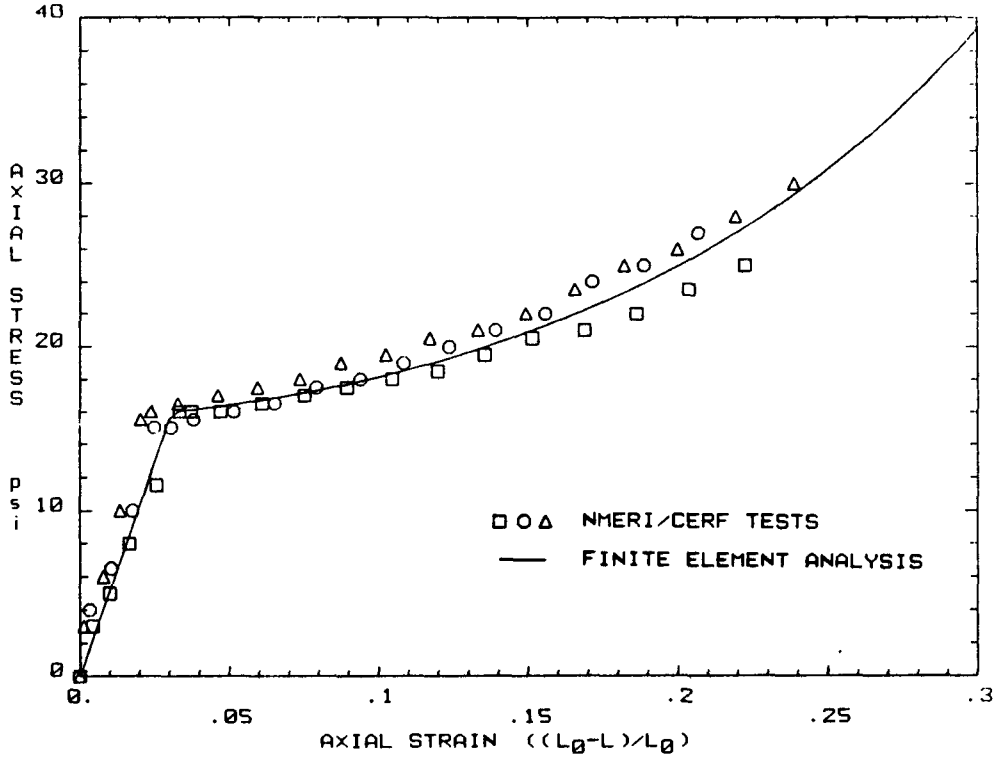

FIGURE 4.11b. Comparison of Analytical and Experimental Results - Axial Responses from Hydrostatic Tests on Foam 6602

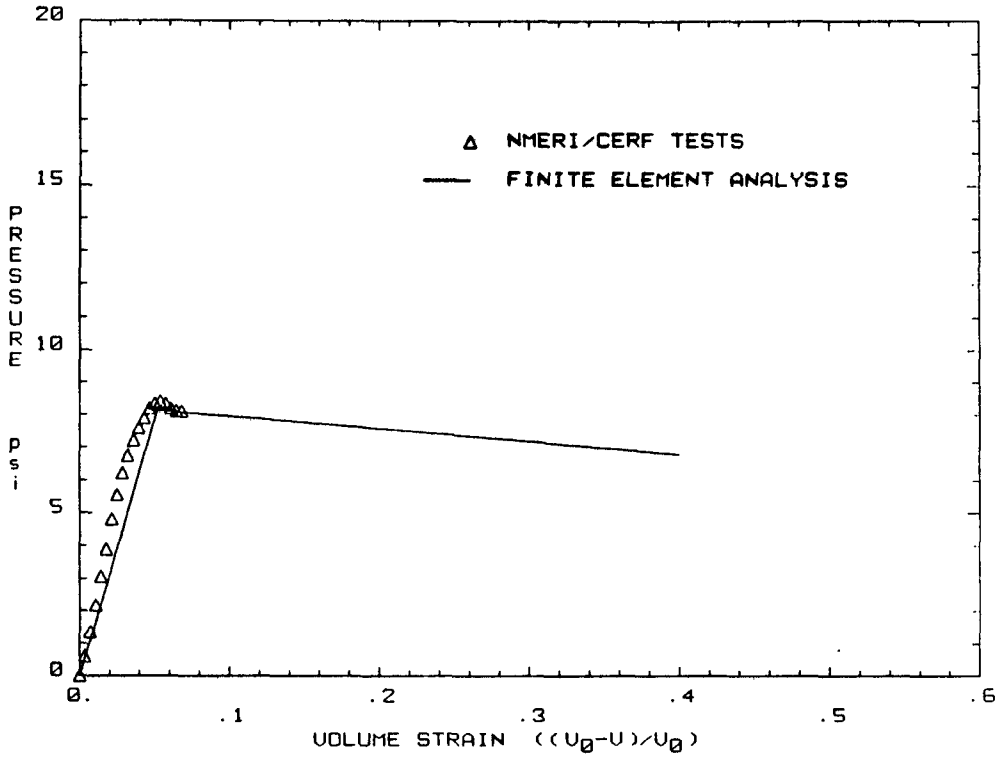

FIGURE 4.12a. Comparison of Analytical and Experimental Results - Volumetric Response from Uniaxial Test on Foam 6602

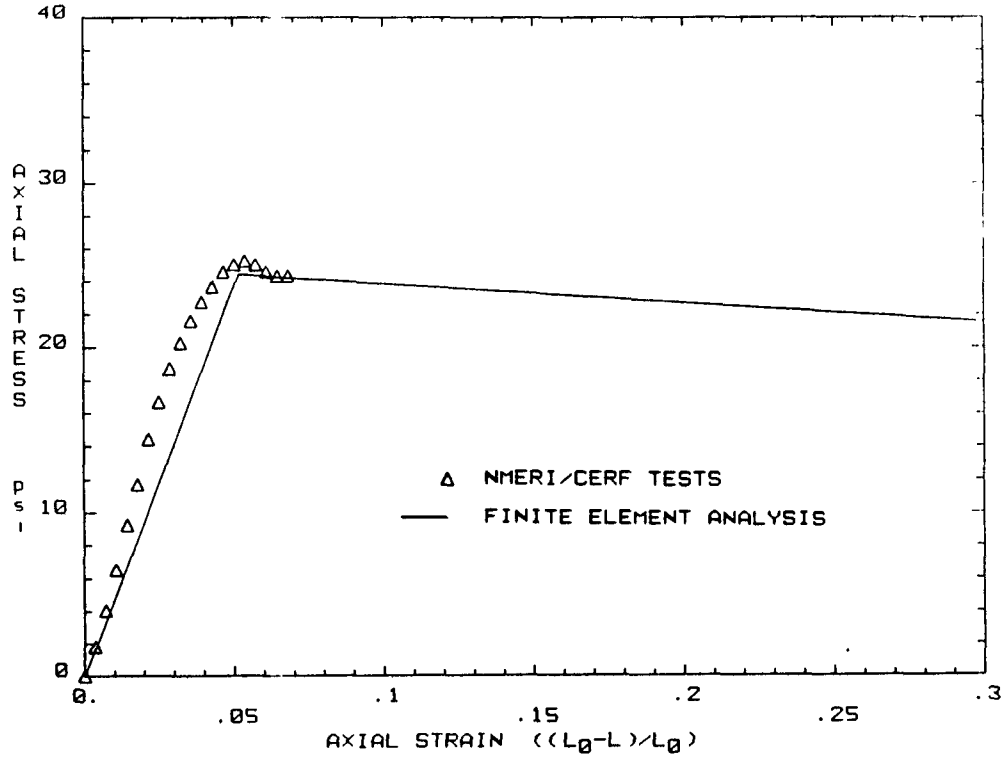

FIGURE 4.12b. Comparison of Analytical and Experimental Results - Axial Response from Uniaxial Test on Foam 6602

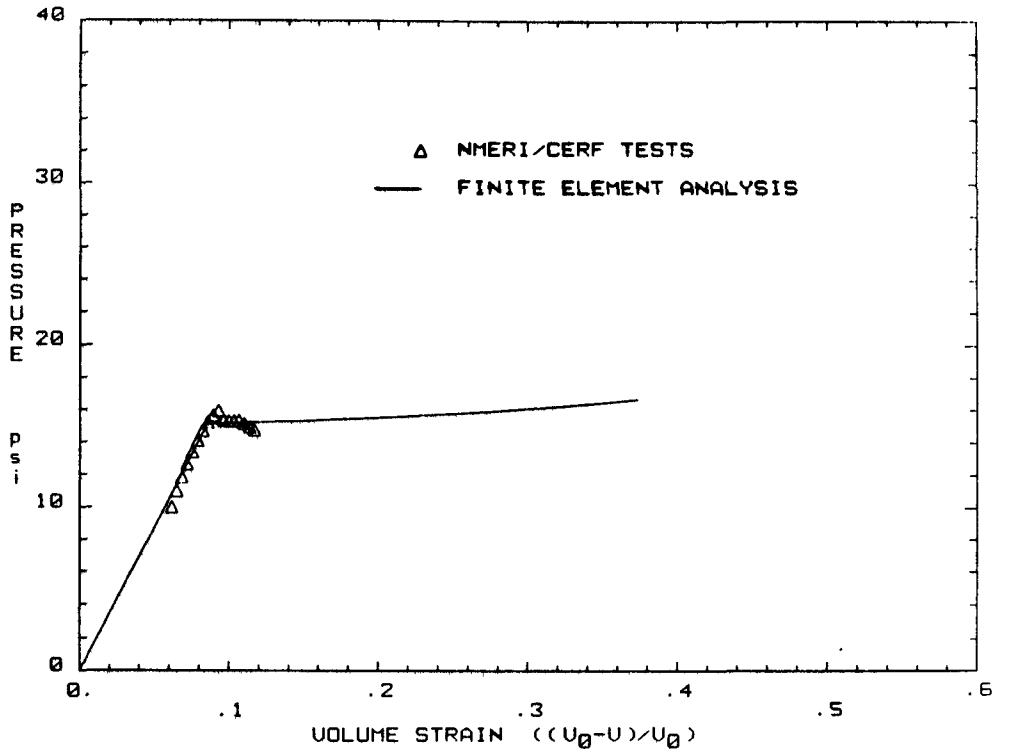

FIGURE 4.13a. Comparison of Analytical and Experimental Results - Volumetric Response from Triaxial Test on Foam 6602 (P=10 psi)

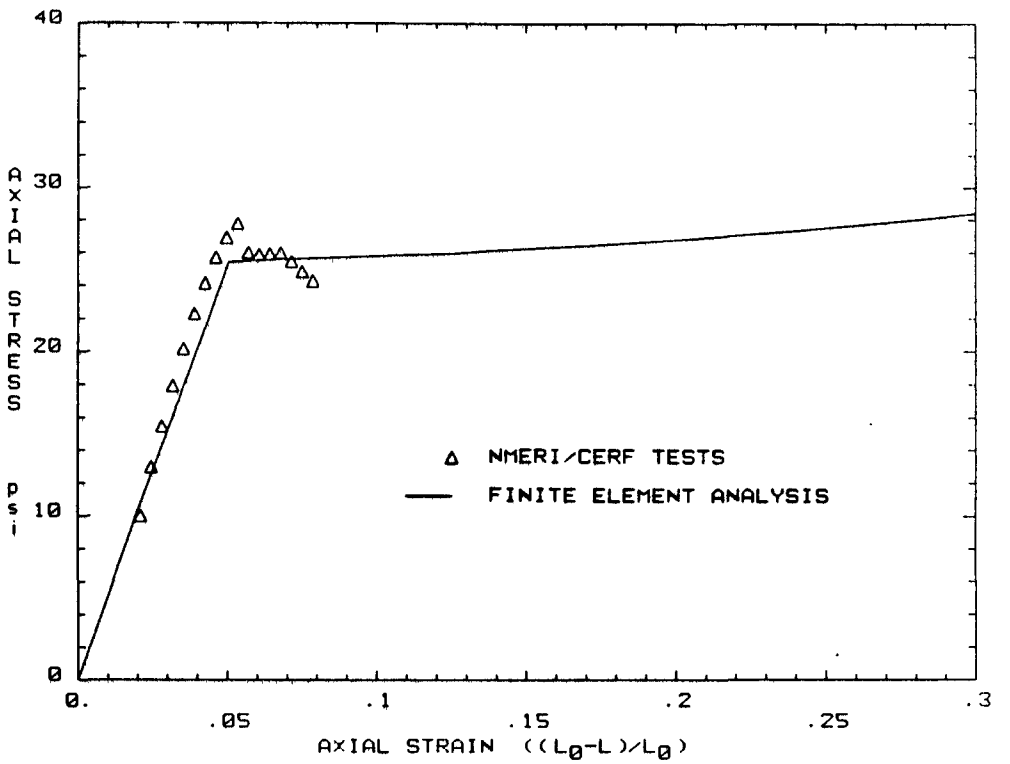

FIGURE 4.13b. Comparison of Analytical and Experimental Results - Axial Response from Triaxial Test on Foam 6602 (P=10 psi)

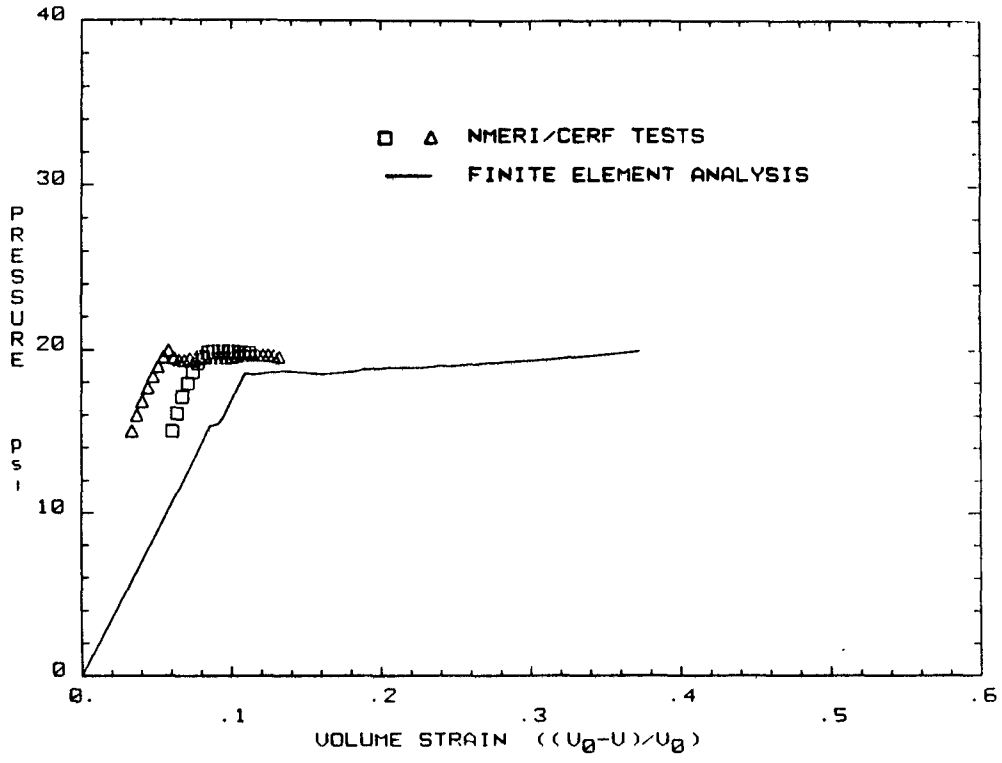

FIGURE 4.14a. Comparison of Analytical and Experimental Results - Volumetric Response from Triaxial Test on Foam 6602 (P=15 psi)

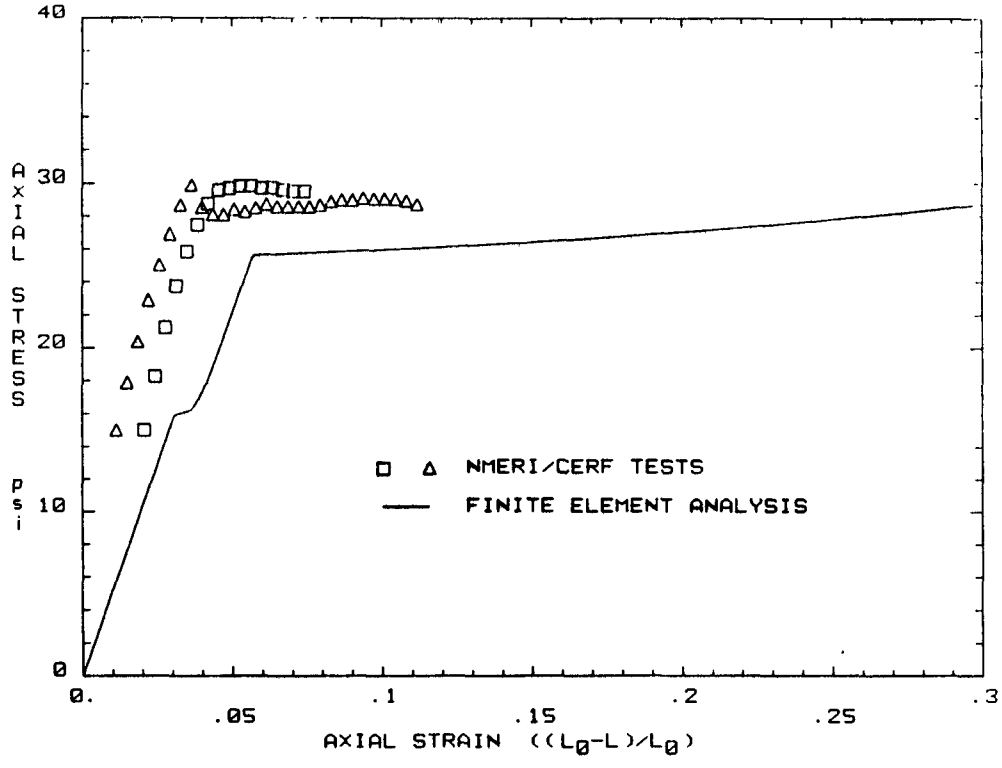

FIGURE 4.14b. Comparison of Analytical and Experimental Results - Axial Response from Triaxial Test on Foam 6602 (P=15 psi)

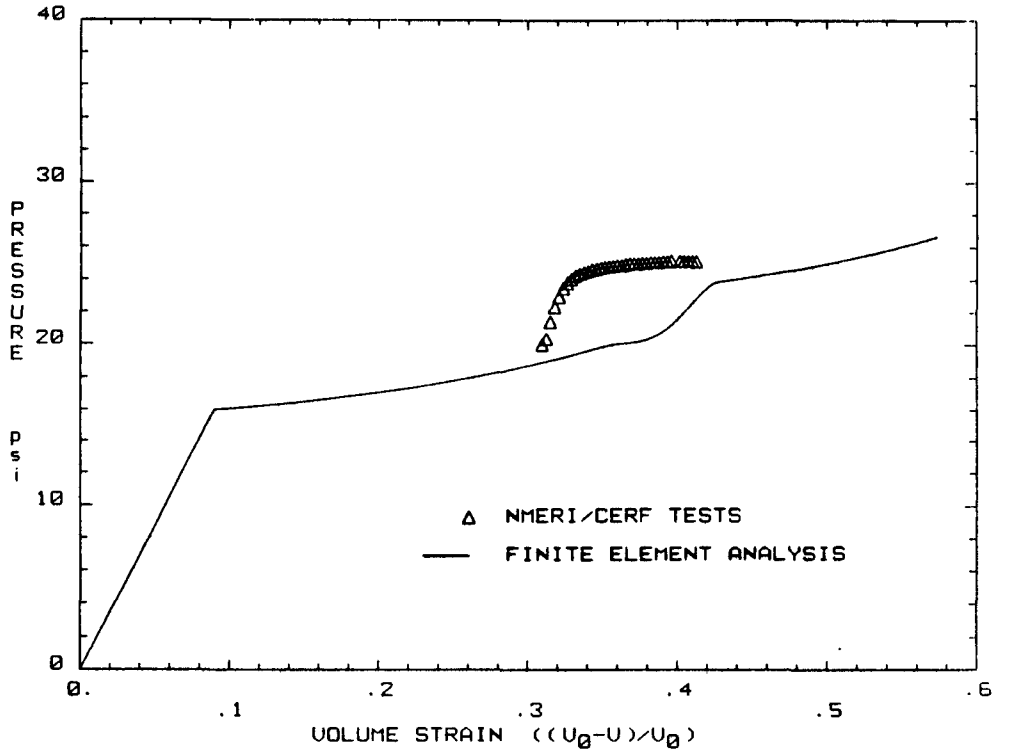

FIGURE 4.15a. Comparison of Analytical and Experimental Results - Volumetric Response from Triaxial Test on Foam 6602 (P=20 psi)

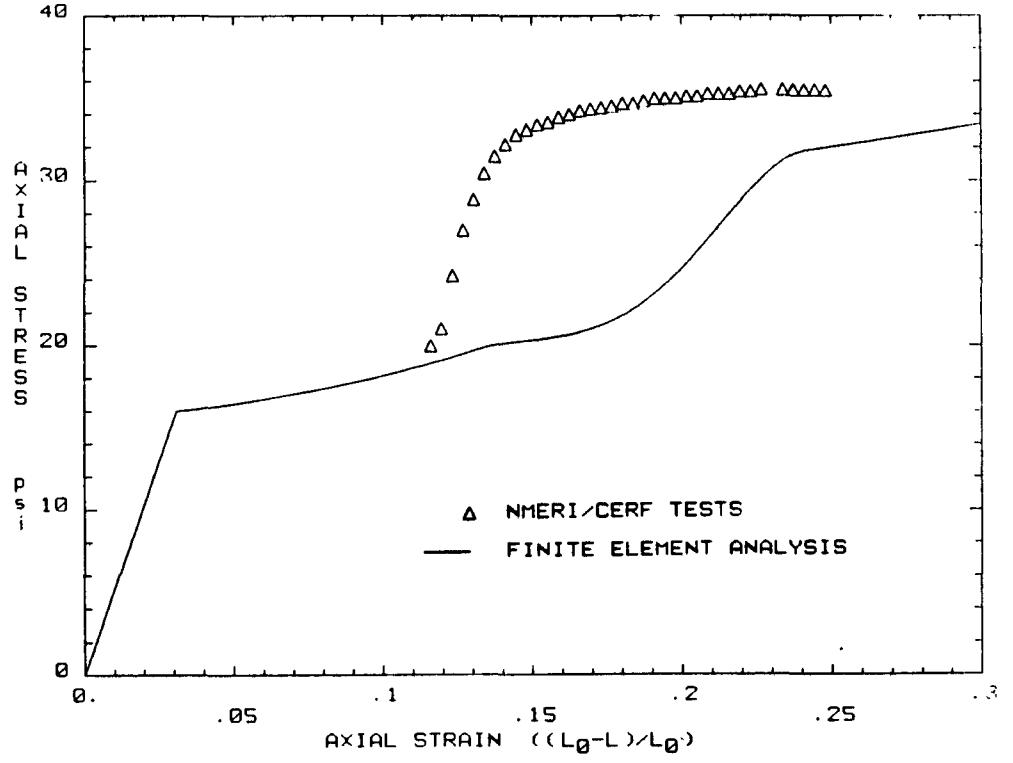

FIGURE 4.15b. Comparison of Analytical and Experimental Results - Axial Response from Triaxial Test on Foam 6602 (P=20 psi)

5. SOLUTION OF A TYPICAL DYNAMIC PROBLEM USING THE NEW CONSTITUTIVE MODEL

A typical dynamic problem was analyzed using the new foam constitutive model and PRONTO. This problem was chosen to demonstrate the capabilities of the model for handling complex stress states. Results from this analysis were compared with results obtained using a conventional deviatoric plasticity model and a combined volumetric plasticity with pressure dependent deviatoric plasticity model to demonstrate the effects of using the various models for the foam material.

This problem consisted of an infinitely long steel cylinder surrounded by a foam layer that was covered with a thin aluminum shell. The two-dimensional, plane strain finite element model shown in Figure 5.1 was used in these analyses. The cylinder was dropped onto a rigid surface at an initial velocity of 528 inches per second, and the resulting deformations and accelerations were computed. Material properties used for this series of analyses are given in Table 5.1. The foam layer was assumed to be 9505 Foam and was modeled with the three different constitutive models discussed above. Material properties for the deviatoric plasticity model were based on results from the uniaxial NMERI/CERF test on 9505 Foam. For this model the material was assumed to be elastic perfectly plastic. Results from both the uniaxial and the hydrostatic NMERI/CERF tests on 9505 Foam were used to determine material properties for the combined volumetric and pressure dependent deviatoric plasticity model. The volumetric response for this model was based on results from the hydrostatic tests and the deviatoric response for this model was based on results from the uniaxial test. Material properties for the new constitutive model were also based on results from both the uniaxial and the hydrostatic NMERI/CERF tests on 9505 Foam.

Results from this series of analyses are summarized in Table 5.2. Results obtained using the new constitutive model are between results obtained using the conventional deviatoric plasticity model and the combined volumetric plasticity with pressure dependent deviatoric plasticity model. The conventional deviatoric plasticity model does not allow for any volumetric plasticity and is stiffer than the other two models. The

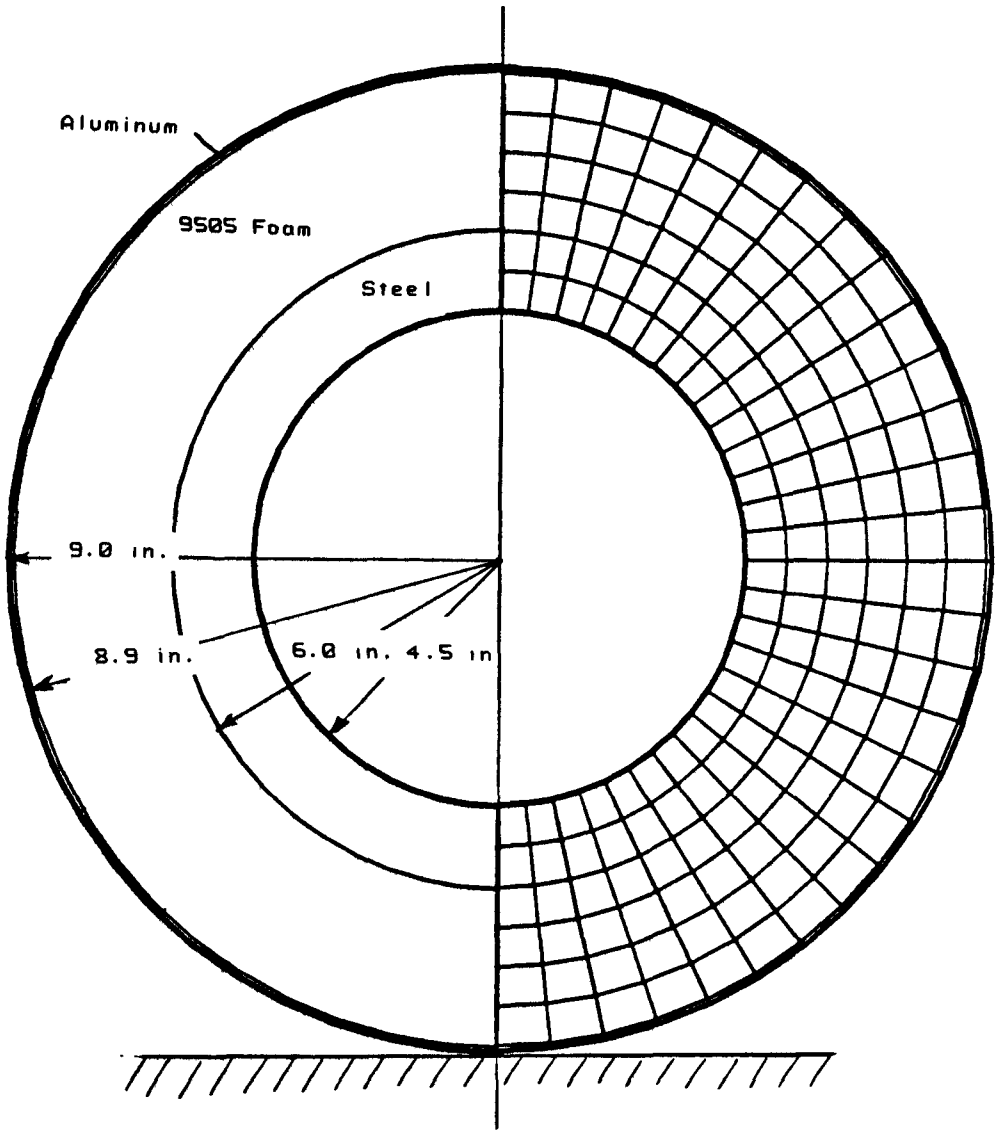

FIGURE 5.1. Finite Element Model

Table 5.1. Material Properties Used in Dynamic Analyses

Aluminum (Elastic)	YOUNG'S MODULUS =	10.E+06	psi
	POISSON'S RATIO =	0.30	
	DENSITY =	2.5E-04	lb s^2/in^4
Steel (Elastic)	YOUNG'S MODULUS =	29.E+06	psi
	POISSON'S RATIO =	0.30	
	DENSITY =	7.0E-04	lb s^2/in^4
Foam (Conventional Deviatoric Plasticity Model)			
	YOUNG'S MODULUS =	3010.	psi
	POISSON'S RATIO =	0.00	
	DENSITY =	7.5E-06	lb s^2/in^4
	YIELD STRENGTH =	110.	psi
	HARDENING MODULUS =	0.	psi
	BETA =	0.	
Foam (Combined Volumetric and Deviatoric Plasticity Model)			
	SHEAR MODULUS =	1505.	psi
	BULK MODULUS =	1003.	psi
	DENSITY =	7.5E-06	lb s^2/in^4
	YIELD FUNCTION CONSTANT - a_0 =	110.	
	YIELD FUNCTION CONSTANT - a_1 =	0.	
	YIELD FUNCTION CONSTANT - a_2 =	0.	
Foam (New Constitutive Model)			
	YOUNG'S MODULUS =	3010.	psi
	DENSITY =	7.5E-06	lb s^2/in^4
VOLUME FRACTION OF SOLID MATERIAL - ϕ =		0.090	
	INITIAL AIR PRESSURE - p_0 =	14.7	psi
	YIELD FUNCTION CONSTANT - A =	49.2	psi
	YIELD FUNCTION CONSTANT - B =	60.8	psi
	YIELD FUNCTION CONSTANT - C =	-0.517	

Table 5.2. Results from Dynamic Analyses		
CONSTITUTIVE MODEL USED	MAXIMUM CRUSH-UP (in.)	MAXIMUM STEEL BODY ACCELERATION (g)
CONVENTIONAL DEVIATORIC PLASTICITY MODEL	1.93	399
NEW FOAM MODEL	2.57	275
COMBINED VOLUMETRIC AND DEVIATORIC PLASTICITY MODEL	2.84	208

combined volumetric plasticity with pressure dependent deviatoric plasticity model does not allow for any change in volumetric response due to the occurrence of deviatoric loading. Experimental results indicated that the occurrence of deviatoric loading would stiffen the volumetric response. The combined volumetric plasticity with pressure dependent deviatoric plasticity model is softer than the other two models. The new constitutive model captures both volumetric plasticity and changes in the volumetric response due to the occurrence of deviatoric loading. Displaced shapes of the finite element model at maximum crush-up are shown in Figures 5.2 and 5.3. Plots of displacement and acceleration of the steel cylinder as a function of time are shown in Figures 5.4 and 5.5, respectively. The acceleration plots were filtered with a lowpass filter with a cut-off frequency of 1000 Hz.

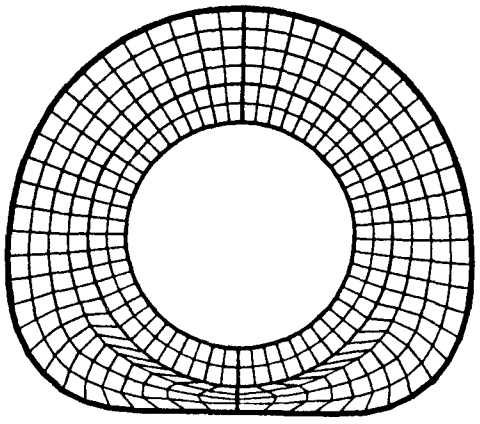

conventional deviatoric plasticity model

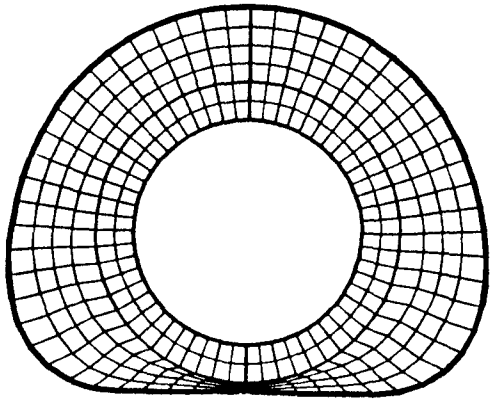

new foam model

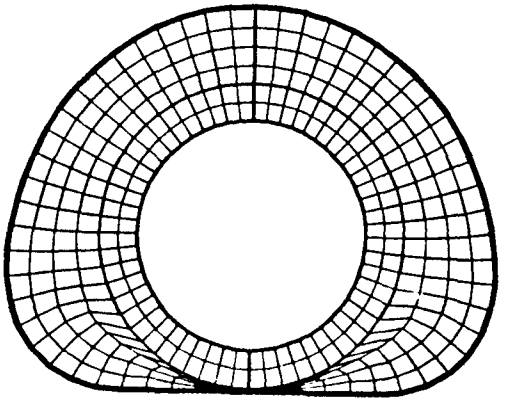

combined volumetric and deviatoric plasticity model

FIGURE 5.2. Displaced Shapes of Finite Element Model at Maximum Crush-up

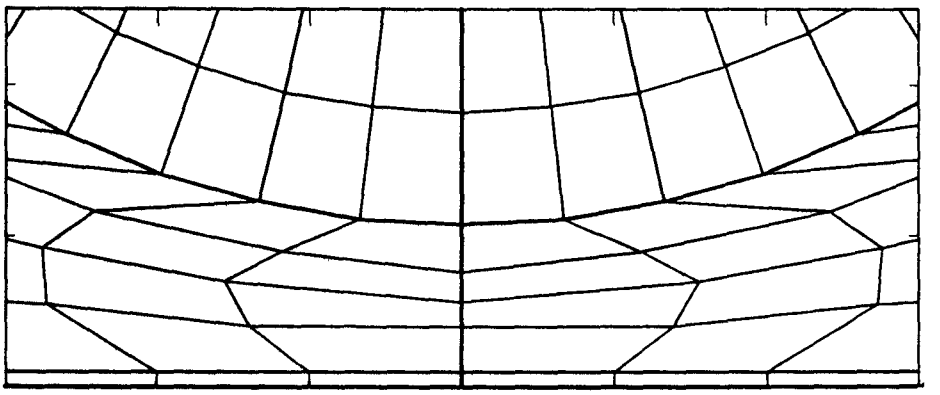

conventional deviatoric plasticity model

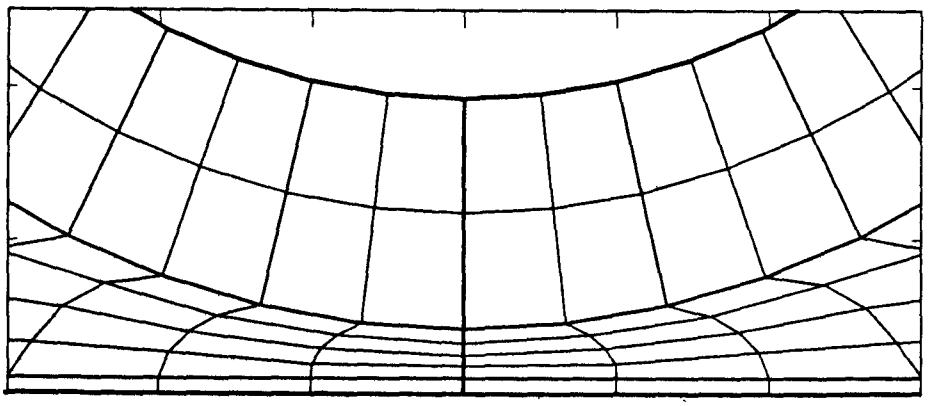

new foam model

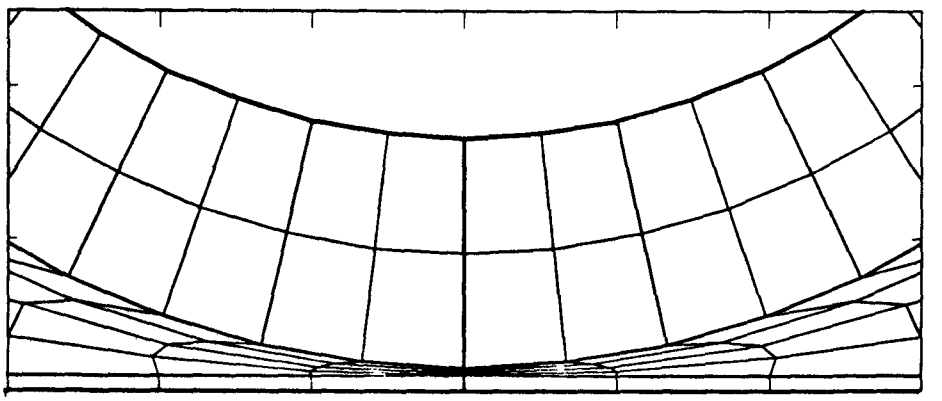

combined volumetric and deviatoric plasticity model

FIGURE 5.3. Close-up of Displaced Foam Layer in Finite Element Model at Maximum Crush-up

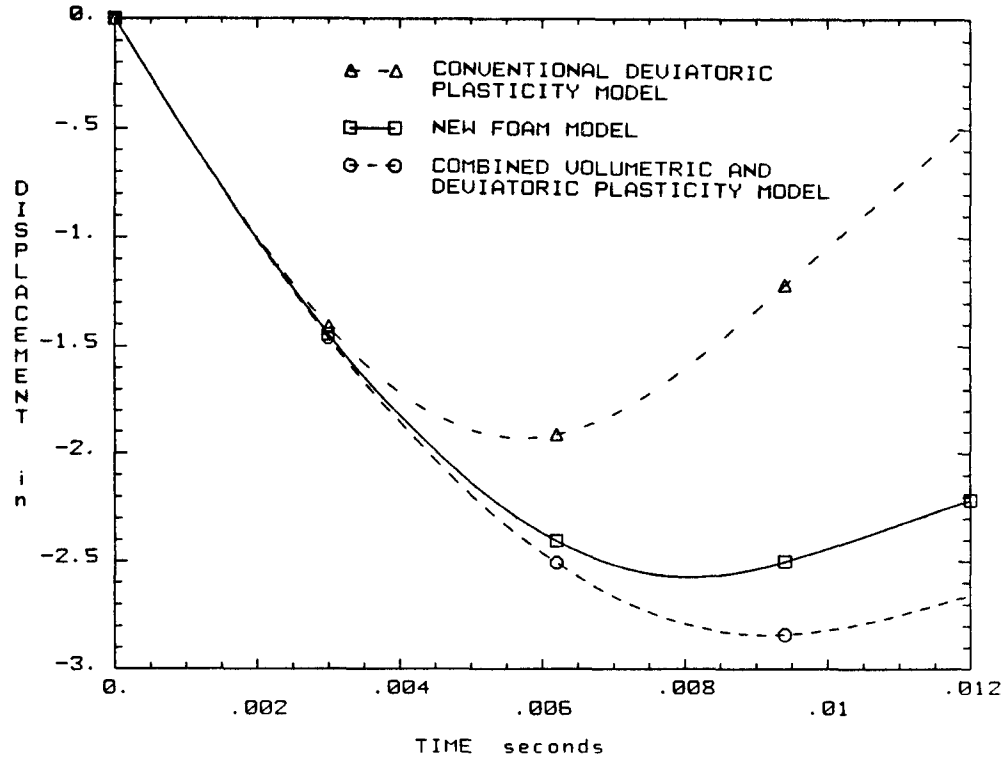

FIGURE 5.4. Displacement of Steel Cylinder

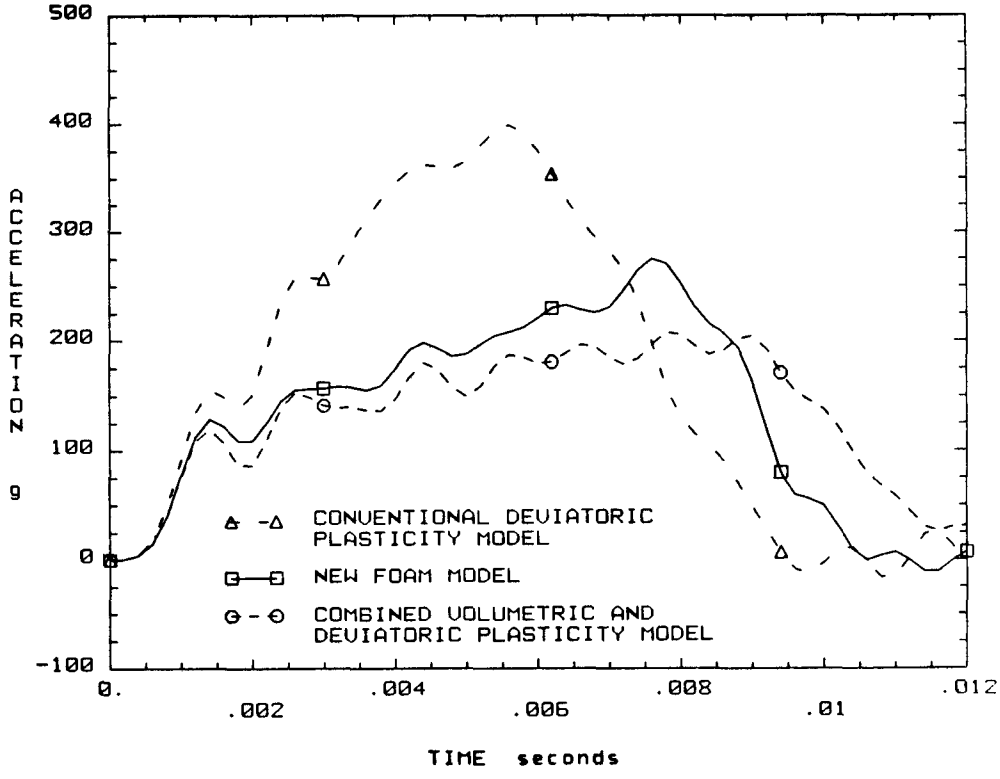

FIGURE 5.5. Acceleration of Steel Cylinder

6. CONCLUSIONS AND FUTURE WORK

The behavior of rigid, closed-cell, polyurethane foam was experimentally investigated. It was found that these foams undergo large plastic volumetric strains when subjected to sufficient load and that the deviatoric and volumetric behaviors for these foams are coupled.

A conventional deviatoric plasticity model and a combined volumetric plasticity with pressure dependent deviatoric plasticity model did not capture the coupling that occurred between the deviatoric and volumetric behaviors in the NMERI/CERF tests. Therefore, a new constitutive model for low density polyurethane foams was developed. This new constitutive model captured all foam behaviors that were observed in the NMERI/CERF tests. This model was implemented in two finite element codes, SANCHO and PRONTO. A typical problem was analyzed using this new constitutive model and two other constitutive models to demonstrate differences between the various models. Results from this series of analyses indicated that the new constitutive model generated displacement and acceleration predictions that were between predictions obtained using the other two models. This result was expected.

Because the experimental NMERI/CERF tests were all static tests there was no way to determine if rate effects were important; therefore, no rate effects were included in the new constitutive model. In the future, dynamic tests should be completed to determine the effects of strain rates. The effects of temperature changes were also not investigated as part of the NMERI/CERF tests. In the new constitutive model it was assumed that the air behaves as an ideal gas and that temperature changes have no effect on the polymer skeleton. Polyurethane is expected to have a strong temperature dependence above the glassy transition temperature, but the resulting effect upon cell wall collapse is unknown. This should be investigated in laboratory tests. Once the new constitutive model has been modified to include any important rate or temperature effects, it could then be used with confidence to analyze dynamic events. Future comparisons between experimental results and analyses with this constitutive model would further increase confidence in its accuracy.

Finally, most shipping containers that use polyurethane foam impact limiters have a thin layer of some metal around the impact limiter. Accurate analyses of such shipping containers will require the implementation of elements that accurately and efficiently model thin layers in the finite element codes in which the foam model is used.

7. REFERENCES

1. Doyle, E. N., "The Development and Use of Polyurethane Products," McGraw-Hill Book Co., 1971, pp. 256-263.

2. "Safety Analysis Report for the NUPAC 125-B Fuel Shipping Cask," Document Number 71-9200, Nuclear Packaging, Inc., Federal Way, Washington, May 1985.

3. "Transuranic Package Transporter TRUPACT Safety Analysis Report for Packaging," SAND 83-7077, Sandia National Laboratories, Albuquerque, New Mexico, May 1986.

4. Hamberg, D., NMERI/CERF, letter to R. May, K. Schuler, and R. Yoshimura, Sandia National Laboratories, Albuquerque, New Mexico, February 29, 1980.

5. Kraynik, A. W. and Warren, W. E., "The Linear Elastic Properties of Foams," Presented at Winter Meeting, Society of Rheology, Santa Monica, CA, January 1987.

6. Wellman, G. W., "Transportation System Impact Limiter Design Using Rigid Polyurethane Foam," SAND84-2271, Sandia National Laboratories, Albuquerque, New Mexico, 1985.

7. Krieg, R. D., "A Simple Constitutive Description for Soils and Crushable Foams," SC-DR-72-0883, Sandia National Laboratories, Albuquerque, New Mexico, 1972.

8. Stone, C. M., Krieg, R. D., and Beisinger, Z. E., "SANCHO - A Finite Element Computer Program for the Quasistatic, Large Deformation, Inelastic Response of Two-Dimensional Solids," SAND84-2618, Sandia National Laboratories, Albuquerque, New Mexico, 1985.

9. Taylor, L. M. and Flanagan, D. P., "A Two-Dimensional Transient Solid Dynamics Program," SAND86-0594, Sandia National Laboratories, Albuquerque, New Mexico, 1986.

APPENDIX A

To verify that the new constitutive model captured the foam behavior observed during the NMERI/CERF tests, a series of analyses was completed using the new model in SANCHO and PRONTO. This series of analyses was completed using an axisymmetric, one element model of a NMERI/CERF test sample. Boundary conditions on the model were varied to represent the various NMERI/CERF tests. Results from this series of analyses are compared with results from the NMERI/CERF tests in this appendix. These results indicate that the new constitutive model does capture the foam behavior observed during the NMERI/CERF tests.

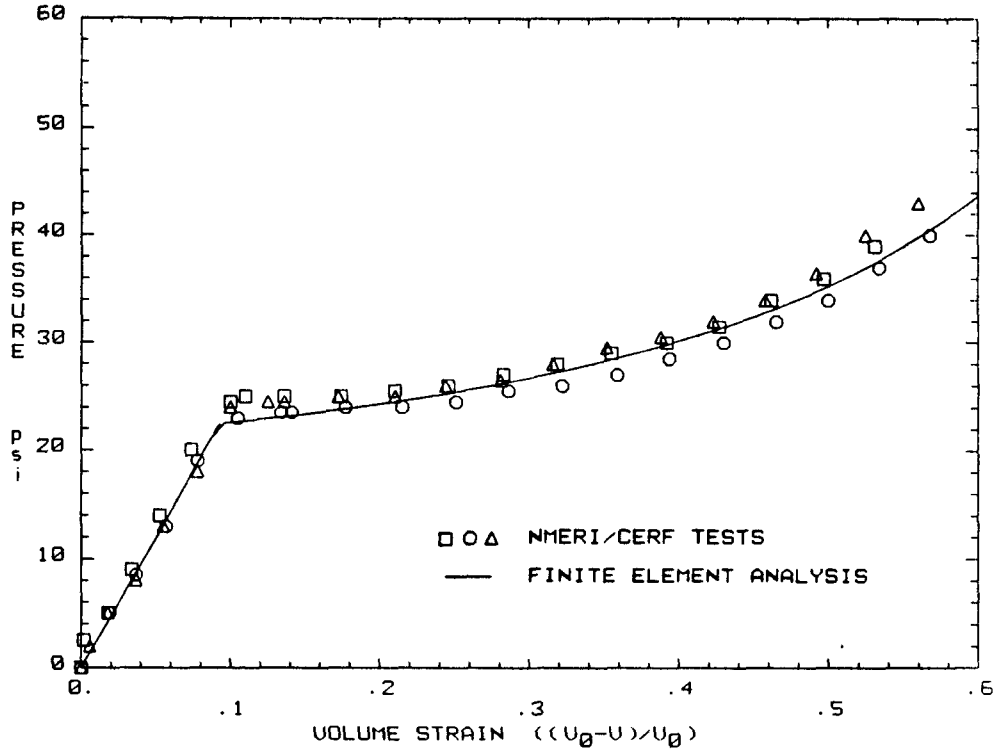

FIGURE A.1a. Comparison of Analytical and Experimental Results - Volumetric Responses from Hydrostatic Tests on Foam 6703

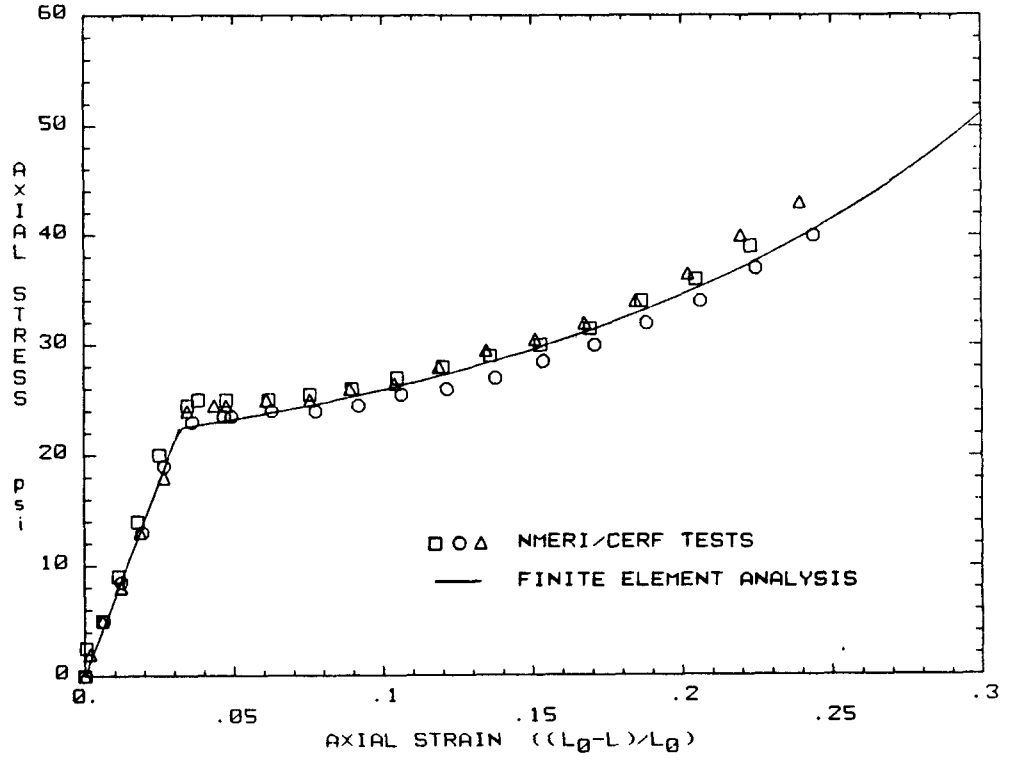

FIGURE A.1b. Comparison of Analytical and Experimental Results - Axial Responses from Hydrostatic Tests on Foam 6703

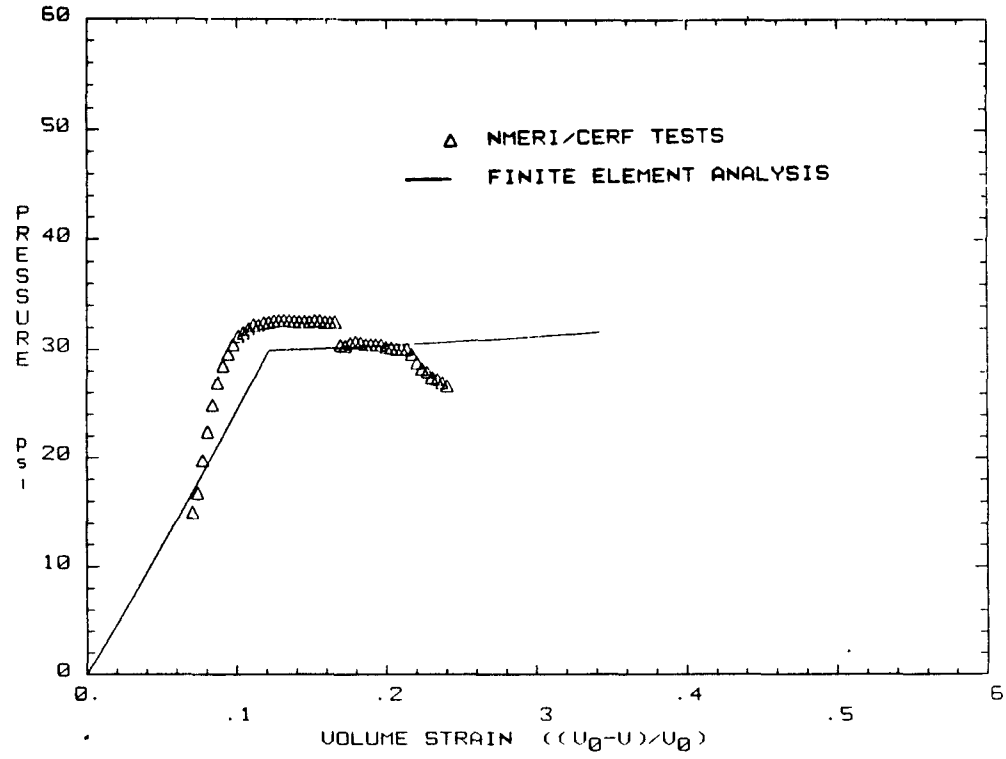

FIGURE A.2a. Comparison of Analytical and Experimental Results - Volumetric Response from Triaxial Test on Foam 6703 (P=15 psi)

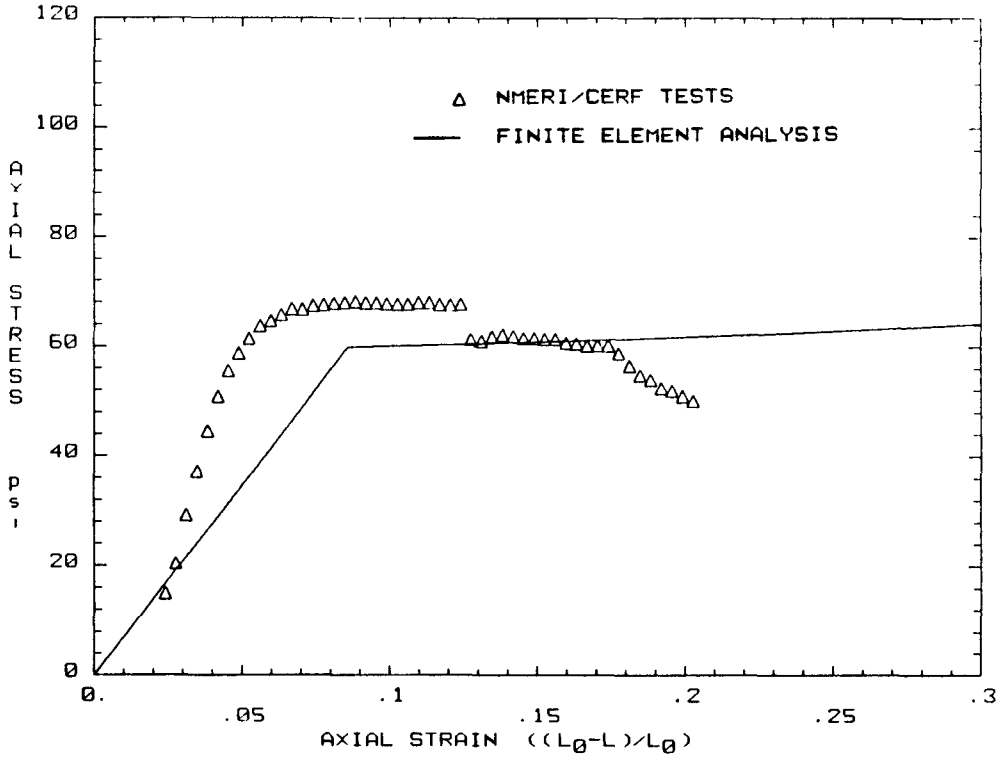

FIGURE A.2b. Comparison of Analytical and Experimental Results - Axial Response from Triaxial Test on Foam 6703 (P=15 psi)

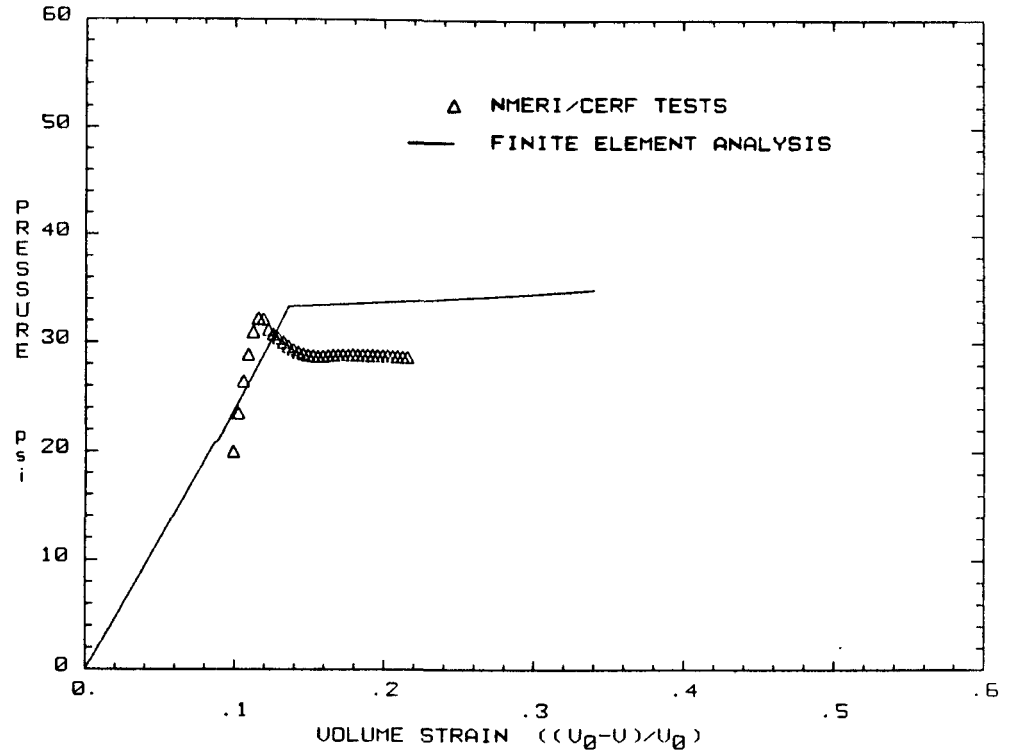

FIGURE A.3a. Comparison of Analytical and Experimental Results - Volumetric Response from Triaxial Test on Foam 6703 (P=20 psi)

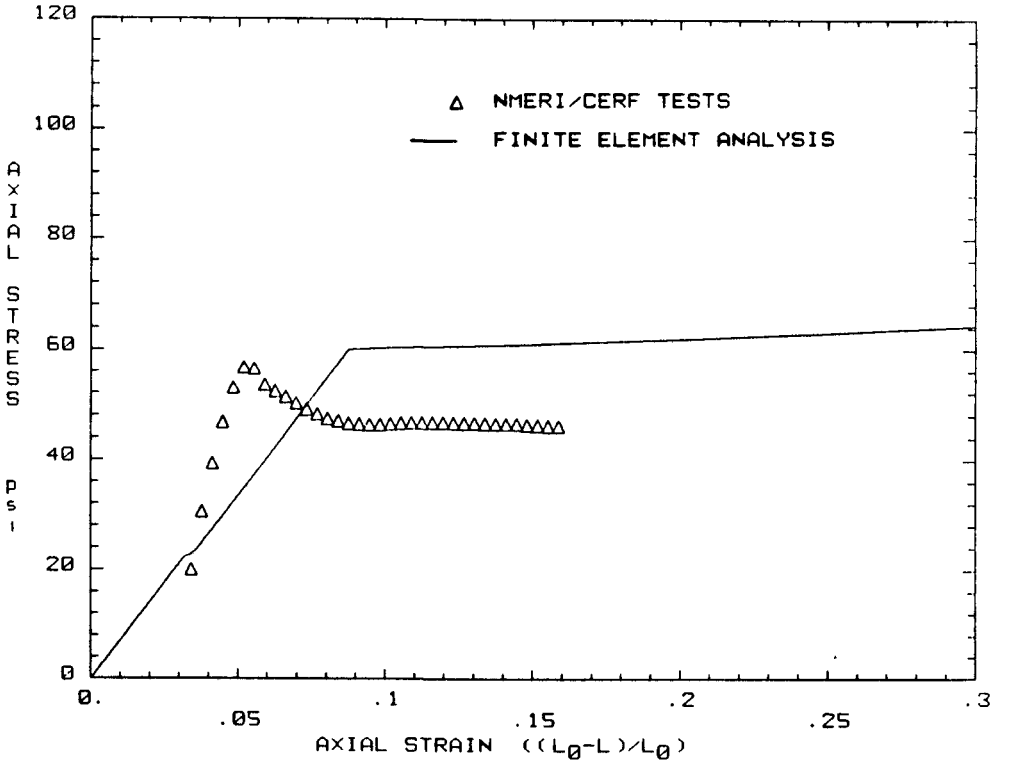

FIGURE A.3b. Comparison of Analytical and Experimental Results - Axial Response from Triaxial Test on Foam 6703 (P=20 psi)

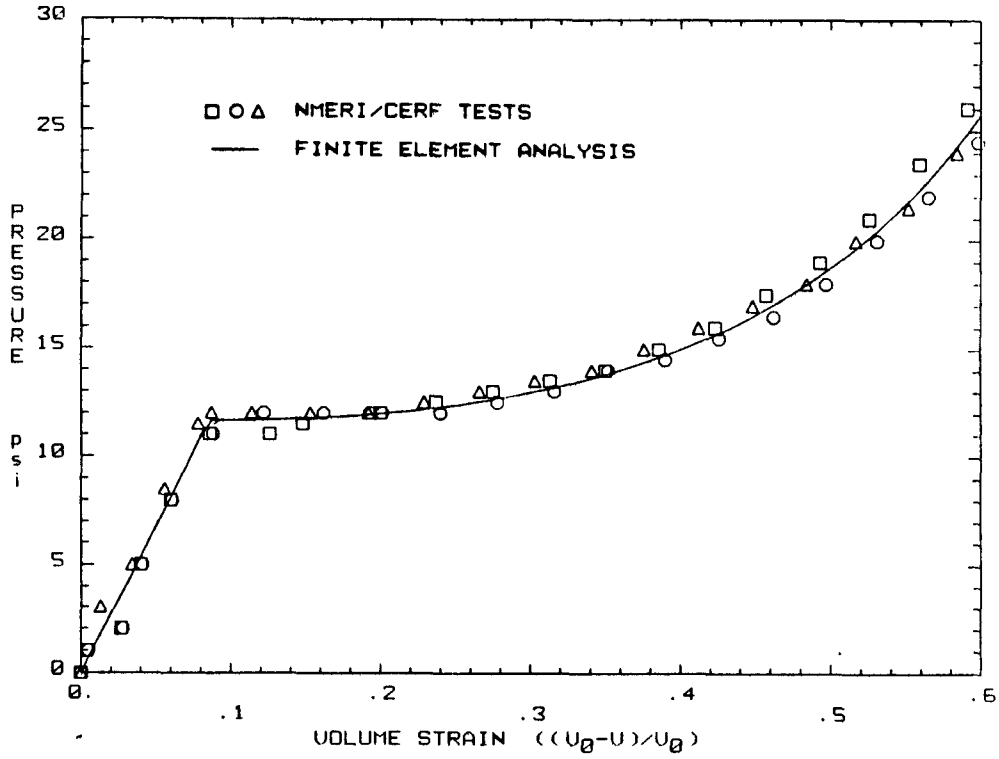

FIGURE A.4a. Comparison of Analytical and Experimental Results - Volumetric Responses from Hydrostatic Tests on Foam 9703

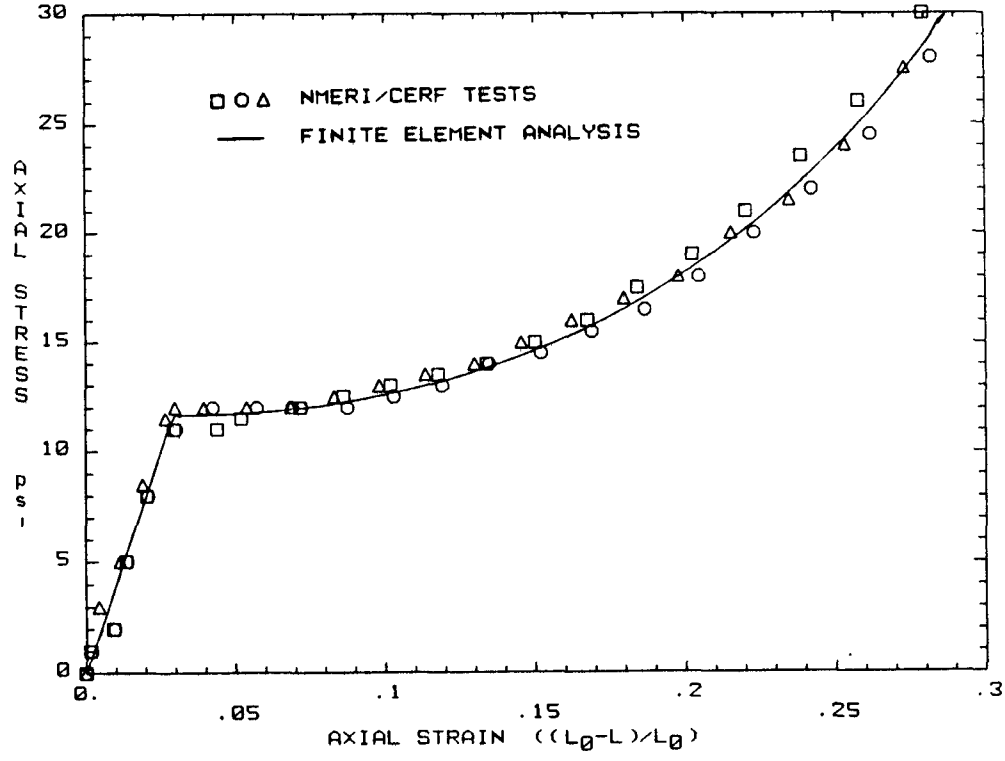

FIGURE A.4b. Comparison of Analytical and Experimental Results - Axial Responses from Hydrostatic Tests on Foam 9703

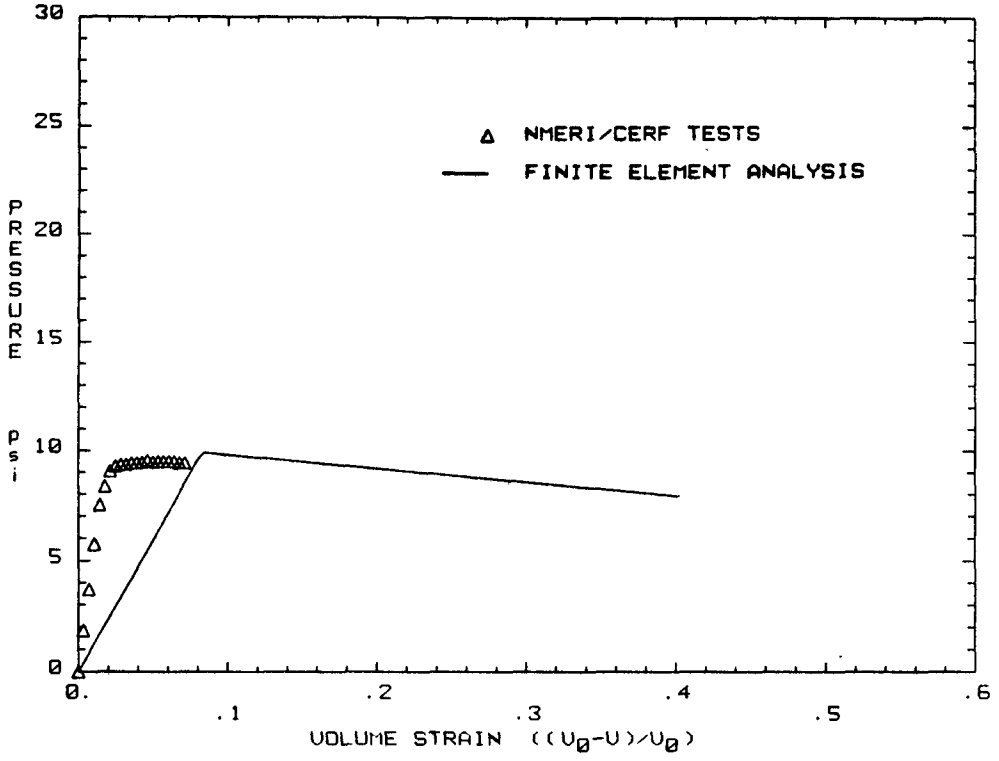

FIGURE A.5a. Comparison of Analytical and Experimental Results - Volumetric Response from Uniaxial Test on Foam 9703

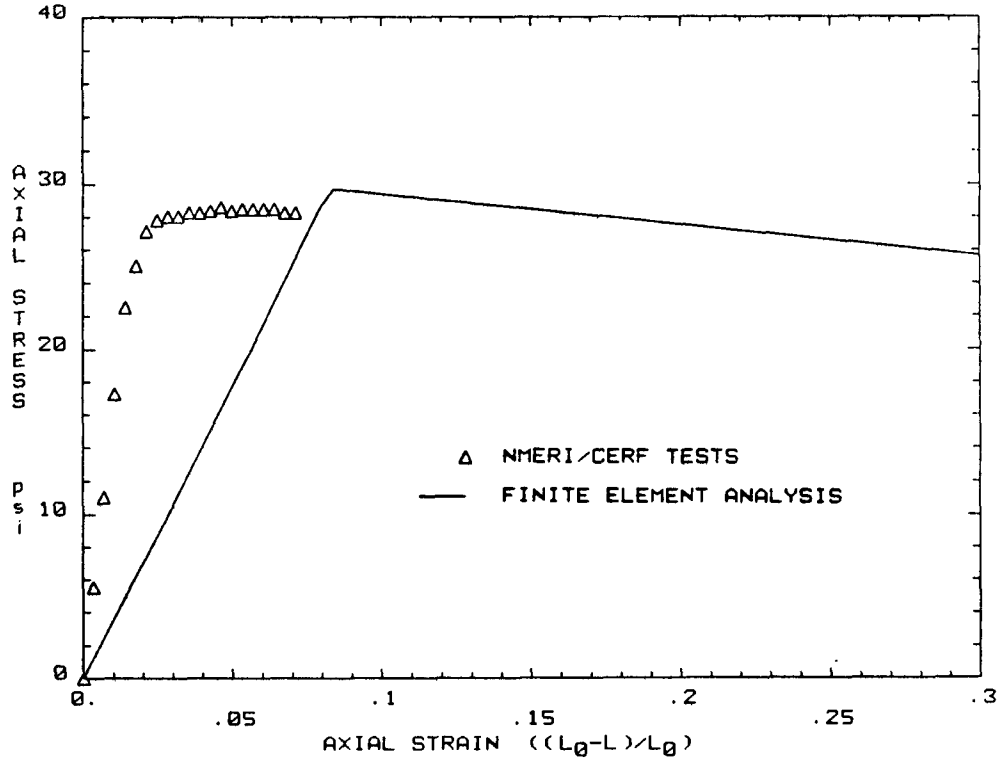

FIGURE A.5b. Comparison of Analytical and Experimental Results - Axial Response from Uniaxial Test on Foam 9703

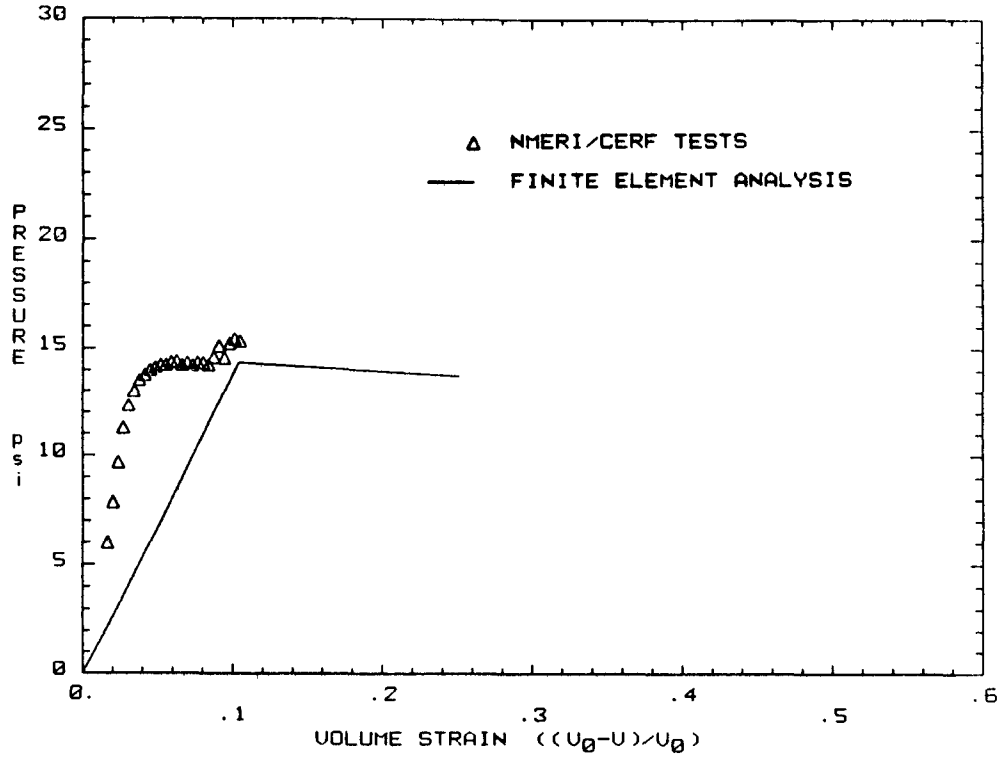

FIGURE A.6a. Comparison of Analytical and Experimental Results - Volumetric Response from Triaxial Test on Foam 9703 (P=6 psi)

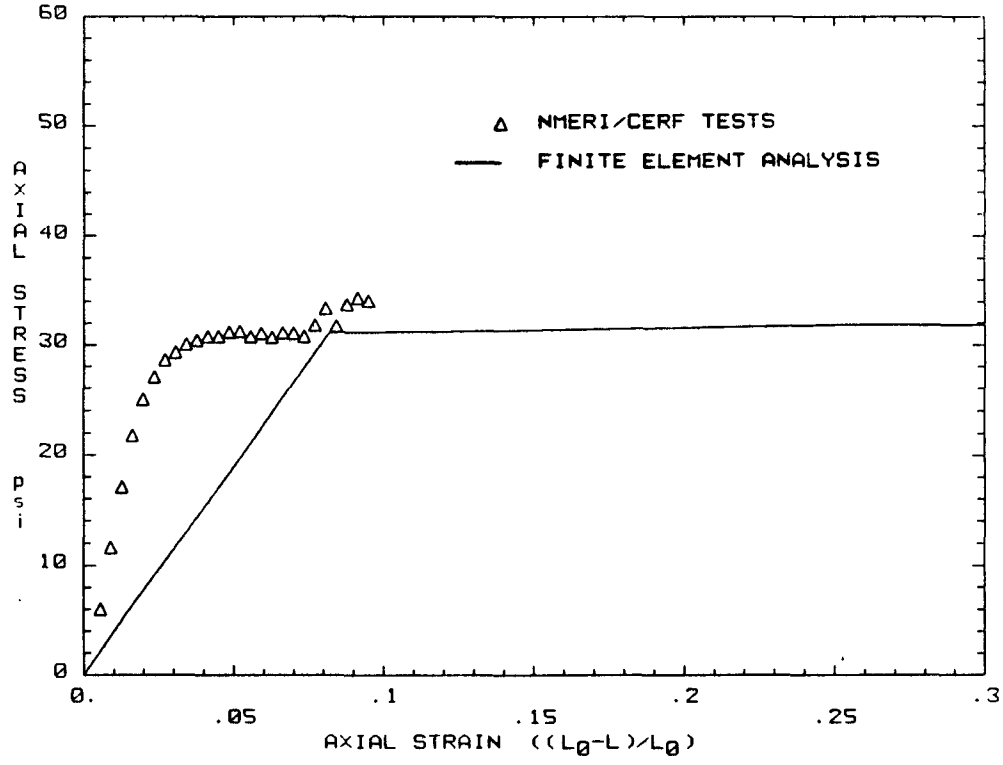

FIGURE A.6b. Comparison of Analytical and Experimental Results - Axial Response from Triaxial Test on Foam 9703 (P=6 psi)

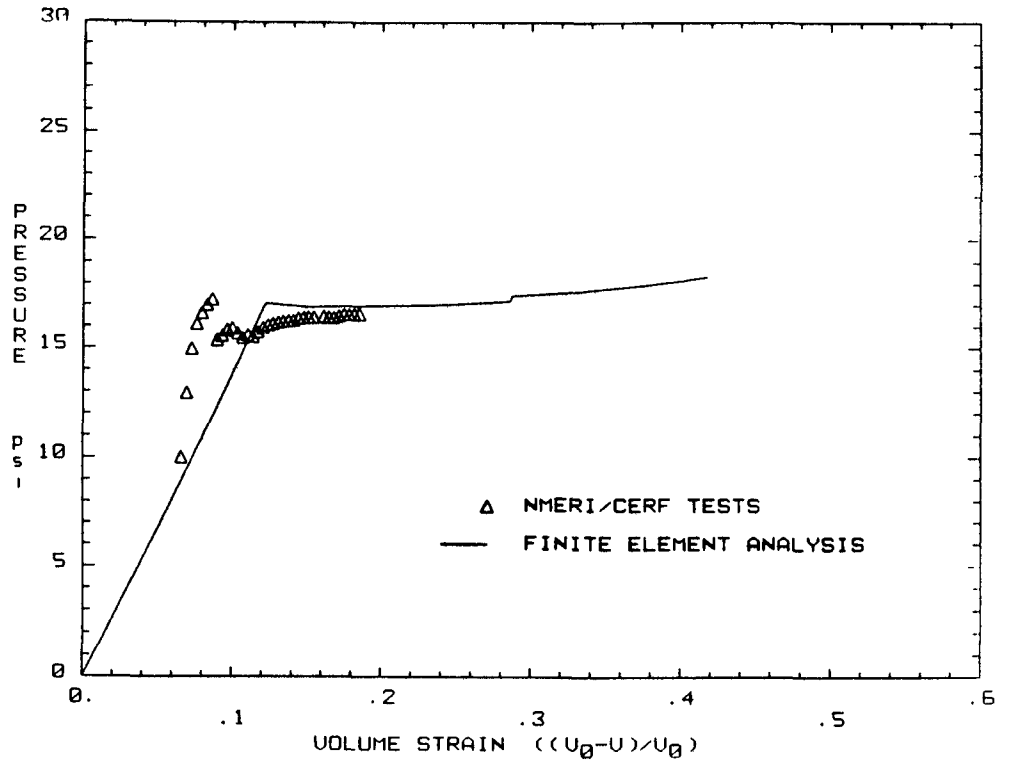

FIGURE A.7a. Comparison of Analytical and Experimental Results - Volumetric Response from Triaxial Test on Foam 9703 (P=10 psi)

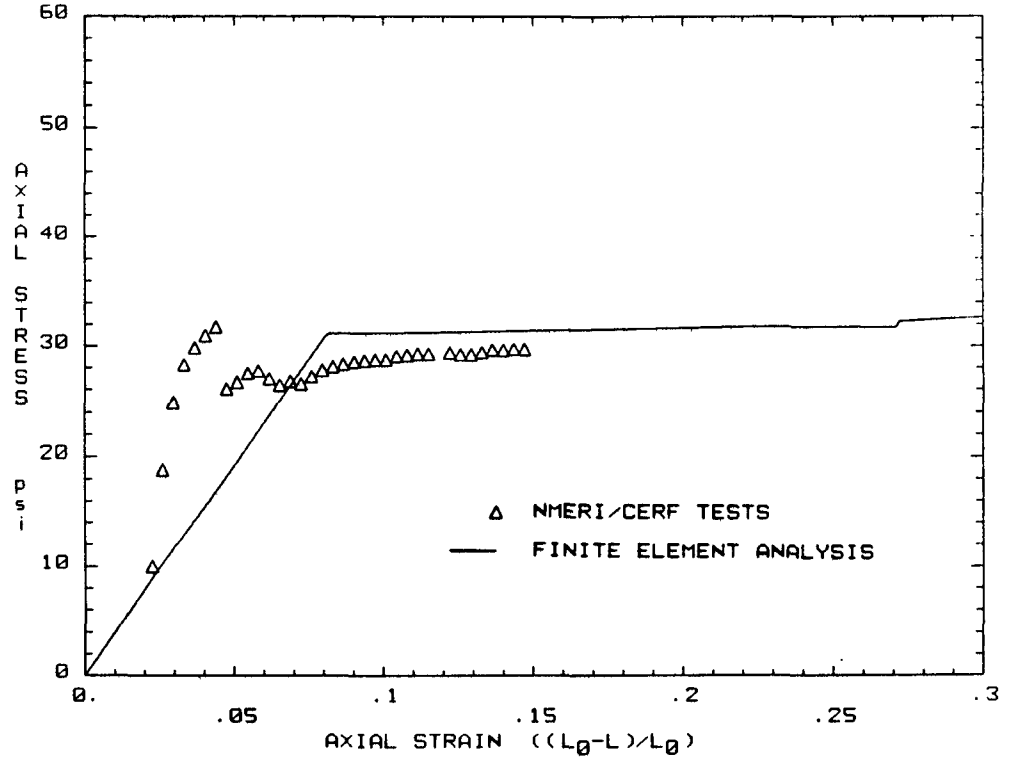

FIGURE A.7b. Comparison of Analytical and Experimental Results - Axial Response from Triaxial Test on Foam 9703 (P=10 psi)

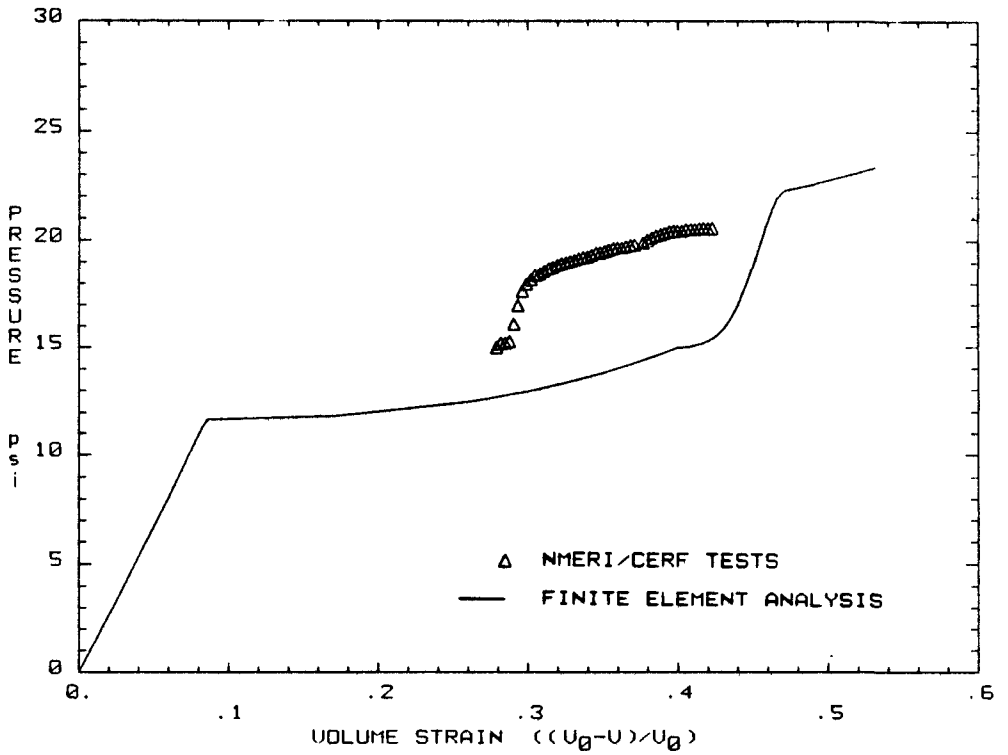

FIGURE A.8a. Comparison of Analytical and Experimental Results - Volumetric Response from Triaxial Test on Foam 9703 (P=15 psi)

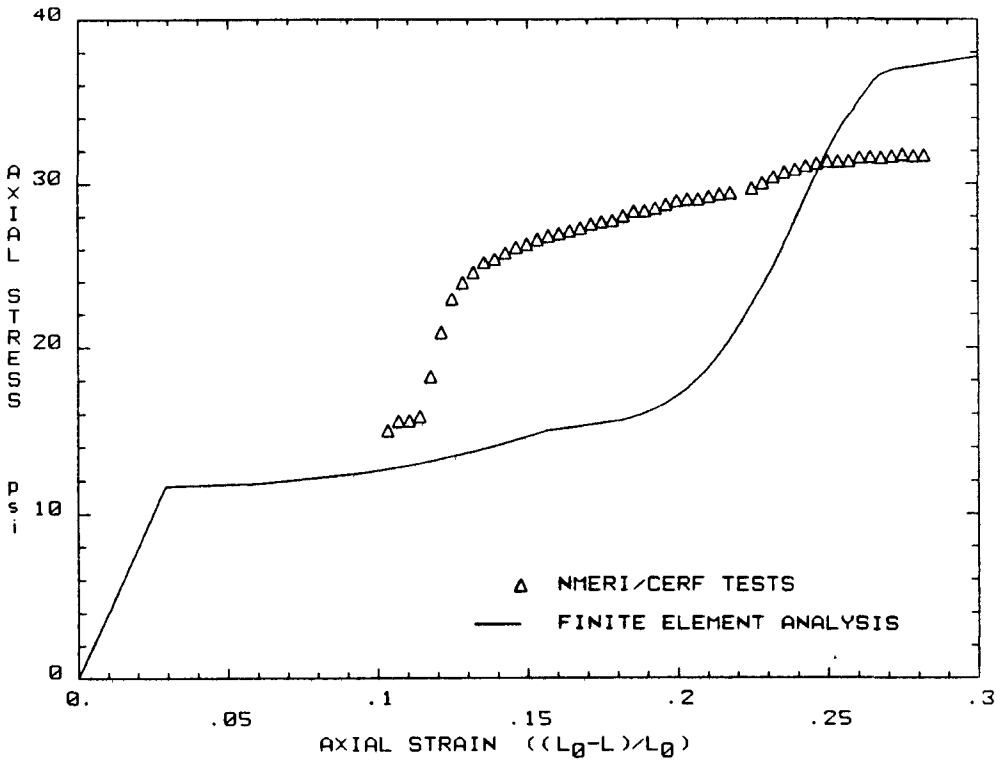

FIGURE A.8b. Comparison of Analytical and Experimental Results - Axial Response from Triaxial Test on Foam 9703 (P=15 psi)

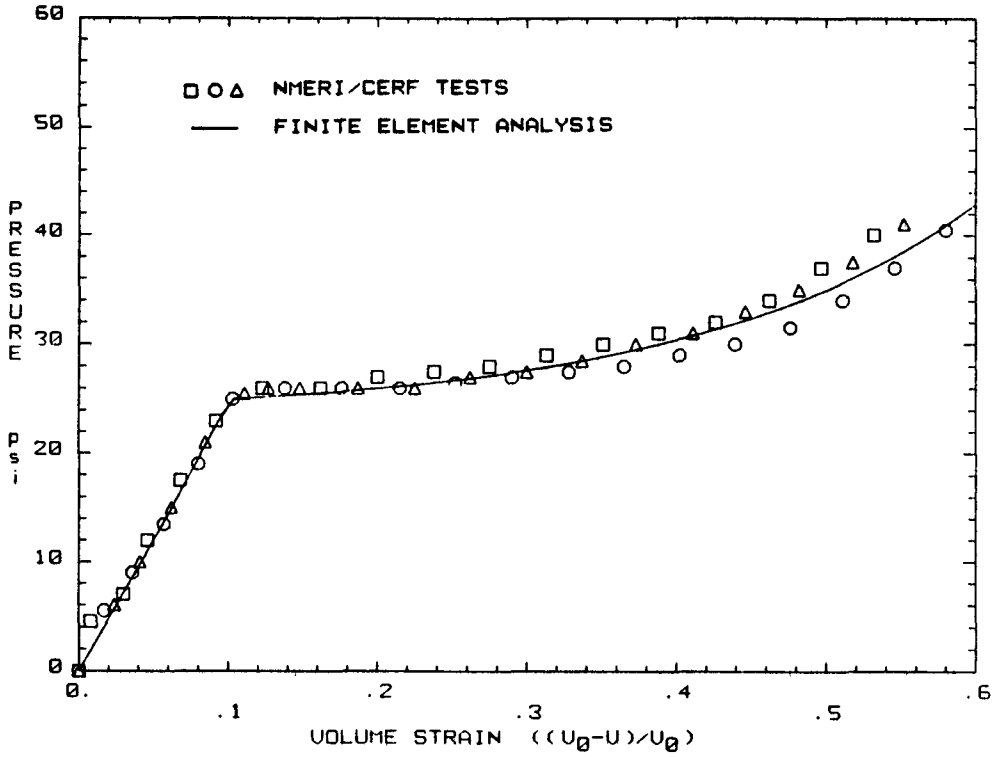

FIGURE A.9a. Comparison of Analytical and Experimental Results - Volumetric Responses from Hydrostatic Tests on Foam 9503

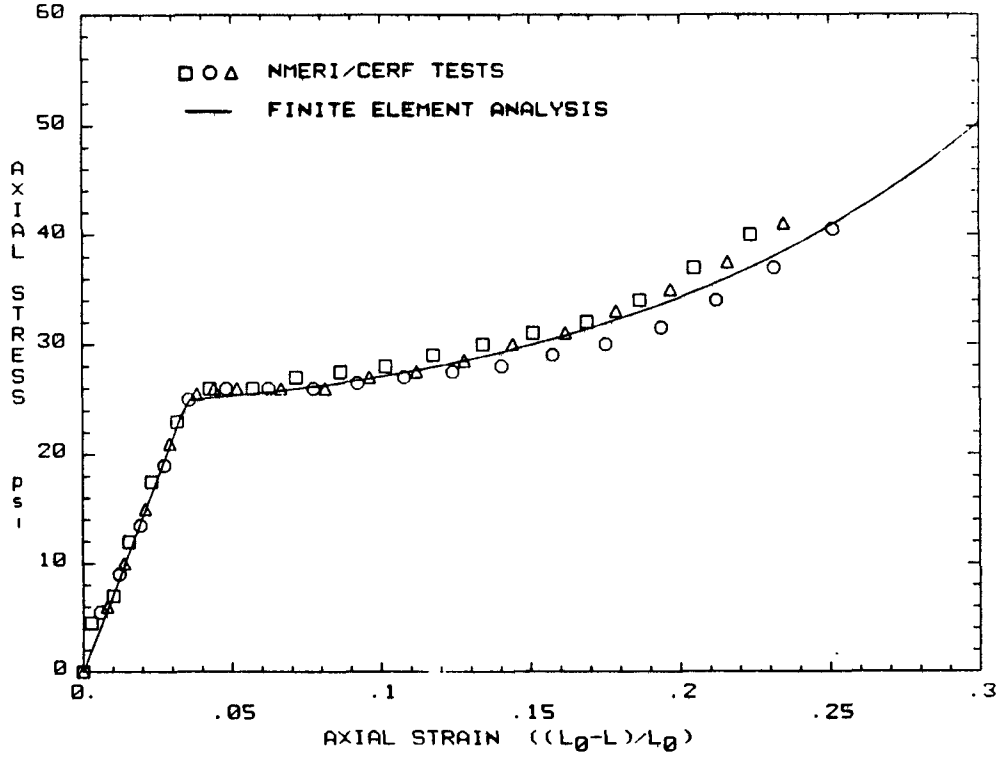

FIGURE A.9b. Comparison of Analytical and Experimental Results - Axial Responses from Hydrostatic Tests on Foam 9503

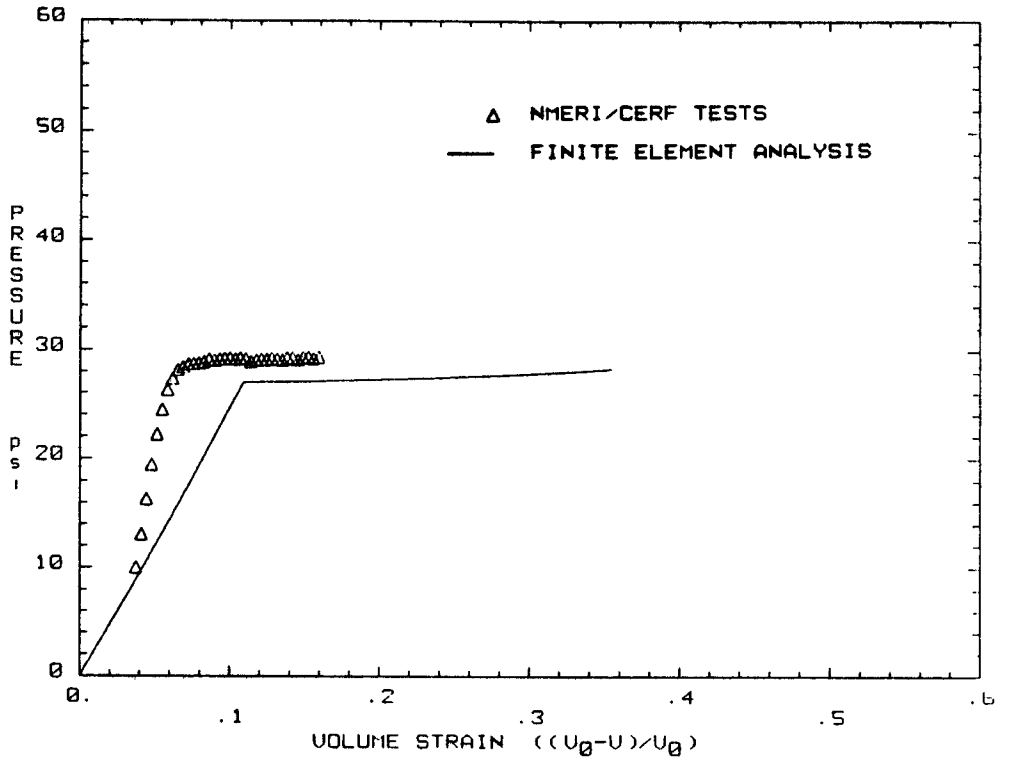

FIGURE A.10a. Comparison of Analytical and Experimental Results - Volumetric Response from Triaxial Test on Foam 9503 (P=10 psi)

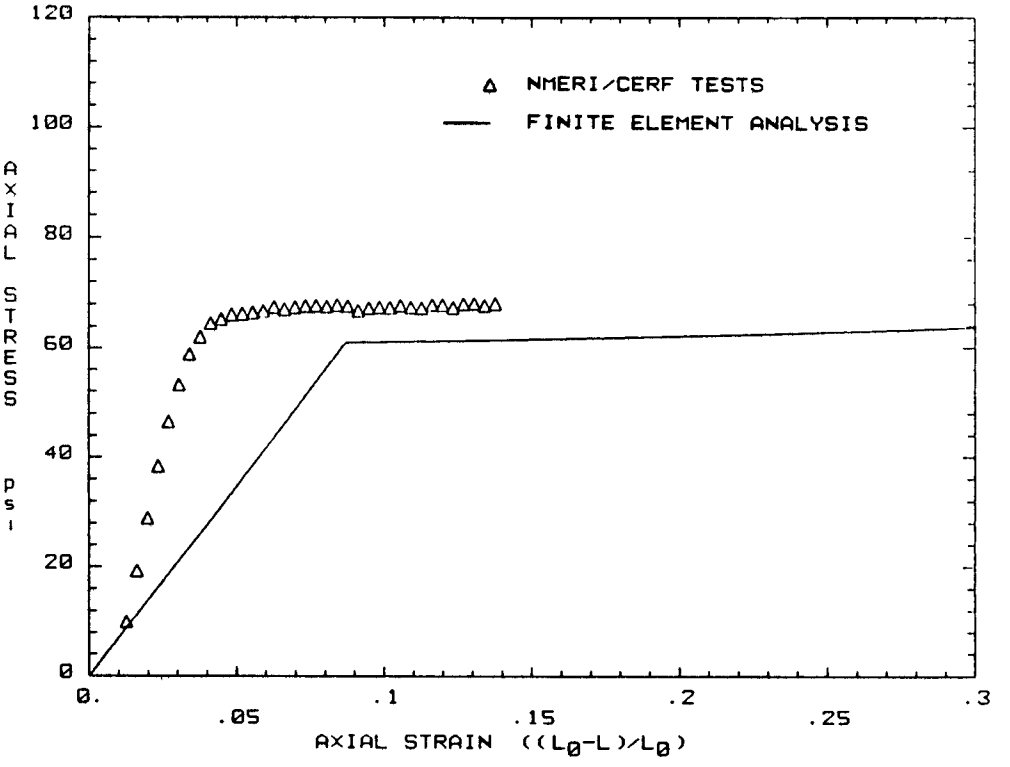

FIGURE A.10b. Comparison of Analytical and Experimental Results - Axial Response from Triaxial Test on Foam 9503 (P=10 psi)

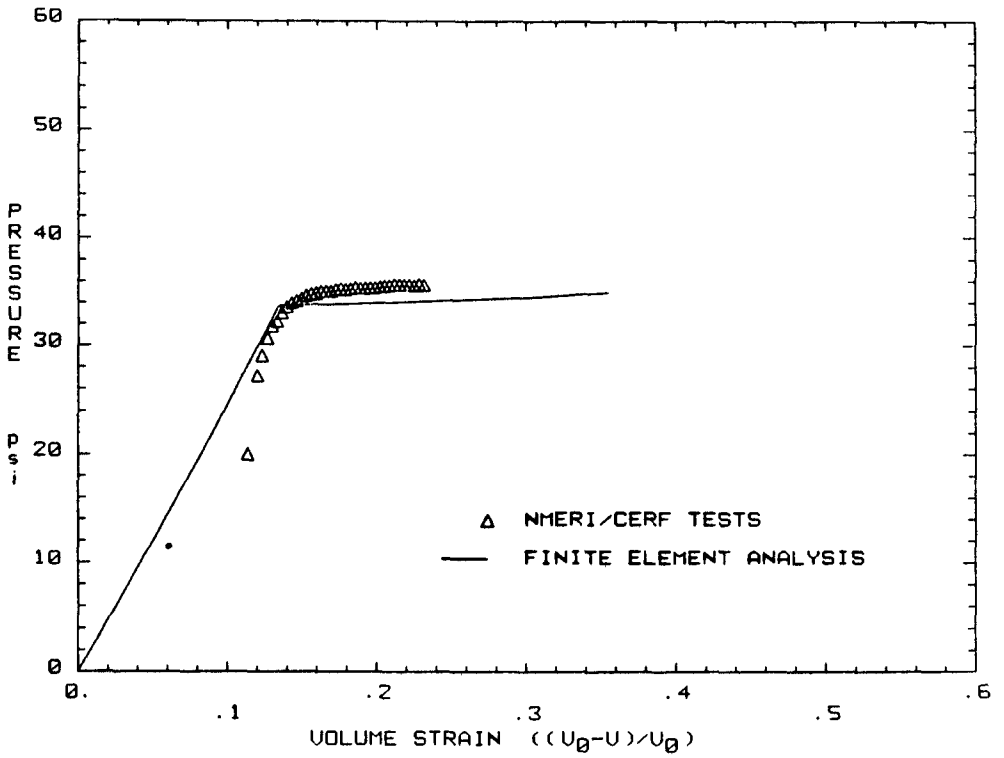

FIGURE A.11a. Comparison of Analytical and Experimental Results - Volumetric Response from Triaxial Test on Foam 9503 (P=20 psi)

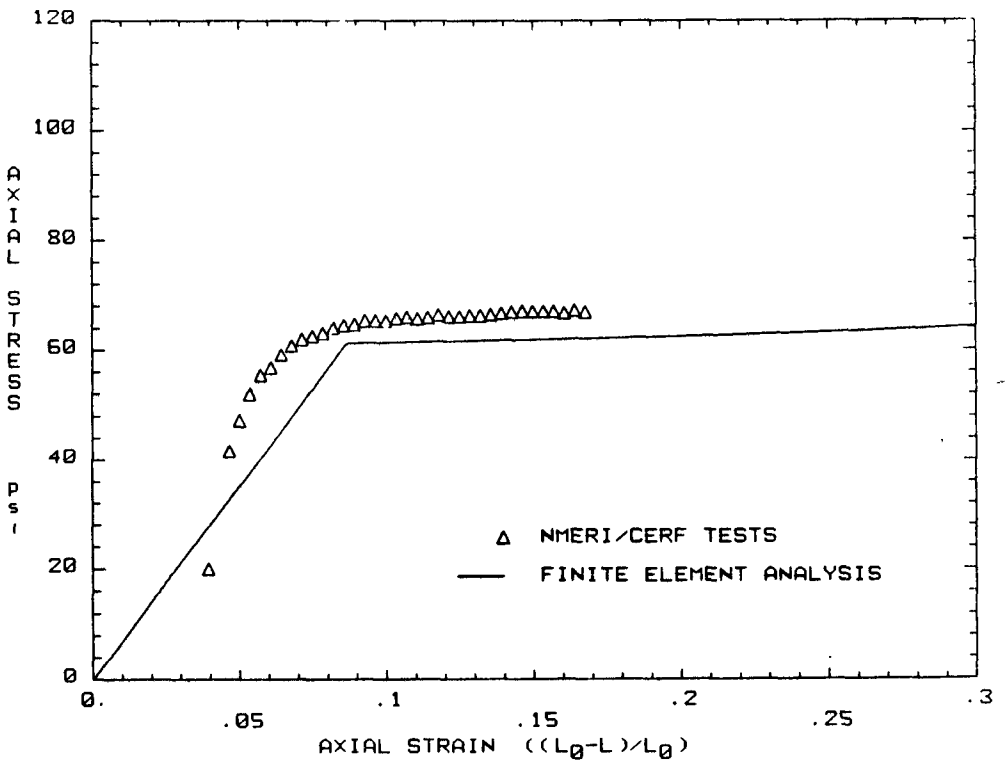

FIGURE A.11b. Comparison of Analytical and Experimental Results - Axial Response from Triaxial Test on Foam 9503 (P=20 psi)

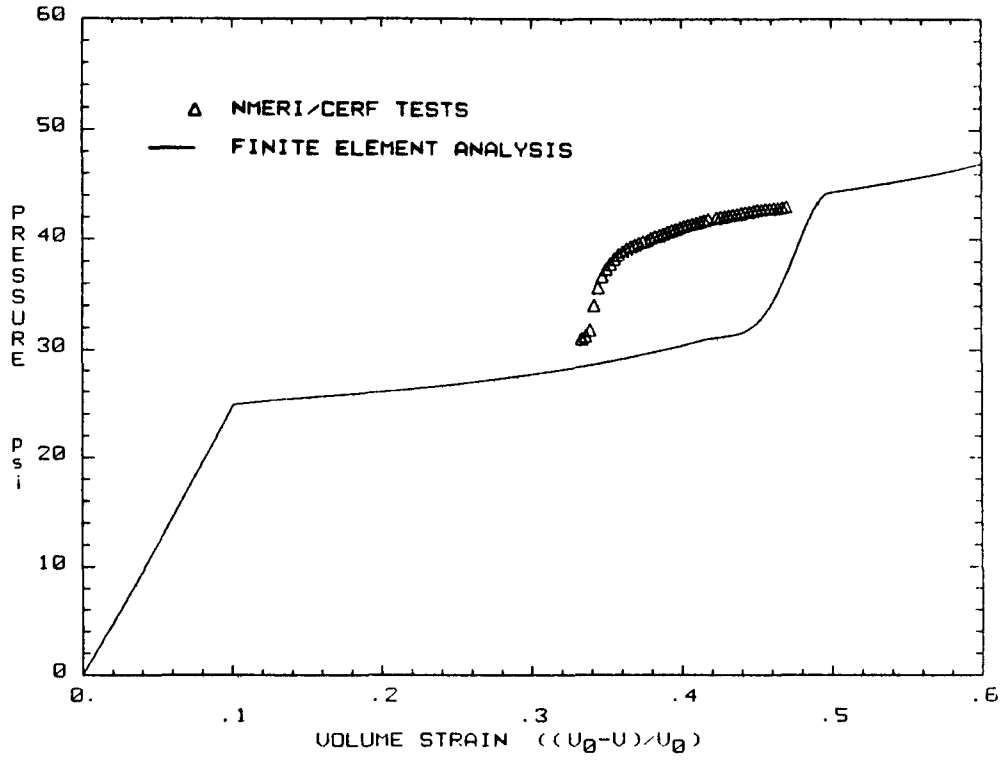

FIGURE A.12a. Comparison of Analytical and Experimental Results - Volumetric Response from Triaxial Test on Foam 9503 (P=31 psi)

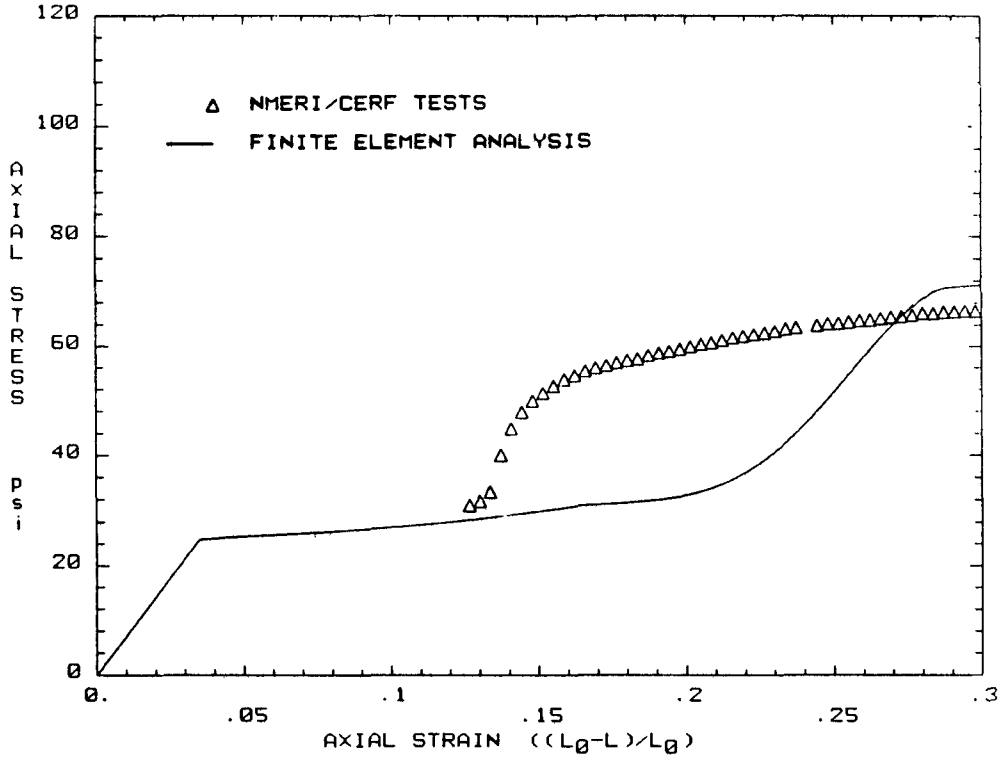

FIGURE A.12b. Comparison of Analytical and Experimental Results - Axial Response from Triaxial Test on Foam 9503 (P=31 psi)

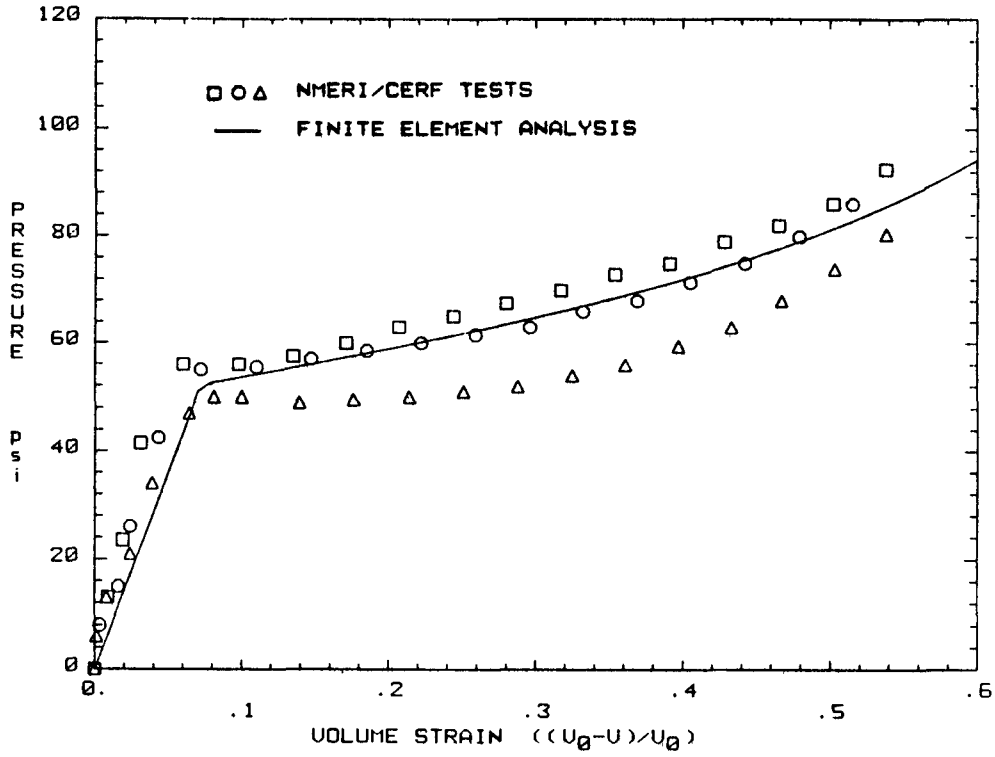

FIGURE A.13a. Comparison of Analytical and Experimental Results - Volumetric Responses from Hydrostatic Tests on Foam 6704

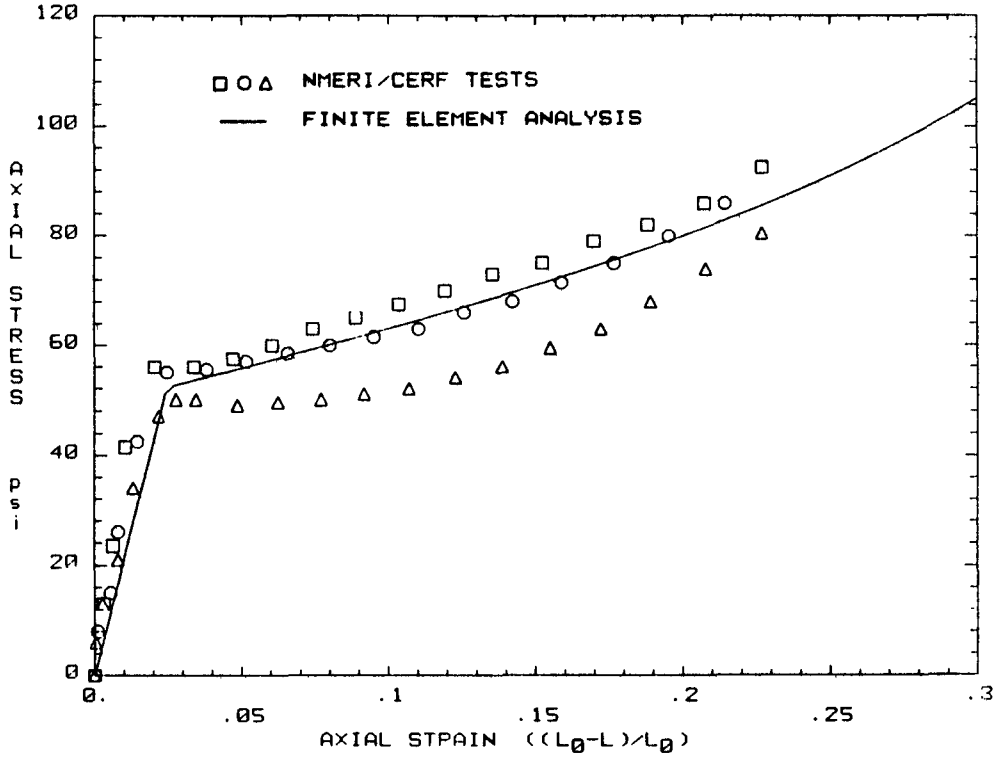

FIGURE A.13b. Comparison of Analytical and Experimental Results - Axial Responses from Hydrostatic Tests on Foam 6704

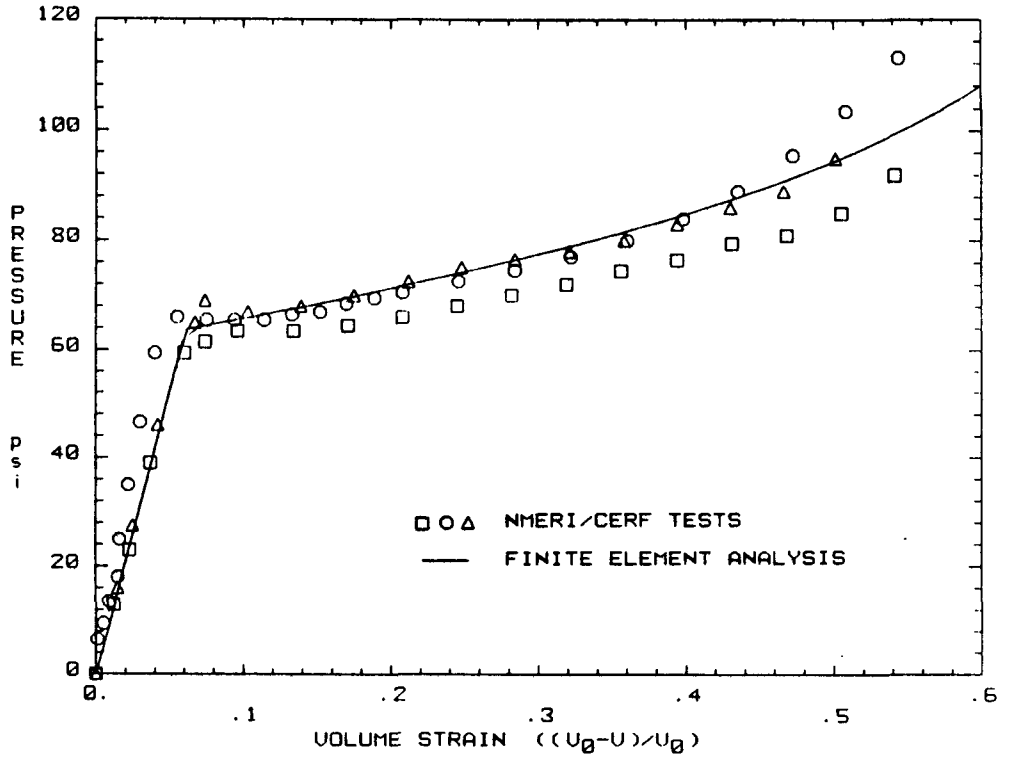

FIGURE A.14a. Comparison of Analytical and Experimental Results - Volumetric Responses from Hydrostatic Tests on Foam 9505

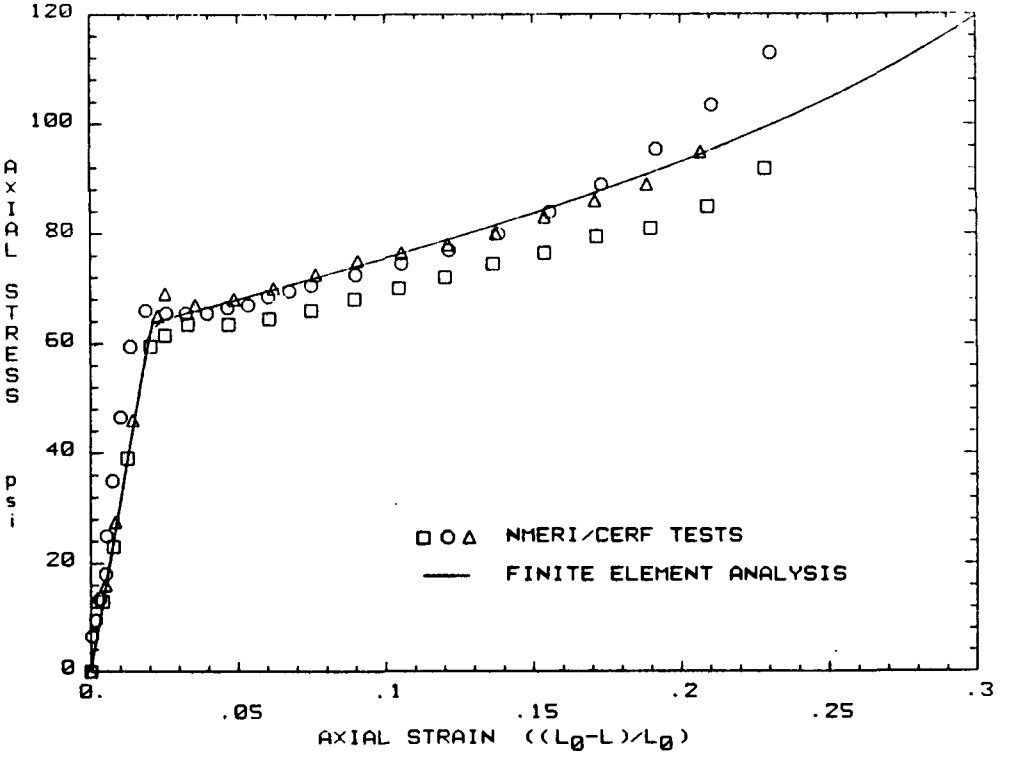

FIGURE A.14b. Comparison of Analytical and Experimental Results - Axial Responses from Hydrostatic Tests on Foam 9505

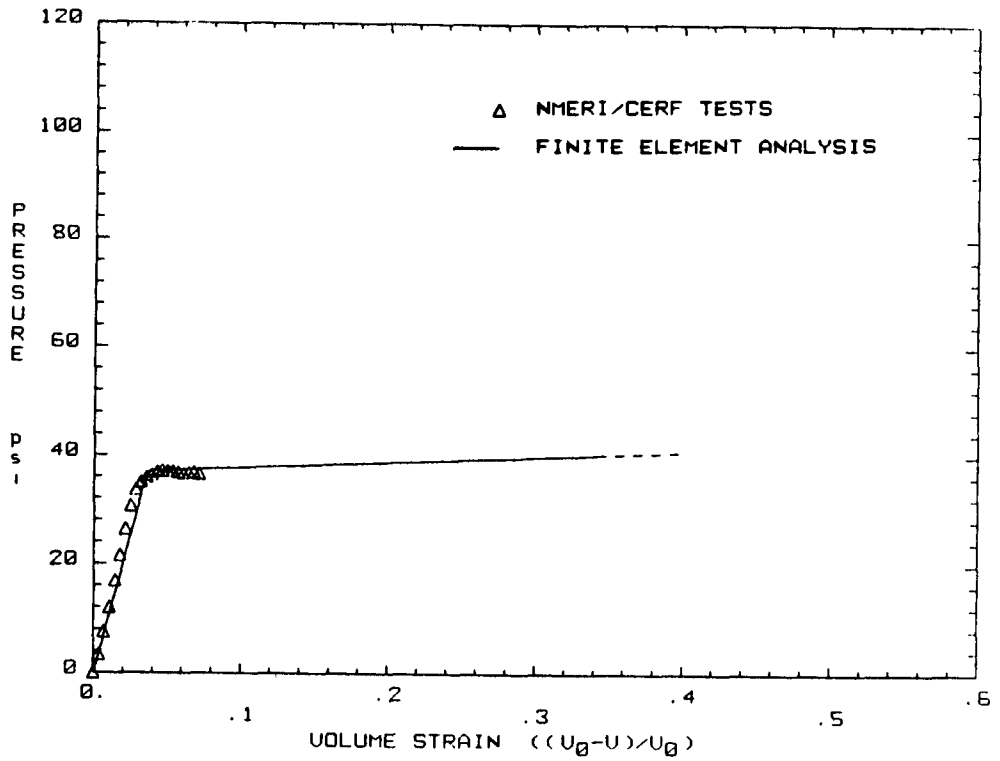

FIGURE A.15a. Comparison of Analytical and Experimental Results - Volumetric Response from Uniaxial Test on Foam 9505

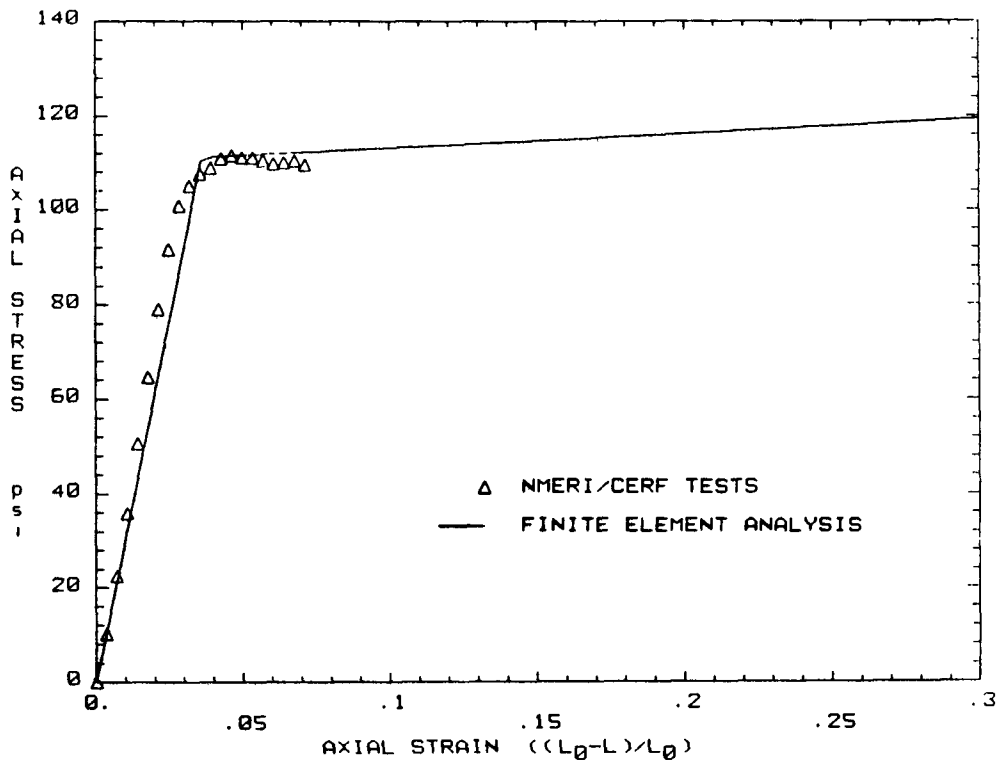

FIGURE A.15b. Comparison of Analytical and Experimental Results - Axial Response from Uniaxial Test on Foam 9505

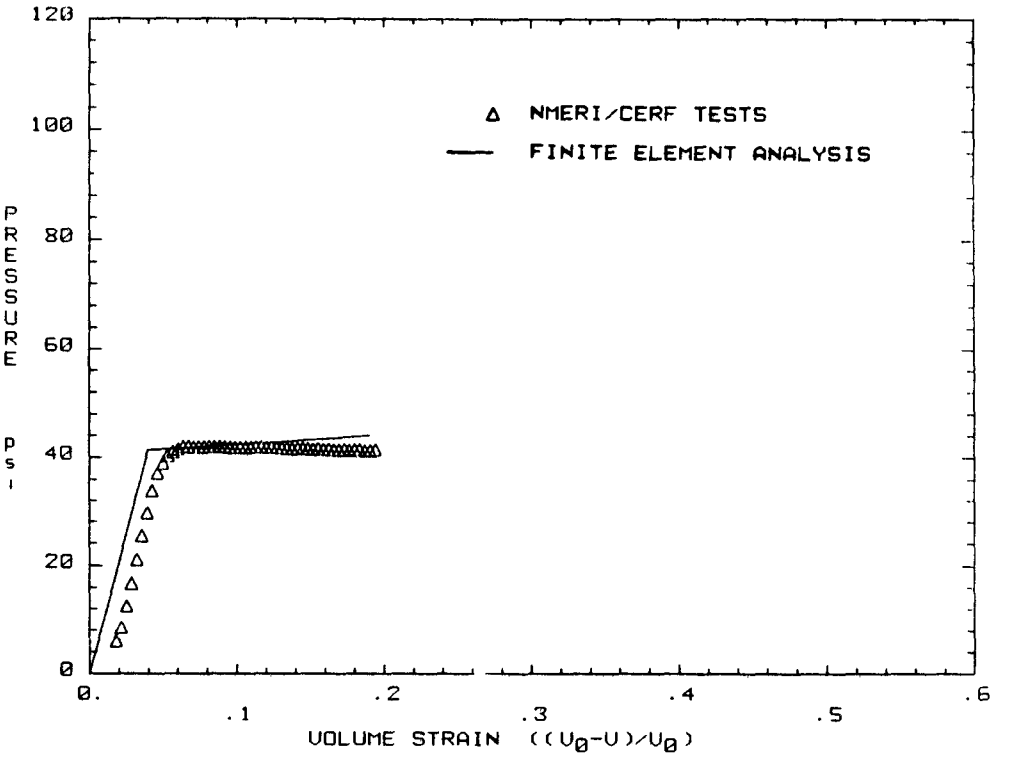

FIGURE A.16a. Comparison of Analytical and Experimental Results - Volumetric Response from Triaxial Test on Foam 9505 (P=6 psi)

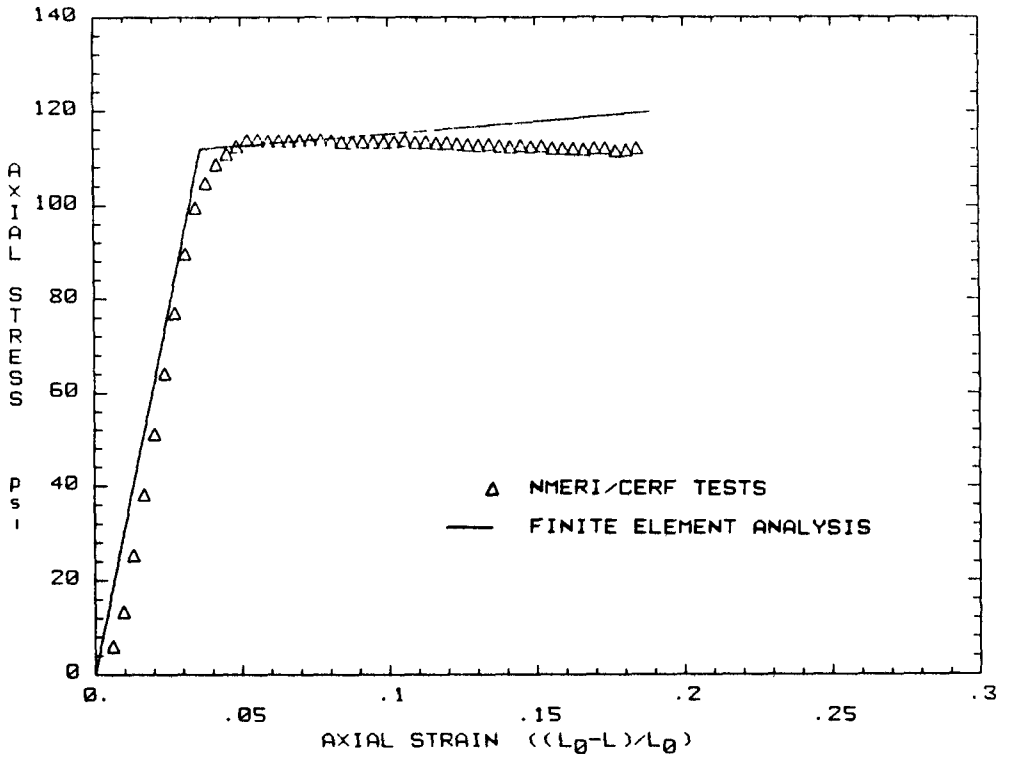

FIGURE A.16b. Comparison of Analytical and Experimental Results - Axial Response from Triaxial Test on Foam 9505 (P=6 psi)

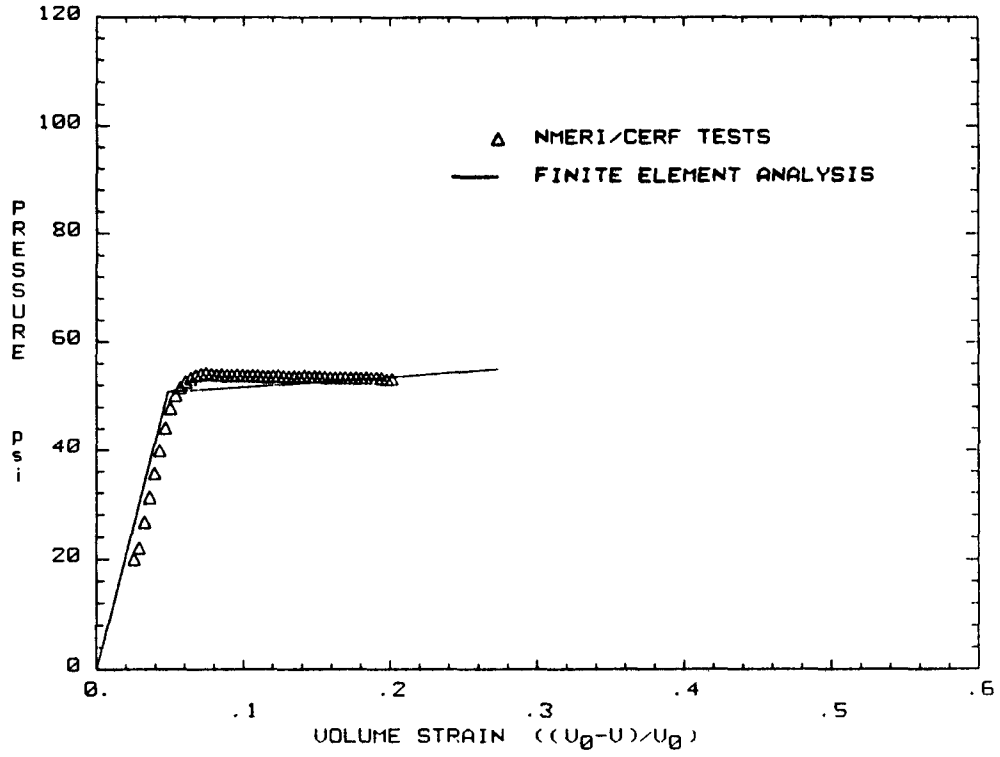

FIGURE A.17a. Comparison of Analytical and Experimental Results - Volumetric Response from Triaxial Test on Foam 9505 (P=20 psi)

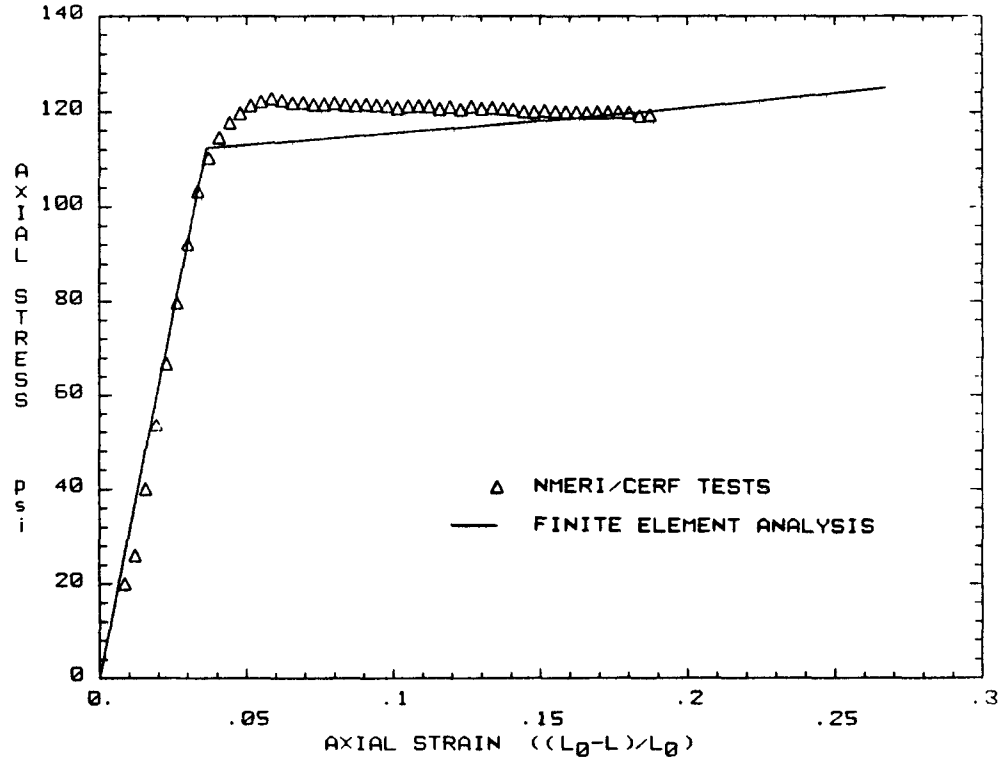

FIGURE A.17b. Comparison of Analytical and Experimental Results - Axial Response from Triaxial Test on Foam 9505 (P=20 psi)

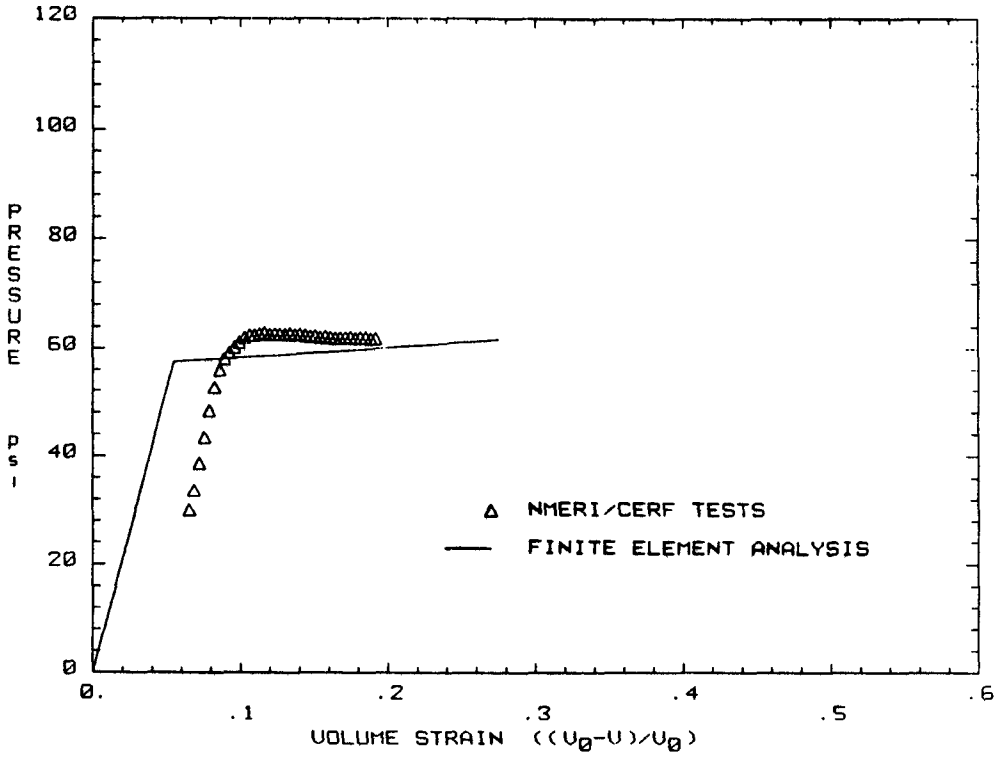

FIGURE A.18a. Comparison of Analytical and Experimental Results - Volumetric Response from Triaxial Test on Foam 9505 (P=30 psi)

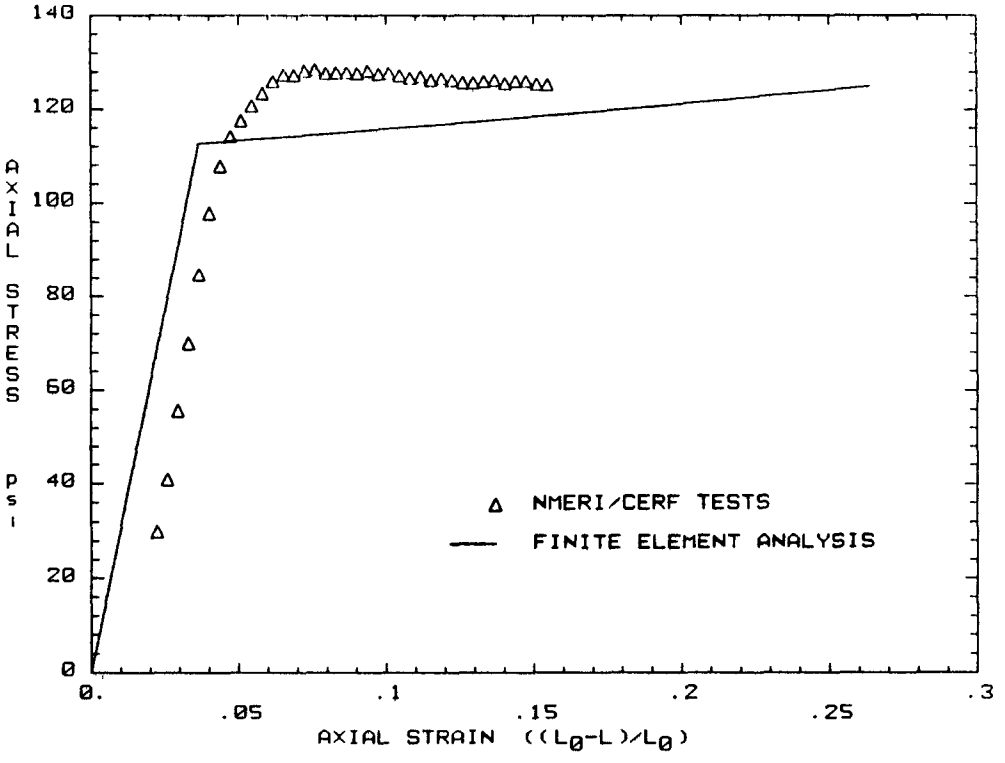

FIGURE A.18b. Comparison of Analytical and Experimental Results - Axial Response from Triaxial Test on Foam 9505 (P=30 psi)

Distribution:

U. S. Department of Energy
Office of Scientific & Technical Information (226)
Oak Ridge, TN 37830
Attn: DOE/OSTI-4500-R74 UC-71

U. S. Department of Energy
Routing RW-33
1000 Independence SW
Washington, DC 20585
Attn: L. Barrett
E. Wilmot
G. Callahan
S. Denny
L. Marks
R. Philpott

U. S. Department of Energy
Routing DP 123
Washington, DC 20545
Attn: J. Lytle
L. Harmon
F. Falci

Office of Security Evaluations
Defense Programs - DP-4, GTN
Washington, DC 20545
Attn: Dr. Julio L. Torres

U. S. Department of Energy
Albuquerque Operations Office
4308 Carlisle, NE
Albuquerque, NM 87107
Attn: J. McGough
K. Golliher

U. S. Department of Energy
Chicago Operations Office
9800 S. Cass Avenue, Bldg. 350
Argonne, IL 60439
Attn: S. Mann
C. Boggs-Mayes

U. S. Department of Energy
Idaho Operations Office
550 Second Street
Idaho Falls, ID 83401
Attn: C. P. Gertz
W. W. Bixby

Joint Integration Office
4308 Carlisle, NE
Albuquerque, NM 87107
Attn: J. Roll, Westinghouse
K. McKinley, Rockwell
R. M. Jefferson

SANDIA INTERNAL:
1510 J. W. Nunziato
1511 D. K. Gartling
1511 A. M. Kraynik
1520 W. Herrmann (acting)
1521 R. D. Krieg (10)
1521 M. K. Neilsen (15)
1521 H. S. Morgan (5)
1521 C. M. Stone
1521 G. W. Wellman
1522 R. C. Reuter
1522 E. D. Reedy
1522 K. W. Schuler
1523 J. H. Biffle
1523 L. M. Taylor
1524 A. K. Miller
1524 K. W. Gwinn
1530 L. W. Davison
1540 W. C. Luth
Attn: W. R. Wawersik
1550 R. C. Maydew
1810 R. G. Kepler
1813 J. G. Curro
1813 W. E. Warren (5)
3141 S. A. Landenberger (5)
3151 W. L. Garner (3)
3154-1 C. H. Dalin, For DOE/OSTI (28)
3310 W. D. Burnett
6000 D. L. Hartley
6300 R. W. Lynch
6320 J. E. Stiegler
Attn: TTC Master File
6320 TTC Library (25)
6321 R. E. Luna
6322 J. M. Freedman
6323 G. C. Allen, Jr.
6323 R. H. Yoshimura (5)
7544 R. A. May
8024 P. W. Dean
8240 C. W. Robinson
8242 L. I. Weingarten
8243 M. L. Callabresi